NTNU

Norwegian University of
Science and Technology

Distributed Sacrificial Cathodic Protection

A New Cost Effective Solution to Prevent
Corrosion on Subsea Structures

Geir Quale

Subsea Technology
Submission date: June 2016
Supervisor: Roy Johnsen, IPM
Co-supervisor: Mariano Iannuzzi, GE

Norwegian University of Science and Technology
Department of Engineering Design and Materials

NTNU - NORWEGIAN UNIVERSITY
OF SCIENCE AND TECHNOLOGY
DEPARTMENT OF ENGINEERING DESIGN
AND MATERIALS

MASTER THESIS SPRING 2016
FOR
STUD.TECHN. GEIR QUALE

CATHODIC PROTECTION WITH DISTRIBUTED ANODES

Katodisk beskyttelse ved hjelp av fordelt anode

Background:

Today, subsea components are protected against corrosion with a solution combining coating (paint) and sacrificial anodes installed across the structures. GE Oil and Gas has proposed a radical new approach to CP design in which the anodes are replaced, in part, by a bilayer metallic coating system. In GE's concept, traditional thermally sprayed aluminum (TSA) of 95% Al and 5% Mg (AlMg5) constitutes the first layer and a sacrificial TSA layer made from a commercial Al-Zn-In alloy is deposited on top. The idea behind this solution is to reduce the total "anode mass" on a subsea structure and, in this way, reduce the overall weight of a subsea structure. GE's calculations showed that the proposed methodology could reduce anode demand by at least 90%. Such reduction translates into enormous weight saving opportunities across subsea system components.

Objective:

The following objectives have been put up for the MSc project:

1. Document the electrochemical properties of the sacrificial TSA anode coating compared to a traditional anode.
2. Document the self-corrosion rate (i.e. anode utilisation) of the coating and compare it to a conventional anode.
3. Document the ability for the sacrificial TSA coating to protect a defect, i.e. an area exposing the conventional TSA coating (AlMg5) to the seawater environment.

Activities:

According to public information in the literature, no attempt has been performed to spray a commercial aluminium anode alloy with the Thermal Spraying (TS) method or by any other deposition technology. The first activity in the project is to prepare a 2 mm wire matching the chemical composition of an Al-Zn-In anode. We will achieve this by using a commercial NORSOK certified anode as starting point in the wire manufacturing process. We will use IPM's facilities to manufacture the wire. Preparation for this work has already begun. An IPM technician will conduct this task, but the student shall follow the production process. The entire manufacturing process will be documented in detail.

After the wire has been prepared, an NORSOK certified and GE approved TS company will apply a coating on test material (plates) made from carbon steel.

The main activity in the MSc the project will be to test and document the corrosion protection properties of the distributed aluminium anode and compare these with the properties of the similar traditional anode. DNV RP-B401 and NORSOK M-503 describe how to test sacrificial anodes. These documents will be important reference material when designing the final test programme (at least part of them).

The following will be included in the corrosion test program:

1. Document TS layers (normal AlMg5 and distributed anode) in SEM/EDS.
2. Documentation of electrochemical properties of the distributed anode and normal anodes according to DNV RP-B401/NORSOK M-503.
3. Measure electrochemical polarization curves and OCP (over time).
4. Exposure of samples with 1% damage in outer TSA coating (distributed anode) – measure OCP and analyze samples after exposure. The 1% defect area will be simulated by galvanically coupling an intact coated sample to a bare/uncoated carbon steel coupon with an area ratio of 100 (coated sample):1 (bare coupon).

Tests will be run in at normal inlet seawater temperature (SEALAB) and room temperature (Gløshaugen). Some tests will also be executed at a higher temperature (e.g. 40-60^0).

The experimental work will be done in SEALAB and the Corrosion Lab at Gløshaugen.

GE Oil and Gas sponsors this project.

Formal requirements:

Three weeks after the start of the thesis work, an A3 sheet illustrating the work is to be handed in. A template for this presentation is available on the IPM's website under the menu "Masteroppgave" (https://www.ntnu.edu/web/ipm/master-thesis). This sheet should be updated one week before the master's thesis is submitted.

Risk assessment of experimental activities shall always be performed. Experimental work defined in the problem description shall be planned and risk assessed up-front and within three (3) weeks after receiving the problem text. Any specific experimental activities that are not adequately covered by the general risk assessment shall be particularly assessed before performing the experimental work. Risk assessments should be signed by the supervisor and copies shall be included in the appendix of the thesis.

The thesis should include the signed problem text, and be written as a research report with summary both in English and Norwegian, conclusion, literature references, table of contents, etc. During preparation of the text, the candidate should make efforts to create a well arranged and well-written report. It is important to cross-reference text, tables and figures to facilitate the evaluation of the thesis. For evaluation of the work, a thorough discussion of results is appreciated.

The thesis shall be submitted electronically via DAIM, NTNU's system for Digital Archiving and Submission of Master's theses.

Co-supervisor: Mariano Iannuzzi, (GE Oil & Gas and IPM)

Torgeir Welo
Head of Division

Roy Johnsen
Professor/Supervisor

NTNU
Norges teknisk-
naturvitenskapelige universitet
Institutt for produktutvikling
og materialer

Preface

This master's thesis is submitted to the Norwegian University of Science and Technology (NTNU) as the final work for the master's degree program Subsea Technology at the Department of Engineering Design and Materials. The project has been a close collaboration between NTNU and General Electric Oil & Gas (GE), with Professor Roy Johnsen as the main-supervisor together with Professor Mariano Iannuzzi from GE and IPM as co-supervisor.

Acknowledgement

First of all, I would like to give a special thanks to my supervisor Professor Roy Johnsen for all his help and guidance throughout the project period. His availability, engagement and feedback are highly appreciated. I would also thank my co-supervisor Professor Mariano Iannuzzi for excellent feedback, discussion and engagement, and for always being available through internet communication.

I would also like to give a special thanks to Ph.D. candidate Cristian Torres for his excellent help solving both practical and theoretical problems. Last but not least, I would like to thank Nils-Inge J. Nilsen for practical help in the lab.

Trondheim, June 10, 2016

Geir Quale

Abstract

Over the last 50 years, only minor changes have been made to the cathodic protection (CP) design, whereas optimization has not been considered as a cost saving opportunity to date. For subsea structures, sacrificial anodes combined with organic coatings are the main corrosion protection strategy. Depending on the lifetime of the subsea system, the complexity of the structure to be protected, and the environmental conditions, the total anode mass can be substantial. The anode mass does not only increase fabrication costs, but also affects the total structure weight in a way that puts special requirements on lifting vessels and cranes. Reducing this weight may not only be cost efficient, but also improve the safety during installation due to less complex lifting operations.

In this study, the electrochemical properties of a new concept named CP by distributed sacrificial anode (DSA) was investigated, with the main focus on the anodic capabilities in comparison to those of conventional sacrificial Al-Zn-In anodes and thermally sprayed aluminum (TSA-Al99.5). The main principle of CP by DSA is to convert the cathode area to anode area by distributing anode mass on the surface of the equipment to be protected. DSA was achieved by deposition of a dual layer metallic coating, consisting of a TSA layer applied on carbon steel (CS) plates, followed by sacrificial outer Al-Zn-In layer on top. This was done by arc-spraying, a thermal spray technique. Freely exposed specimens as well as galvanic couplings between DSA, TSA, conventional anode and CS with area ratio 1:1, 10:1 and 100:1 were immersed in nearly stagnant flowing seawater at $10 \pm 2\,°C$ and $40 \pm 5\,°C$. Continuously monitoring of the open circuit potential (OCP) and the current demand for the couplings were conducted as well as periodically obtaining potentiodynamic polarization curves in order to investigate the electrochemical properties with respect to exposure time. After 30 days exposure, surface and cross-section examination was conducted using scanning electron microscope (SEM) coupled to an energy-dispersive spectroscopy (EDS).

The results from this study indicate that DSA have similar anodic properties as for those of conventional sacrificial anodes, and can supply sufficient CP to a substantial larger defect compared to TSA coatings. When used as a CP system, protecting a 10% holiday i.e. exposed CS, the coupling potential was not affected and held the same potential as for freely exposed DSA, at -1000 mV$_{Ag/AgCl}$. The effective polarization properties provides initial high current output to the CS area, but decreases rapidly due to a dense calcareous deposition, contributes to an overall lower degradation rate of the coating in comparison to TSA under similar conditions. The cathodic properties for DSA is changed with respect to the bulk material, the sacrificial anode. The reason is either due to reduced content of Zinc and Indium as a result of the thermal spraying process and/or due to increased oxidation properties. This also affected the OCP, contributing to a nobler potential. The cathodic properties are similar to those of TSA at cathodic polarization between -1100 mV$_{Ag/AgCl}$ and -1550 mV$_{Ag/AgCl,}$ thus when connected to a conventional sacrificial anode, the current drain is similar as for TSA, between 6-10 mA/m^2.

Sammendrag

I løpet av de siste 50 årene har få endringer blitt gjort når det gjelder designet av katodisk beskyttelse (CP), mens optimalisering ikke har vært ansett som en kostnadsbesparende mulighet til dagens dato. For undervannsstrukturer, offeranoder kombinert med organiske belegg er hovedstrategien for CP. Avhengig av levetiden for det undersjøiske systemet, dens kompleksitet og de miljømessige forholdene, kan den totale anodemassen være betydelig stor. Anodemassen påvirker ikke bare de økte fabrikasjonskostnadene, men også den totale vekten av strukturen på en måte som stiller spesielle krave på løftefartøy og kraner. Reduksjon av denne vekten vil dermed ikke bare være kostnadsbesparende, men også øke sikkerheten under installasjonen på grunn av en reduksjon av antall kompliserte løfteoperasjoner.

I denne studien ble de elektrokjemiske egenskapene til et nytt konsept kalt CP ved distribuert anode (DSA) undersøkt, med hovedfokus på de anodiske egenskapene i forhold til konvensjonelle offer anode av typen Al-Zn-In og termisk sprøytet aluminium (TSA – Al99.5). Hovedprinsippet bak CP ved DSA er å omdanne katodeområdet til anodeområde ved å fordele anodemasse på overflaten av utstyret som skal beskyttes. Dette ble oppnådd ved avsetning av et tolags metallisk belegg bestående av et indre TSA lage påført karbonstålplater (CS), etterfulgt av et av et ytre Al-Zn-In lag som skal fungere som en offeranode. Dette ble gjennomført ved bruk av lysbue-sprøyting, en termisk sprøyte teknikk. Fritt eksponerte prøver i tillegg til galvaniske koblinger mellom DSA, TSA, konvensjonell anode og CS med arealforhold 1:1, 10:1 og 100:1 ble nedsenket i tilnærmet stillestående sirkulert sjøvann ved $10 \pm 2℃$ og $40 \pm 5℃$. Kontinuerlig overvåkning av det åpne kretspotensialet (OCP) og strømbehovet for koblingene ble utført, i tillegg til periodisk opptak av polarisasjonskurver. Etter 30 dagers eksponering ble det gjennomført både overflate og tverrsnittsundersøkelse ved bruk av et scanning elektronmikroskop (SEM) koblet til en enegi-dispersiv spektroskopi (EDS).

Resultatene fra denne studien indikerer at DSA har tilsvarende anodiske egenskaper som for konvensjonelle offeranoder, og kan levere tilstrekkelig CP til et betydelig større eksponert CS område i forhold til hva TSA kan tilføre. DSA brukt som CP system for en 10% helligdag hvor CS er eksponert, holdt samme koblingspotensial som for fritt eksponert DSA, ved -1000 mV$_{Ag/AgCl}$. De effektive polariseringsegenskapene for DSA, gir en innledende høy strømtilførsel til CS-området, men avtar hurtig grunnet tett kalkavsetning som bidrar til å redusere den totale nedbrytningshastigheten av belegget i forhold til TSA under lignende forhold. De katodiske egenskapene for DSA har blitt endret i forhold til anode materialet. Årsaken er enten som følge av redusert innhold av sink og indium som et resultat av den termiske sprøyte prosessen og / eller som følge av økt oksidasjonsegenskaper. Dette har i tillegg påvirket OCP ved å bidra til et edlere potensial. De katodiske egenskapene for DSA er lik de av TSA under katodisk polarisering mellom -1100 og -1550 mV$_{Ag/AgCl}$, og fører dermed til et nesten tilsvarende strømbehov når koblet mot konvensjonelle anoder, mellom 6-10 mA/m^2.

Content

List of Abbreviations

Ag/AgCl	-	Silver Chloride Electrode
CP	-	Cathodic Protection
b_a	-	Anodic Tafel Constant
b_c	-	Cathodic Tafel Constant
CS	-	Carbon Steel
DIN	-	Deutsches Institut für Normung
DMS	-	Data Management System
DNV	-	Det Norske Veritas
DSA	-	Distributed Sacrificial Anode
E_{corr}	-	Corrosion Potential
EDS	-	Energy-Dispersive Spectroscopy
E_P	-	Pitting Potential
F	-	Faradays Constant
GE	-	General Electric
i	-	Current Density
i_{corr}	-	Corrosion Current
i_p	-	Passive Current Density
ISO	-	International Organization for Standardization
M	-	Molar Weight
MEG	-	Mono-Ethylene Glycol
NORSOK	-	Norsk Sokkels Konkurranseposisjon
NTNU	-	Norwegian University of Science and Technology
OCP	-	Open Circuit Potential
SCE	-	Saturated Calomel Electrode
SEM	-	Scanning Electron Microscope
SHE	-	Standard Hydrogen Electrode
SPS	-	Subsea Production System
T	-	Temperature
TLP	-	Tension Leg platform
TSA	-	Thermally Sprayed Aluminum
TSC	-	Thermally Sprayed Coating
TSZ	-	Thermally Sprayed Zinc
WE	-	Working Electrode
WT%	-	Weight Percent
ρ	-	Density

List of Figures

List of Tables

1   Introduction

1.1 Background

Over the last 50 years, only minor changes have been made to the cathodic protection (CP) design, whereas optimization has not been considered as a cost saving opportunity to date. For subsea structures, sacrificial anodes combined with organic coatings are the main corrosion protection strategy. Depending on the lifetime of the subsea system, the complexity of the structure to be protected, and the environmental conditions, the total anode mass can be substantial. For subsea structures, the anode mass not only increases fabrication costs but also affects the total structure weight in a way that puts special requirements on lifting vessels and cranes. Reducing this weight may not only be cost efficient, but also improve the safety during installation due to less complex lifts.

Thermal Spray Aluminum (TSA) has occasionally been used to replace organic coating on subsea structures, especially to reduce current demand at elevated temperatures or to extend anode life on projects with long design lives (i.e. 40 to 50 years)[1-6]. For risers and tension legs at e.g. the Hutton tension leg platform, TSA showed good protective abilities and was proven to deliver acceptable CP to up to 2.5% coating damage, i.e. carbon steel is exposed, with current density demand according to DNV RP-B401[7]. However, TSA has not been used subsea as an anode replacement to protect subsea structures. In conventional CP design, TSA remains connected to the CP system, draining current from sacrificial anodes to ensure adequate cathodic protection.

Therefore, a new concept named CP by distributed sacrificial anode (DSA) will be presented. The coating consists of a dual layer, where the first layer, a conventional TSA (Al99.5)[1] is applied in order to reduce the current demand, followed by a sacrificial Al-Zn-In layer which will provide cathodic protection to defects. This layer, consists of a conventional anode alloy which will in contrast to TSA theoretically eliminate the cathodic area if the electrochemical properties, are identical to those of conventional Al-Zn-In anodes.

The benefits by the use of DSA as an alternative for optimization of traditional CP system may be big when it comes to weight- and cost savings. As an illustration, for the subsea production system (SPS) at the Gordon project, approximately 26,000 kg of anodes were used in the PTS M2 manifold alone. General Electric (GE), who designed and manufactured the SPS, have calculated that by implementing DSA can translate into a 92 % reduction in the total anode mass, from 26,000 kg to just over 2000 kg [8]. For the whole subsea production system at Gordon, a total weight saving of 522,130 kg may be possible, contributing to one of the largest weight saving opportunity for subsea production system.

---

[1] In the project description it said to use AlMg5 as a first layer. This was changed to Al99.5 in this study.

The enormous weight saving is a result of reduced area to be protected which contributes to fewer anodes and the corresponding carbons steel cores for fastening. In GEs weight saving calculations it's assumed that DSA is best suited for un-insulated gas system operating at elevating temperature at 140℃. However, for the substantial weight saving possibilities to be true, the following hypothesis which have been used in GEs calculation must be true:

- DSA does not drain current from anodes (no potential differences)
- DSA reduces the cathode area but does not provide CP to defects.
- Exposed areas in need of CP are protected by conventional anodes.

In comparison, weight savings achieved by applying higher strength materials (>15%) for the M2 manifold translates into 600,000 kg. However, the initial costs for high strength materials is substantial higher compared to the use of DSA. In addition, the DSA concept holds lower risk than what can be expected form savings due to higher strength materials. This is because the DSA is a somewhat proven technology and does not affect the pressure envelope [8].

At an economic point of view, implementation of DSA for un-insulating gas fields requiring a long design life (e.g. Gorgon), fabrication cost savings in the range of 27-37 % may be possible, according to GE.

In GE's calculations, CP for coating damages are achieved by conventional anodes alone and not from the coating itself. This means that even larger weight- and cost savings can be possible if the DSA surfaces are included in the calculations. As TSA has proven adequate for tension legs and risers under splash zone environments, DSA should theoretically be superior due to its low corrosion potential providing effective polarization to defects at a higher degree than TSA. Figure 1, illustrates the main benefits (theoretically) by applying DSA compared to other CP strategies.
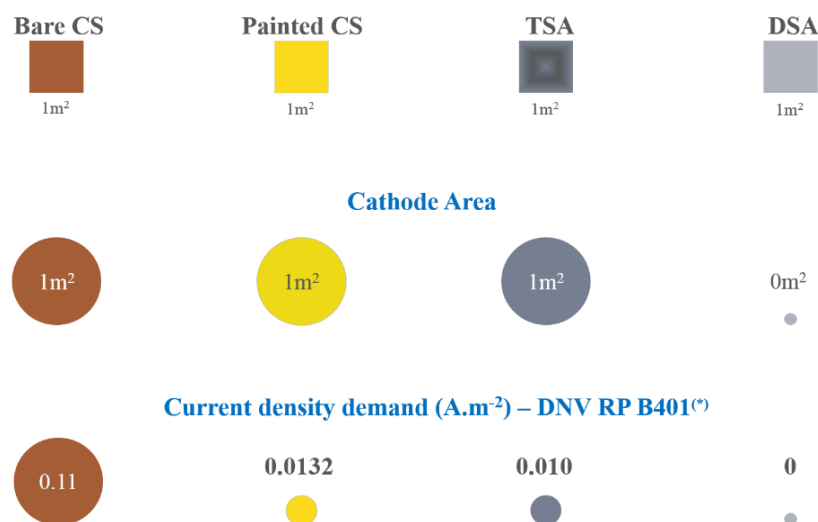
Figure 1 Current density demand for bare carbon steel (CS), painted CS with coating damage and TSA according to DNV [7], in addition to theoretical behavior of DSA connected to conventional sacrificial anodes [8].

1.2 **Objective**

The main objective for this thesis is therefore to document the electrochemical properties and corrosion protection properties for DSA exposed to natural seawater at both 10℃ and 40℃. The electrochemical properties shall be compared to those of conventional sacrificial anode and TSA in order to determine if DSA is an alternative CP strategy for the oil and gas industry. Also, an evaluation of the following hypothesis GE has made for the performance of DSA shall be conducted:

- ▪ DSA have same electrochemical potential as sacrificial anode
- ▪ DSA eliminates the cathode area, i.e. does not drain current from connected sacrificial anodes
- ▪ DSA have similar anodic protective properties as conventional sacrificial anode
- ▪ DSA is an alternative to TSA and/or sacrificial anodes

2   Theoretical background

2.1 Thermally Sprayed Coatings

Thermal spraying is a generic term for a group of coating processes used to apply metallic, ceramic, cermet and some polymeric coatings for different applications. It's a well-established industrial method in order to protect or modify the substrate surfaces for enhanced performance [9]. Different techniques for applying the coating exist, and the different processes are grouped into three major categories: flame spray, electric arc spray and plasma spray. However, the basic of the processes are the same. The coating material is fed into a spraying gun in forms of wire, powder or rod. By the use of electrical or chemical combustion, the material is heated to molten or semi-molten conditions. High velocity air or gas accelerates the particles towards a prepared substrate, where it hits the surface in the forms of splats, solidify and adhere [10]. Bonding between splats occurs, primarily mechanically, resulting in a lamellar microstructure. Depending on the used technique, pores and oxide will be present in different order of magnitude. The use of High Velocity Oxy-Fuel (HVOF) provides excellent adhesion to the substrate and low porosity. However, this is one of the most costly methods, which must be taken into consideration when evaluate which method to use. Selection of the most appropriated thermal spray method is typically determined by:

- Desired coating material
- Coating performance requirements
- Economics
- Part size and portability

Other factors like deposition rate, finish requirements, coating thickness and equipment availability are also important to consider. For materials with low melting temperature like Zinc and Aluminum, the most commonly used method is flame spray or electric arc spray due to economic reasons [10]. In this project, electric arc spray technique have been used for applying both layers consisting of a traditional layer of thermally sprayed aluminum (TSA – 99.5% Al) followed by a sacrificial layer made from a commercial Al-Zn-In anode alloy (DSA) on top. Therefore, only this technique will be discussed.

Electric arc spray, also called twin-wire arc, was developed by M.U. Schoop in 1910 [10]. The process, unlike other thermal spray processes, uses a direct current between two wires of the coating material. The process is shown schematically in Figure 2. The potential differences between the two wires creates an electric arc in the gap when converging, melting the wires together. The wire diameter used for the spraying is usually 2 mm, 3.17 mm or 4.76 mm. Reports have shown that increased diameter can increase the productivity. However, with increasing diameter, the arc becomes more unstable as

the transferred heat from the flame becomes too small in order to melt the wires. This may increase the porosity of the coating and may increase the possibilities for coating defects [11]. As the wires are fed continuously, high-velocity air jet located behind the intersection shears and accelerate the molten particles towards the substrate surface. Compared to any other conventional thermal spray processes, electric arc spray transfers the least heat to the substrate surface (cold process), making it possible to deposit coatings onto polymers, fiberglass, wood etc. In addition, arc spray gives higher temperature to the melted material compared to flame spray, which contributes to increased adhesion to the substrate [9]. Due to its simplicity, low operation cost, portability and high efficiency, the process is often used in the offshore industry to protect equipment and structures against corrosion and wear [12].
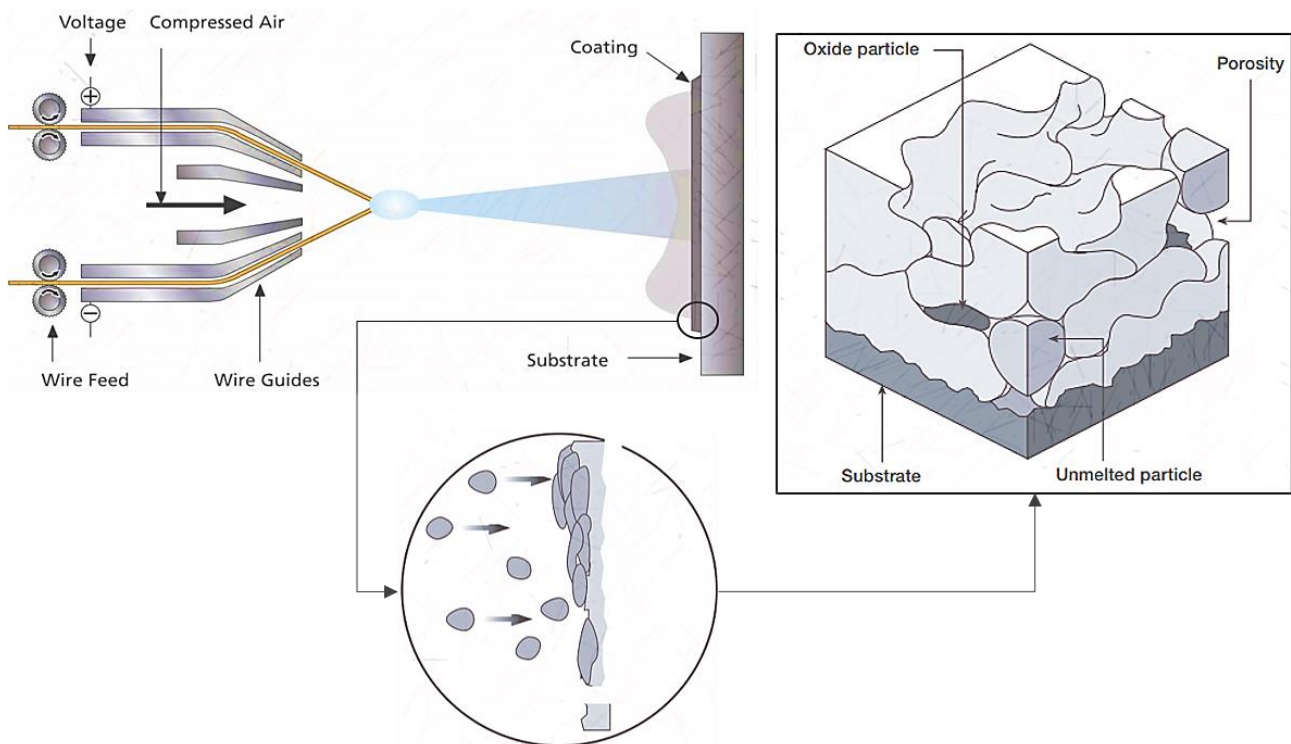
Figure 2 Principle of thermal spraying [13].

2.1.1 Coating Function

Corrosion protection is usually provided by applying a dense coating that act as a barrier against the corrosive environment, preventing it to reach the surface of the protected substrate and thereby reduce or eliminate corrosion. In the past, conventional organic coatings (paint) were mainly used due to low initial cost compared to thermal sprayed coatings (TSCs). However, corrosion progression from coating defects cause by transportation, handling, installation or simple long-term material degradation will occur over time and repair and/or replacement is required. This contributes to an increased overall life-cycle cost of the structure. Studies have shown that the long-term benefits often outweigh the initial higher cost of TSCs, making it cost-competitive with other coating systems [14]. This can be

seen from reports by the US Navy, who in 1978 evaluated the corrosion performance of TSA for steam valves at 515℃. After 8 years, 3000 steam valves showed no sign of corrosion damages, and the overall cost savings was estimated to 800,000 USD [15].

In the offshore industry, thermal spray coatings are increasingly used to mitigate corrosion on subsea pipelines and structures. Studies, either long-term field testing or laboratory testing have indicated that TSA coatings can provide adequate protection to steel substrates in all marine areas. This include marine atmosphere, splash and immersion zones [2]. According to Fischer et al, a 200 µm thermal sprayed aluminum coating exposed for splash-zone service, can achieve a lifetime in excess of 30 years, without maintenance [1].

In addition to give superior corrosion protection, thermally sprayed coatings are easy to apply, has low operating costs, no curing time, robust and can be used in many applications to reduce maintenance costs, improve performance and/or increase the lifetime [16]. The broad choice of coating materials gives high flexibility to solve specific performance problems. Due to the very wide selection of coating materials, TSCs for corrosion control are generally divided into three main groups: anodic coatings, cathodic coatings and neutral coatings.

Anodic coatings, where the coating has a more negative open circuit potential (OCP) relative to the substrate, provide cathodic protection to defects or parts where the coating is imperfect and the substrate is exposed to a corrosive medium. Aluminum and Zinc alloys are mainly used, however aluminum have shown to be the most effective metal for protection of steel in offshore structures [16].

For cathodic coatings, the major different is their behavior at such defects in the coating, as illustrated in Figure 3. At a defect in the cathodic coating, the substrate will be subjected to galvanic corrosion, in contrast to the anodic coating. Severe localized corrosion will often occur due to the area ratio between the cathodic coating and the anodic spot is often very high. Complete barrier of the coating is therefore more crucial for cathodic coatings compared to anodic coatings [10].
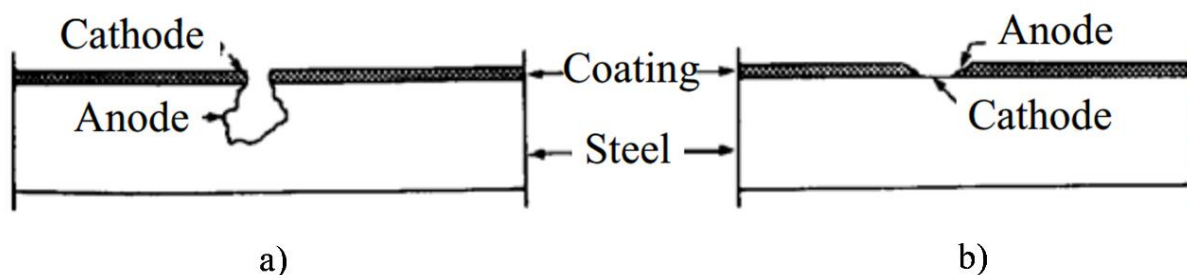
Figure 3 Localization of corrosion at a defect in a metal coating on steel, a) cathodic coating, b) anodic coating [17].

Neutral coatings like alumina and chromium oxide ceramics provides excellent corrosion protection in most cases by acting as a barrier, preventing exposure of the substrate. A damage in the coating will in general not accelerate nor deaccelerate the corrosion rate of the substrate, meaning that an exposed area of the substrate will corrode in the rate of its open circuit corrosion potential. Sealing of the coating is recommended to avoid the corrosive medium to penetrate through the pores of the coating, which can reduce adhesion between the coating and the substrate, causing coating separation [16].

2.1.2 Surface Preparation

Surface preparation is of absolute importance in order for the coating to perform to its designed expectation. Usually two stages are implemented in this process: surface degreasing and surface roughening [10]. Surface degreasing is achieved by applying solvents (e.g. Acetone or Methyl ethylene ketone) in order to remove all contaminations on the substrate such as oil, grease, paint, rust, scale and moisture. Any contaminations between the coating and substrate will reduce metal-to-metal contact at the interface, due to interlocking with the contamination and not the substrate directly. This will contribute to a coating with poor adhesion.

After degreasing, surface roughening is the most critical step to ensure good coating adhesion [10]. Dry abrasive grit blasting is the most used surface roughening technique. Roughening provides an increased surface area for particles-to-substrate contact, increase possibilities for mechanical interlocking and metallurgical interactions. Different types of surface preparations can be selected depending on the conditions of the substrate and coating system. Due to the major importance of these two parameters in order to achieve acceptable adhesion, standards exists. In NORSOK standard M-501, it specifies that surface roughness and cleanliness shall be in according to respectively ISO 8503 and ISO 8501-1 [18].

For TSA coatings used for the Norwegian oil and gas industry, the steel surface shall be pre-treated according to coating system no.2 in NORSOK M-501. The cleanliness of the substrate surface should be graded Sa 2½, meaning that the surface should be very thoroughly blast cleaned and free from any contamination viewed with the naked eye. The roughness of the substrate should be of Grade Medium G (50 µm to 85 µm, Ry5), meaning abrasive grit and not abrasive shot should be used for the blast cleaning. Graded medium contribute to a surface topography where the average between the highest and lowest point is between 50 and 85 µm. The abrasives must be sharp angular and not become rounded after frequently used. Sand containing more than 1 % free SiO_2 (quarts) are not allowed to be used in Norway and the majorities of countries in Europe [11].

2.1.3 **Thermally Sprayed Aluminum**

Thermal sprayed aluminum (TSA) coatings are widely used in the offshore industry for protection of steel structures, risers, pipe components and ship. The most typically used aluminum alloys are pure aluminum (99.5% Al) or alloy of the 5000 series like AlMg5, which both are regarded as seawater resistance alloys [19]. The main reason for this is due to its electrochemical behavior to the substrate, as mentioned earlier, causing the coating to act as a sacrificial anode in case of any coating damages due to lower potential compared to most used materials offshore. This will protect the substrate from corrosion, but on the other hand increase the deterioration rate of the coating. TSCs consisting of a mix between Zinc and Aluminum, 85% Zn – 15% Al are also widely used. The zinc content increases the galvanic effect of the coating whereas Al gives a less-reactive barrier layer. However, this is not optimal for splash-zone conditions due the high consumption rate leading to a rapid breakdown of the coating. In order to achieve good protection, properties like adhesion, surface preparation, porosity and oxide content are of major importance [20].

Adhesion between the coating and the substrate material, in addition to cohesion between the deposited particles are of crucial importance when it comes to the mechanically performance of the coating [20]. The basic bonding mechanisms for thermal spray coatings can be categorized into three groups: Mechanically interlocking, chemical-metallurgical and physical forces. Mechanically interlocking are of most importance for TSA. When the accelerated heated particles hits the substrate surface in the forms of splats, rapid cooling and shrinking of the particles occurs, resulting in interlocking between the coating and the rough substrate surface. In some cases, the velocity and heat from the particles are transferred to the substrate, causing micro-welding or atomic diffusion between the coating and the substrate. This type of bonding is called chemical-metallurgical bonding, and contributes to the highest adhesion strength between the coating and the substrate. The third mechanism is the least important bonding, and consist of weak Van-der-Waals forces (inter-atomic attraction within the metal) [20].

Although the use of TSA have demonstrated excellent performance under highly corrosive environment with a maintenance free period for up to 30 years, incidence of coating failure due to blistering have been recorded [21]. Blistering will reduce the lifetime of the coating considerably compared to the coating dissolution rate, and have shown to increase in occurrence with increased temperature [2]. High adhesion to the substrate is of great importance in order to reduce the possibilities for blistering. In addition, the ratio of porosity in the coating may influence the degree of blistering [21]. The higher porosity will contribute to an increased permeability of the coating, which may cause formation of corrosion products at the coating-substrate interface. This creates internal stresses in the coating and blistering may occur. The porosity may be eliminated by increasing the coating thickness but to thick coating may give poor adhesion to the substrate due to thermal expansion mismatch, and have shown to increase blister sizes on Al/Zn alloy coatings immersed in

seawater [5, 21]. It's therefore recommended to apply an organic sealer on top of the TSA, which have shown to prevent blistering [2, 5].

In mild environments, TSA are commonly used without a sealer. Self-sealing will occur to some extend by corrosion products filling the pores, but this process may take some time. Therefore, due to the porous nature of thermal spray coatings necessitates the use of organic sealant for different applications when exposed to harsh environments such as marine atmosphere and/or saltwater immersion.

According to NORSOK M-503, metal coatings shall be sealed or over-coated as specified. The selected sealant shall penetrate and fill pores and micro cracks in the coating structure, and shall be applied until absorption is completed. A low viscosity sealant ought to be used in order to achieve full and deep penetration without adding thickness to the coating. To ensure a smooth surface with little to no contamination which will further reduce the corrosion rate, the sealer should be applied as soon as possible after application of the TSA [6, 18].

The most commonly used sealers are silicon, vinyl or epoxy based, where the silicone based have proven most adequate in immersion and splash-zone conditions at both ambient and high temperature, up to 480℃. In addition, the use of a sealer have shown to prevent blistering

The primary function of the sealer is to prevent corrosion degradation of the substrate material by enhancing the barrier effect of the coating, preventing the corrosive medium from penetrating the coating and attacking the coating/substrate interface [10]. In addition, the use of a silicone sealer have shown to extend the life of the coating by reducing the free corrosion rate of the coating by a factor of two or three at OCP or lower. At higher potential, the corrosion rate is not affected [4]. Studies conducted by SINTEF showed that the corrosion rate for a sealed TSA surface (99.5%Al and AlMg5) are typically in the order of 1 micrometer/year after 11 months of exposure. The experiment was performed at nearly stagnant seawater conditions at low temperature (9-12℃). Increased flowrate and/or temperature will influence the corrosion rate, as will be further discussed in section 2.2.4.

For applications where TSA is used without separate sacrificial anodes, a high anodic activity is desirable. Holidays or damages in the coating exposing the steel substrate must hence be protected from the anodic current of the TSA coating. Sealing of the coating will reduce the cathodic current demand in addition to reduce the current output under anodic polarization. The reduced anodic capability have shown to be sufficient in order to achieve cathodic polarization of holidays or damaged areas. The sealer will reduce unnecessary consumption of the TSA-coating, and thereby enhance the service life of the coating [19]. For the Hutton tension leg platform, Thomasson calculated that a 4.8% coating damage could be protected by a 200 μm thick TSA coating with a current output of 3.0 Ah/cm^3 for 30 years. A cathodic protection current demand of 60 mA/m^2 for bar steel surface was used in his

calculation. This is a rather conservative values of the carbon steel surface as the cathodic current demand for a damaged area should be lower on a TSA-coating due to an effective polarization, causing formation of calcareous deposits. However, according to DNV (Det Norske Veritas) the mean design current density under similar conditions is 90 mA/m^2 [7].With this design, a maximum coating damage of 2.5 % can be sustained, which due to the good impact resistance and excellent adhesion for TSA-coatings should be possible to achieve [19].

Table 1 Maximum coating damage for flame sprayed coatings, current output 3.0 Ah/cm^3 with 10 to 90 mA/m^2 current demand for 30 years' service life [19].

CP current demand in damage areas [mA/m^2]	Max coating damage [%]
10	22.8
20*	11.4
30	7.6
40**	5.7
50	4.6
60	4.8
70	3.2
80	2.8
90***	2.5

*	Expected current demand on a hot surface (60-80℃)
**	Expected current demand on a cold surface
***	DNV design current demand for bare steel at ambient temperature (depth 100-300m)

2.2 **Corrosion Mechanisms for Aluminum**

Aluminum has been used in marine applications for many years due to its corrosion resistant properties and the strength-to-weight ratio. In particular, Al-Mg (5000 series) and Al-Mg-Si (6000 series) are widely used. Higher strength alloys in the 2000 and 7000 series are mostly used in aerospace applications. These are stronger but have shown poor performance in marine environments due to galvanic reaction with alloyed copper. A general definition of the term corrosion according to DIN 50900 is:

> "*Corrosion is the reaction of a metal with its environment that leads to a measurable change of the material and can impair the function of a part or of a system*"

When a metal like aluminum is immersed in an electrolyte, i.e. water, an electro chemical reactions takes place. Detachment of metal ions into the electrolyte will occur according to Equation (2.1) or Equation (2.2) if exposed to a more alkaline electrolyte, leaving the material surface negative charged. The released electrons will flow through the metal to the cathode region where reduction reaction will take place at the surface, consuming the negative charge electrons, either by oxygen reduction or hydrogen evolution according to Equation (2.3) and (2.4), respectively. The oxidation and reduction reactions are together called charge-transfer reactions as there is a flow of current between the cathode and anode sites. Continuously replacing the water will result in continuously metal dissolution as it will not reach the equilibrium potential.

$$Al \rightarrow Al^{3+} + 3e^- \tag{2.1}$$
$$Al + 4OH^- \rightarrow Al(OH)_4^- + 3e^- \tag{2.2}$$
$$O_2 + 2H_2O + 4e^- \rightarrow 4OH^- \tag{2.3}$$
$$2H_2O + 2e^- \rightarrow H_2 + 2OH^- \tag{2.4}$$
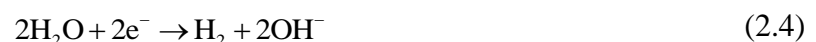
The main reason for the exceptional corrosion properties for many aluminum alloys is due to its passivating abilities. When aluminum is exposed to an oxidizing medium, a thin oxide film (Al_2O_3) forms immediately at the surface according to Equation (2.5). The oxide layer will immediately recover (self-healing) after damaged by for example mechanical impact. In contrary to the passivation of an active-passive metal like steel, the oxidation of aluminum will occur whether oxygen is dissolved in the electrolyte or not. This is done by splitting the water molecules releasing hydrogen, Equation (2.4), which again can be used as an energy source [22].

$$3Al^{3+} + 3H_2O \rightarrow Al_2O_3 + 6H^+ + 6e^- \tag{2.5}$$
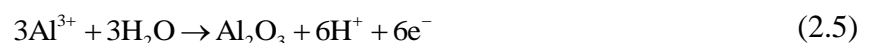
The aluminum oxide is an amphoteric compound, meaning it increases its solubility with increased acid or alkalinity. Based on the Pourbaix diagram for pure aluminum in seawater, the oxide is stable with a pH-value in the area of 2.5-4.3 and a potential greater than -1.7 mV$_{SHE}$, Figure 4. Lower potential will move us into the immune region depending on the pH, hence no corrosion will take place. However, studies have shown that aluminum practically does not have an immune region due to the formation of aluminum hydrides which destabilizes the oxide layer [22]. From this point of view, aluminum should theoretically not be suited for seawater exposure, as the pH usually is around 8.2. Nevertheless, some alloys are regarded as seawater resistant due to alloying elements. Figure 4 shows the potential-pH diagram for alloy 5086 in seawater. The diagram is based on experiments, and shows how alloying elements like Mn and Mg increases the passive region by preventing formation of Fe$_3$Al-particles compared to pure aluminum, making these alloys well suited for seawater applications where the pH is around 8.2 and the potential is between -0.85 and -1.2 mV$_{SCE}$ [23].
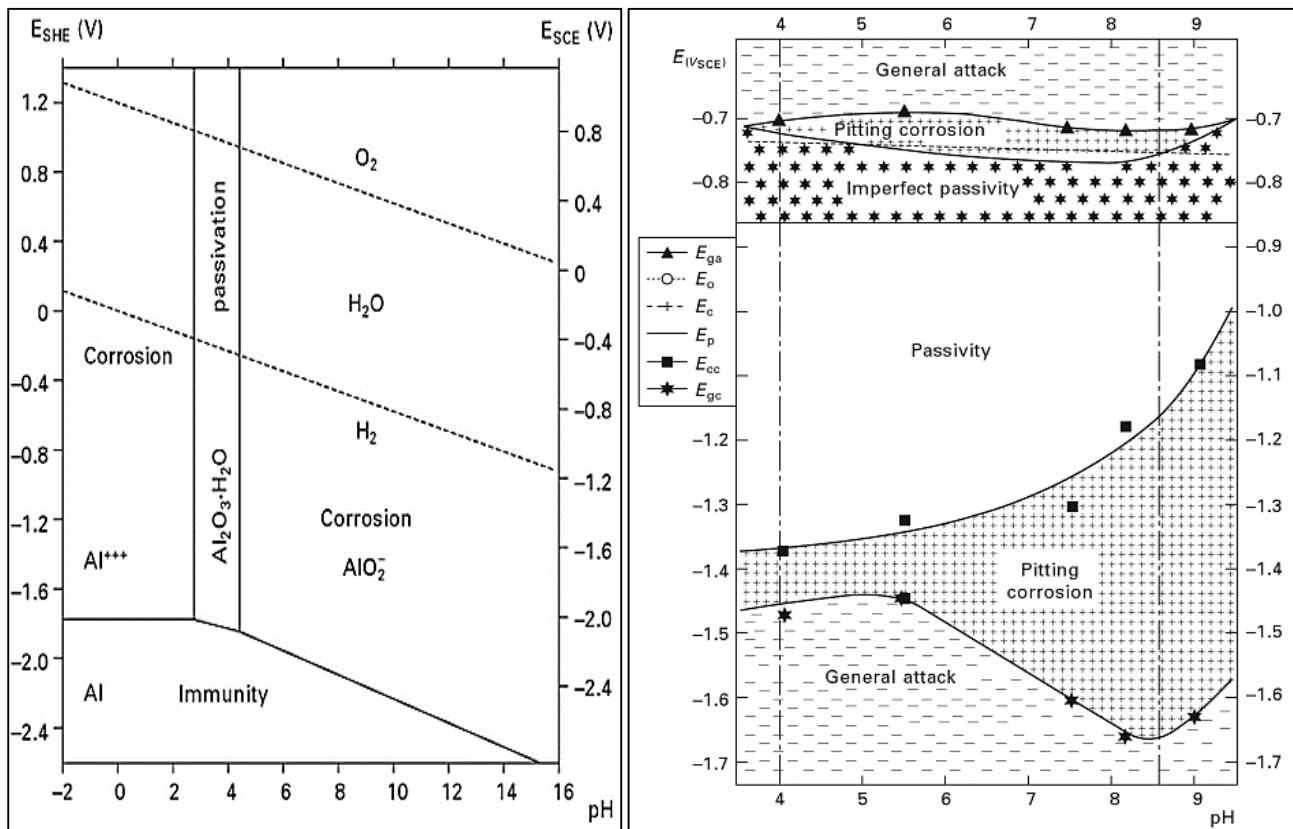
Figure 4 From left, Pourbaix diagram for pure aluminum in seawater and potential-pH diagram for aluminum alloy 5086 in a chloride solution (experimental) [23].

A study done by Reinhart and Jenkin where 60 different alloys were submerged in the Pacific Ocean for 189 days, showed that the corrosion rate of 6061-T6 was less than 0.0762 mm/year [24]. He further conclude that the corrosion rate calculated from weight loss are meaningless when it comes to aluminum. This is because aluminum corrode mainly by pitting and crevice corrosion making the severity of the corrosion much higher than estimated by the weight loss method.

The mechanism by which aluminum corrodes depends on environmental factor such as pH level, presence of aggressive species such as chloride ions and potential level. Uniform corrosion of the aluminum surface can only take place in highly aggressive environments where the oxide layer is unstable, meaning in both acidic and alkaline environments. From Figure 5, the corrosion rate of aluminum as a function of pH is drawn, showing that the oxide is highly sensitive to alkaline environments. Uniform corrosion occurs under, e.g. cathodic polarization. Increased reduction reactions promotes accumulation of OH⁻ ions adjacent to the surface causing a chemical dissolution of the oxide layer according to Equation (2.6) [25]. Thus, the corrosion attack is spread evenly on the surface making it easier to detect. This is not the case for pitting corrosion, making it a more dangerous form of corrosion, and is the most common corrosion mechanism for active-passive materials [19].

$$Al(OH)_3 + OH^- \rightarrow Al(OH)_4^- \tag{2.6}$$
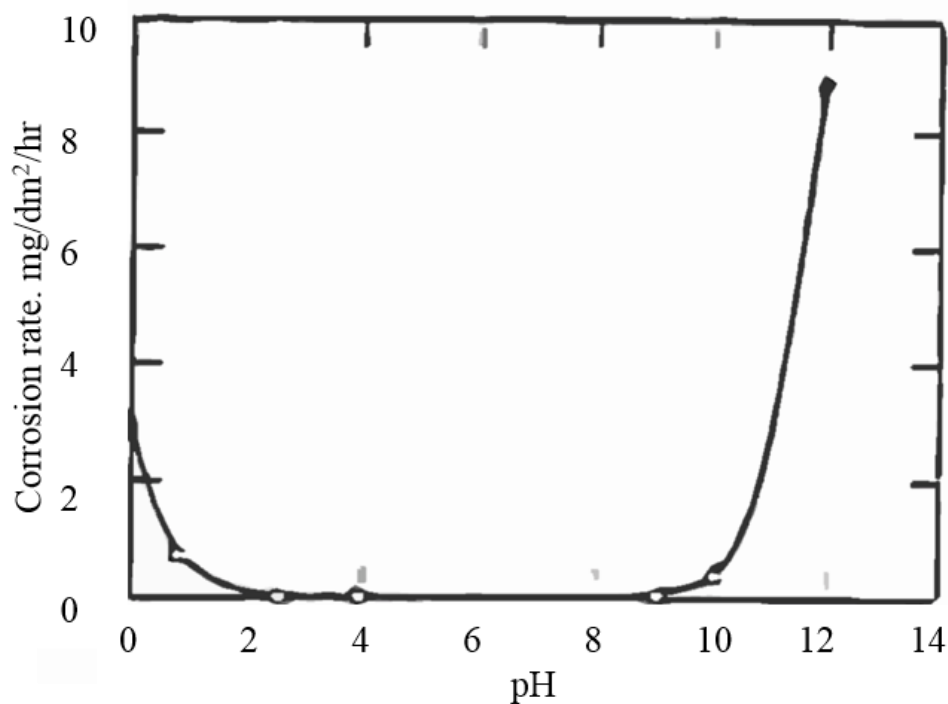
Figure 5 The corrosion rate as a function of pH [19].

15

2.2.1 **Pitting Corrosion**

The most common type of corrosion for aluminum alloys is in the form of pitting corrosion due to the passive film and intermetallic particles from alloying elements like iron and copper. The potential different between e.g. $FeAl_3$ and the aluminum matrix is in the order of 1.2 V and will act as a site for reduction reactions [26]. At these sites, flaws may exist in the oxide layer in addition to potential differences between the particles and the matrix, which may cause nucleation and growth of pits [27]. This is a much more dangerous form of corrosion compared to uniform corrosion because it's difficult to detect, predict and causes a rapid degradation of the metal thickness in localized areas due to high corrosion rate. Crack initiation and reduced mechanical strength can occur in addition to wall penetration causing leakage of gas or liquid. Knowing the extent of pitting corrosion is necessary to predict the life time of an application and choosing the most resistance material. Figure 6 illustrate the growth of pits around an intermetallic particle.
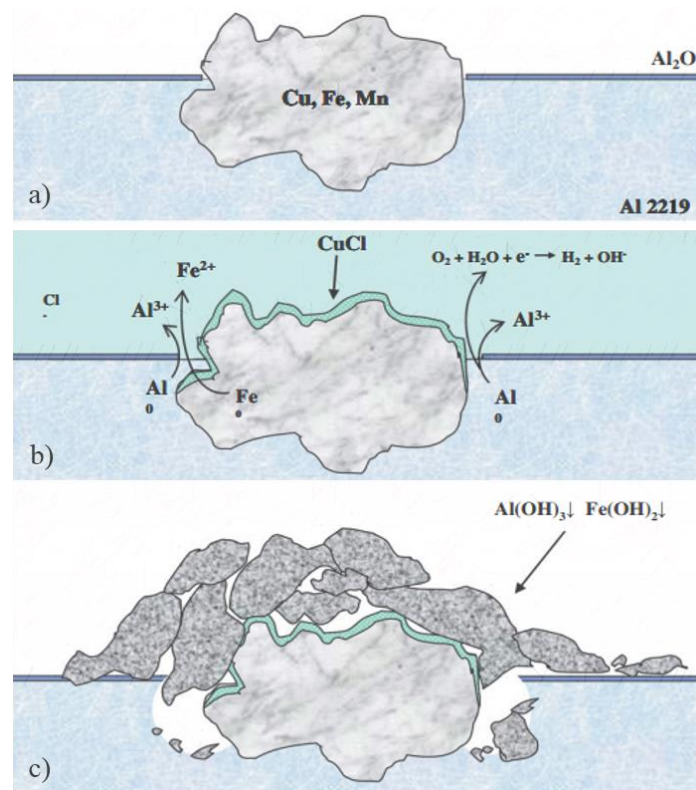
Figure 6 Illustration of (a) an intermetallic particle covered by an oxide layer, (b) corrosion process when immersed in seawater and (c) corrosion deposits after long exposure time [28].

The mechanism for pit initiation is not fully understood, and many theories exists. In general it is said that the pits initiates where the oxide layer is weak due to mechanical damage or around intermetallic particles were the film is weaker [23]. Due to aggressive chloride anions or other halide ions in addition to have an electrical potential above a critical value, pitting corrosion will occur. The transport of metal ions increases in line with the increased concentration of chloride ions in the film, resulting in deep

localized pits in the metal. The large cathode area outside the pit compared to the localized anode causes aggressive corrosion.

Propagation of the pit is the same mechanism as for the formation of crevice corrosion. The anode reaction takes place in the bottom of the pit where aluminum oxidizes to aluminum ions, Figure 7. Outside the pit, reduction of oxygen and/or hydrogen evolution occurs around cathodic intermetallic particles, resulting in an increased pH outside (alkaline). Charge balance is needed to maintain equilibrium in the pit, hence chloride ions migrates into the pit causing metal hydrolyses. The pH decreases in the pit as a result of the formation of hydrochloride acid, which accelerate the propagation rate of the pit. The alkaline environment outside the pit destabilizes the aluminum oxide layer, and etching of the aluminum matrix initiates. Around the mouth of the pit, solid aluminum oxide will form and with time the pit will gradually close and thereby hinder further exchange of ions, reducing the corrosion rate [29]. For aluminum alloys AlMg, AlMgSi and AlMgMn submerged in seawater, the pit depth is estimated to be only 0.2-1 mm [30]. A study performed in 1950, 25 different waters in Canada were used for evaluating the pitting corrosion rate of aluminum alloys [31]. The result showed that the deepening of the pit follows Equation (2.7).
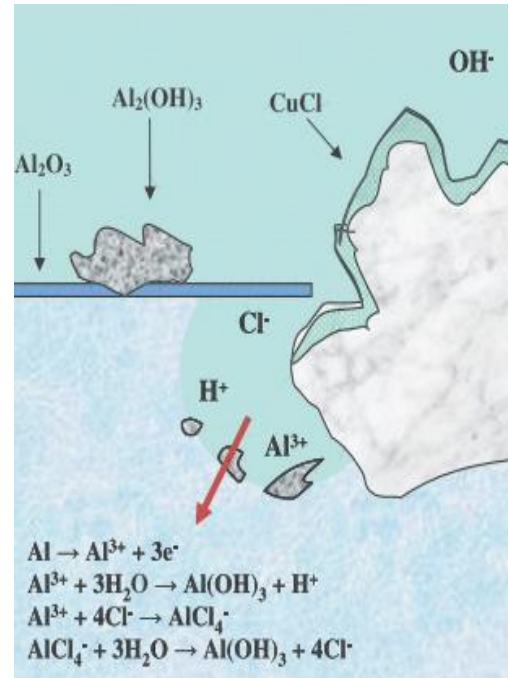
Figure 7 Reactions to maintain equilibrium inside the pit [27].

$$d = K\sqrt[3]{t} \tag{2.7}$$

Where:

- d - The depth of the pit
- t - The time
- K - Constant which is dependent on the alloy and service conditions

The equation shows that the rate of pitting corrosion, in most cases, decreases with time. The life time of structures can therefore be several decades long, making the alloy well suited as a construction material in many environments.

TSA and solid aluminum behave differently in some degree when it comes to the corrosion behavior. This is related to the surface structure and topography of the material in addition to the thickness of

the oxide layer [32]. As mentioned for thermal sprayed process, the oxidation properties of the coating is increased compared to solid aluminum which is beneficial due to improved corrosion resistance. The most important difference is the dissolution rate of the oxide layer, whereas the oxide on TSA dissolves slower than on solid aluminum. In addition, the oxide layer is not affected to the same extend by the water flow rate [32].

Like seen on solid aluminum alloys, the initial corrosion rate for TSA is relatively high due to dissolution of the oxide layer, increasing exposure of intermetallic particles causing localized pitting corrosion. Over time, detachment of the particles will occur, removing impurities from the surface and re-passivation of the pits by corrosion products, hence the corrosion rate decreases. Another contribution to this effect on TSA is that corrosion products tend to fill up the pores and thereby inhibits further corrosion. This can be seen on Figure 8, where the potential of flame sprayed aluminum exposed to seawater initially drops from -900 mV$_{SCE}$ to below -1050 mV$_{SCE}$. Over time the potential gradually increases as the corrosion rate decreases, and reaches its steady state corrosion rate and open circuit potential, OCP [19].
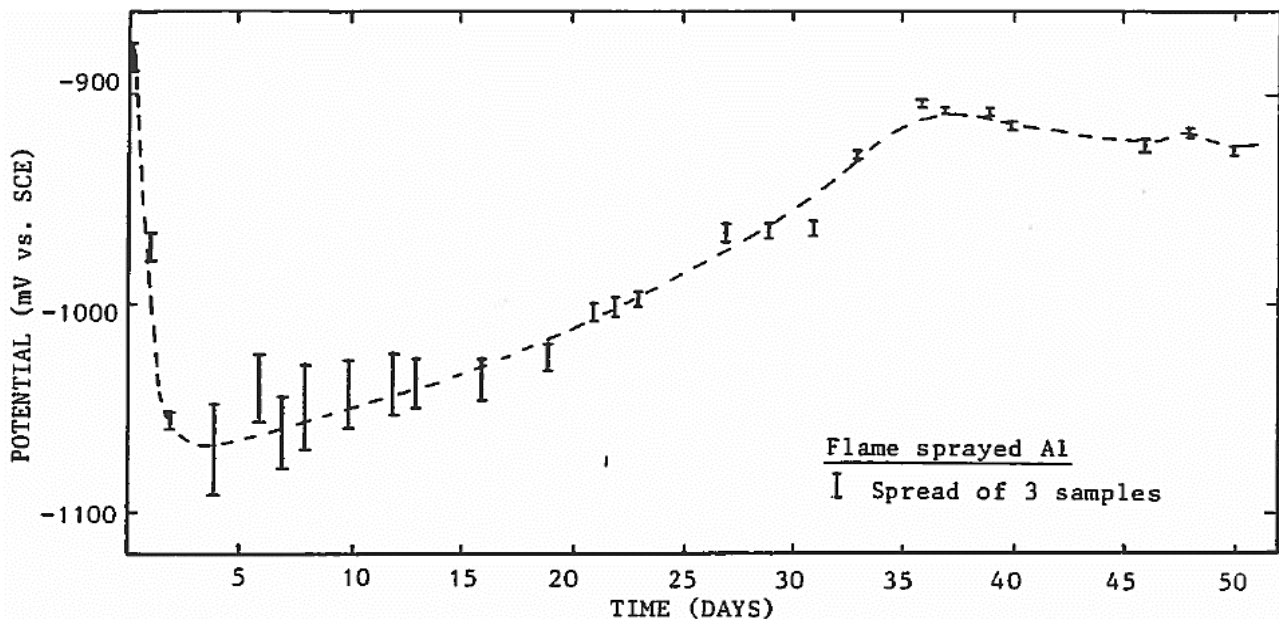
Figure 8 Corrosion potential of flame sprayed aluminum over time [19].

18

2.2.2 **Effect of alloying elements and spraying method**

The OCP is influenced by the alloying elements, as described in section 2.2.1, in addition to the applied method used for the TSA coating. Gartland and Eggen measured the OCP for different TSA coatings, applied by arc -and flame sprayed technique over a period of 11 moths [4]. In addition, some of the coatings were sealed to distinguish its affect, Table 2. The result showed that both the spraying method used and applied sealer had little influence on the corrosion potential of the coatings.

Table 2 Steady state corrosion potential (OCP) after 11 months for different TSA coatings, sealed and un-sealed.

Coating material	Potential [$mV_{Ag/AgCl}$]
Arc sprayed Al	-950
Arc sprayed Al sealed	-940
Flame sprayed Al	-910
Flame sprayed Al sealed	-950
Arc sprayed AlMg	-995
Arc sprayed AlMg sealed	-970
Flame sprayed AlMg	-1000
Flame Sprayed AlMg sealed	-1010
Arc Sprayed ZnAl	-995
Arc Sprayed ZnAl sealed	-920
Flame Sprayed ZnAl	-980
Flame Sprayed ZnAl sealed	-920

2.2.3 **Effect of Temperature**

Most metals have shown to have an increased corrosion rate with increased temperature, as the underlying chemical reactions increases at high temperatures. The general effect of increasing the seawater temperature for TSA is that the corrosion potential decreased, and at temperature above 40℃ the critical pitting potential decreases substantial with increased temperature [19].

Fischer et al. studied this effect on steel pipe spools coated with TSA, exposed to seawater at ambient temperature and at 70 and 100℃. The initial potential was severely lower at higher temperature, which indicates high corrosion rates, see Table 3. However, the potential increased with time and stabilized at a value around −950 mV Ag/AgCl, showing that at high temperature the corrosion rate may be high for a short period before it's reduced to a value close to what is expected at low temperatures [1, 5].

Table 3 Corrosion Potential of TSA as a Function of Temperature[1].

Temperature [°C]	Potential [mV$_{Ag/AgCl}$]		
	Initial (day 1-2)	1 Month	3 Months
8	-800	-1000	
70	-1040	-970	-945
100	-1115	-950	-950

Another effect on the corrosion behavior for aluminum at elevated temperatures, is the pH-range at which the oxide layer is stable. With increasing temperatures, the passive zone in the Pourbaix diagram shifts towards lower pH, meaning the oxide layer will be less stable in alkaline and neutral environments, hence the danger of corrosion increases [22]. This effect is illustrated in Figure 9.
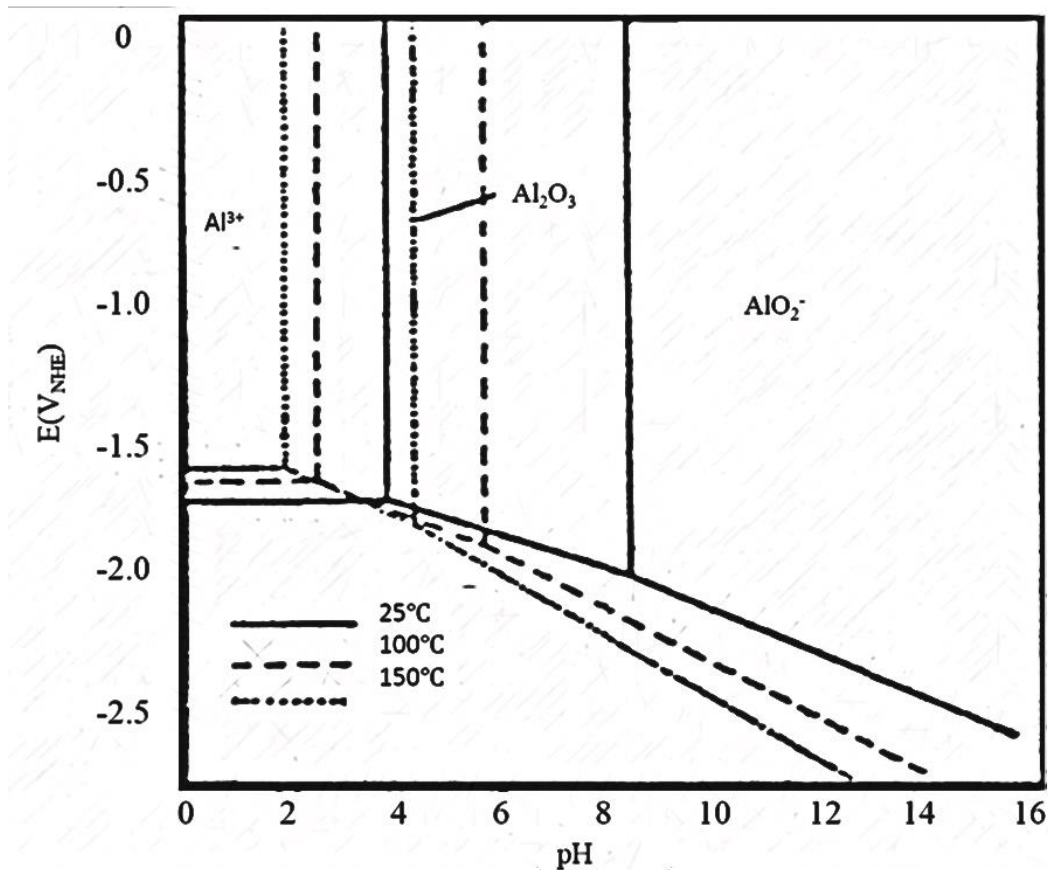
Figure 9 Effect of temperature on the passivity of aluminum in water [22]

2.2.4 **Effect of Seawater Flowrate**

Corrosion of aluminum is, as mentioned, dominated by pitting corrosion under stagnant and laminar flow conditions. Increasing flowrate may cause uniform dissolution of the oxide layer, reducing pitting corrosion with increased uniform corrosion. A test carried out in the Trondheimsfjord by SINTEF showed that increasing the flowrate from 8 cm/s to 1 m/s contributed to an increased uniform corrosion from 0.01 mm/year to 0.06 mm/year. Since erosion-corrosion can only occur in multiphase flow systems, the significant increase in the corrosion rate (if not cavitation), is caused by the transition from laminar to turbulent flow. In this regime, the corrosion rate cannot be reduced by cathodic protection due to that the corrosion process is a chemical process controlled by the dissolution of the oxide film and not an electrochemical process [22, 33]. This is illustrated in Table 4, adapted from the SINTEF study, where the cathodic current density requirements were measured at stagnant conditions as well as at flowrate of 0.1 m/s. For solid aluminum it's expected that the potential decreases with 80 mV for each tenfold increase in the flow rate [19].

Table 4 Cathodic current density requirement at -1038 $mV_{Ag/AgCl}$ after 7 months exposure [19].

Coating	Water flow	
	Nearly stagnant	0.1 m/s
Arc Sprayed Al	8 mA/m^2	0.60 mA/m^2
Arc Sprayed AlMg	1 mA/m^2	0.19 mA/m^2
Flame Sprayed ZnAl	7.5 mA/m^2	5.05 mA/m^2

The self-corrosion rate of TSA under high flowrate was studied by C. Holager. Carbon steel specimens coated with TSA (AlMg5) and solid AlMg5 specimens were placed in a flowing channel. Natural seawater was continuously pumped through the channel at a velocity of 2.5-3.6 m/s and with a temperature ranging from 8.5-10.5℃. Both freely exposed and polarized specimens were test, during which the corrosion potentials and currents were continuously measured. Specimens were polarized to −1050 $mV_{Ag/AgCl}$. Results obtained by the weight loss method showed a significant increase in the corrosion rate for the TSA specimens, which was up to one order of magnitude higher than the solid AlMg5. The same was observed on the polarized specimens. The differences was believed to be caused by either an electrochemical activation of the passive surface on the TSA by an unknown additive, which increased both anodic and cathodic processes on its surface, or cavitation erosion due the rough surface, or both mechanisms acting together [33].

2.2.5 Electrochemical corrosion rate measurements

Measuring the corrosion rate of freely exposed thermally sprayed surfaces cannot be conducted by the weight loss method. This is because the porous nature of the coating, which in the beginning of immersion, will to some extend be filled up by corrosion products, thus the sample may in fact experience a weight gain instead of weight loss [19]. Therefore, for this experiment, electrochemical methods like obtaining the polarization curves and linear polarization resistance measurements (LPR) have been conducted to evaluate the corrosion rate for the TSA coating.

In order to obtain the polarization curves and hence evaluate the corrosion rate of the coating, potentiodynamic polarization can be conducted. By moving the potential of the metal, also called the working electrode (WE), away from its OCP in a stepwise approach, a net current will be applied from the counter electrode (CE) to the working electrode in order to hold the potential. The change in the electrode potential will change the rate of electrochemical reactions at the metal surface by altering the rate of charge transfer. A reference electrode (RE) that is stable under the test conditions is used to monitor and evaluate the potential at the WE. By measuring the net current flow and the potential, the polarization curves can be plotted as E vs. log i (Evans diagram), and the Overvoltage curves can be obtained [17]. Figure 10 shows typical polarization- and overvoltage curves.
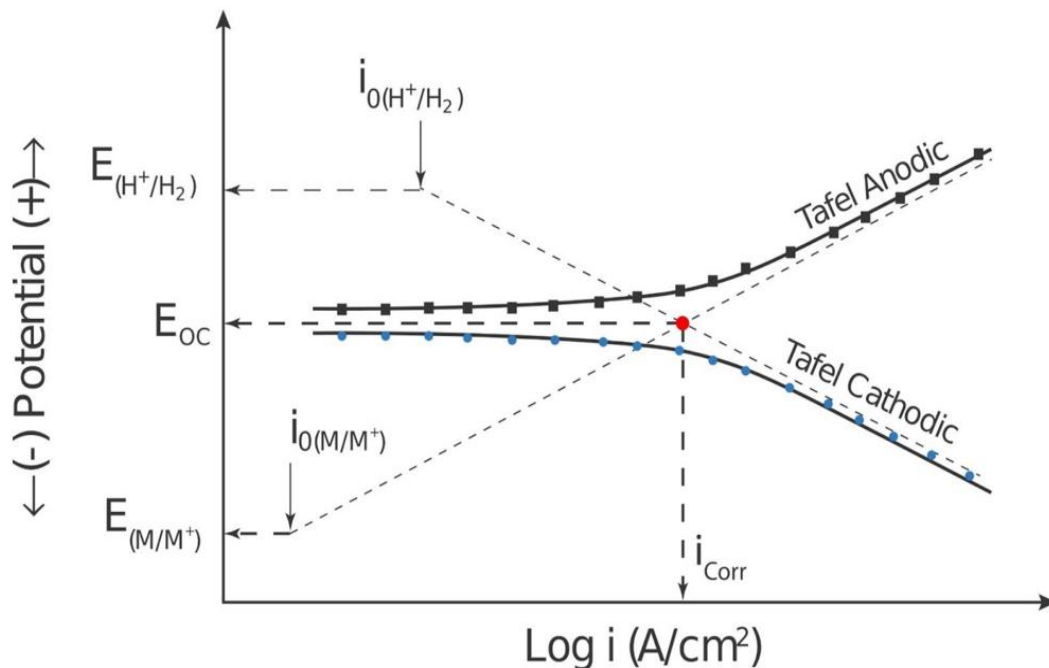
Figure 10 Polarization curves and Overvoltage Curves (Tafel lines) [34].

The Overvoltage curves, also called Tafel lines, are asymptotes of the polarization curves, and can be found by extrapolate the linear part of the polarization curves. The Tafel behavior generally starts at a

potential greater or less than 50 mV from OCP [34]. The intersection[2] between the anodic and cathodic overvoltage curves gives the corrosion current density (i_{corr}) of the WE. From the Tafel lines, the anodic and cathodic Tafel constants b_a and b_c, which are the slope of the overvoltage curves, can be found. These can be used to determine the corrosion rate in a much quicker approach by using the LPR method.

The LPR measurement is conducted by polarizing the material in a small range around the OCP ($\pm 10 - 25$ mV). As the potential is changed, a net current will as mentioned be induced and flow between the working -and counter electrode. Due to the fact that the relationship between the potential and the net current is approximately linear in a small range around the OCP, the corrosions rate can be calculated using the Stern-Geary's Equation (2.8) [17].

$$\frac{\Delta E}{\Delta I} = \frac{b_a \cdot |b_c|}{2.3 \cdot I_{corr} \cdot (b_a + |b_c|)} \tag{2.8}$$

By implementing the Tafel constants, obtained from the overvoltage curves, and the potential/current relationship found from the LPR measurement, the corrosion current (I_{corr}) can be calculated from Equation (2.8). The corrosion current density is given in A/m^2, and should be converted to mm/year for practical reasons. From Faraday's law the corrosion rate can be calculated according to Equation (2.9).

$$CR = K \cdot \frac{i_{corr} \cdot M}{n \cdot \rho} \tag{2.9}$$

Where:

CR	-	Corrosion Rate	$\left[\text{mm / year}\right]$
K	-	3268	-
i_{corr}	-	Corrosion Current	$\left[\text{A / cm}^2\right]$
M	-	Atomic weight of the metal	$\left[\text{g / mol}\right]$
n	-	Electrons exchanged	-
ρ	-	Density	$\left[\text{g / cm}^3\right]$

---

[2] The anodic overvoltage curves usually exhibits a nonlinear behavior causing the anodic and cathodic extrapolations to not intersect at the same point at OCP. In that case, the cathodic curve shall be used to determine i_{corr}.

2.3 **Cathodic Protection**

Cathodic protection (CP) is a well-established and effective method in order to avoid degradation of a structure caused by corrosion. The method was first introduced in 1824 by Sir Humphrey Davy, and is today widely used in marine applications for protection of immersed metallic structures, especially for subsea applications. There are two methods of achieving CP, either by the use of an impressed current CP system or by sacrificial anodes [17]. Both are illustrated in Figure 11 below.
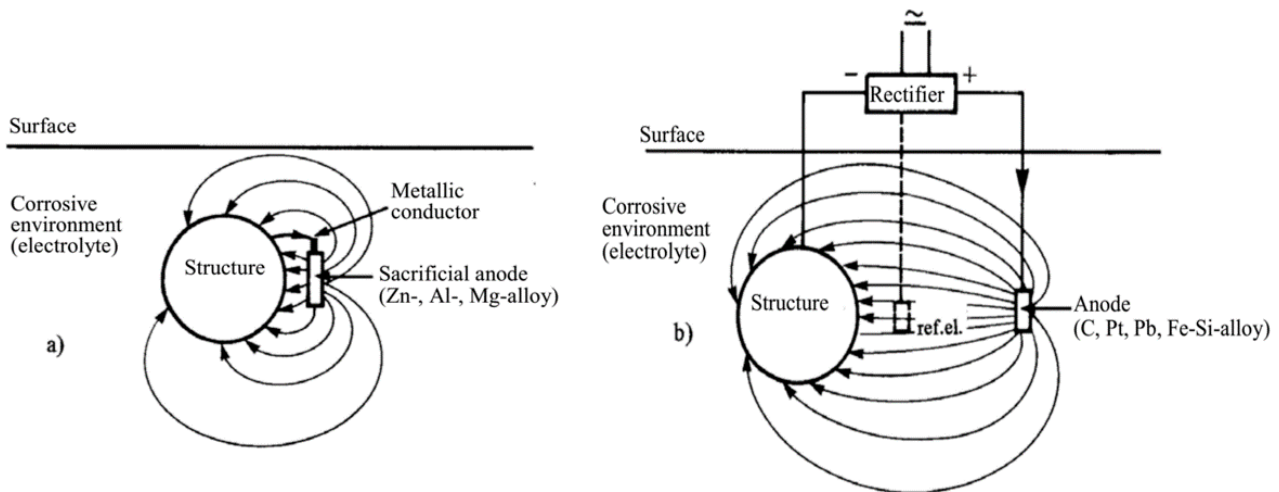
Figure 11 Cathodic protection by a) sacrificial anodes or b) impressed current system [17].

2.3.1 **Sacrificial Anode – Al-Zn-In**

For permanently installed offshore structure, CP by use of sacrificial anodes are usually preferred due to its simplicity, robustness, no external current needed in addition to reduced inspections related to the anode consumption rate [7]. Aluminum alloys are the most used sacrificial anodes in seawater due to their high current conductivity and higher electrochemical capacity compared to zinc anodes. Their low weight is very favorable when long service life is needed. However, due to the passivating abilities of pure aluminum which reduces contact between the metal and the environment, activating alloying elements are necessary in order to enhance its performance, hinder oxidation of the surface. The alloying elements that prevent the oxidation is Zn, Mg, Ga, In, Sn, Bi and Ti. In addition, some alloying elements contributes to a more fine-grained structure, leading to a more uniform metal loss, and some reduces the self-corrosion rate and increase the current yield [35]. Due to its toxicity, Hg elements are seldom used. Aluminum anodes with activating elements of Zn and In have shown excellent performance due to their great polarizabilities and are widely used for protection of subsea pipelines. Several, well-established recommended practices exist in order to design an effective CP system with Al-Zn-In anodes [7, 36, 37].

2.3.2 Effect of Alloying Elements

The Role of Indium

Indium is in general of high nobility and will contributes to cathodic shift in the pitting potential when small amount (i.e. ppm level) are added, which will reduce the passive region of the alloy. As a result, the surface will become more active as the oxide layer destabilizes. Also, the OCP increases in the cathodic direction when aluminum is alloyed by In or when In^{3+}-ions are added in a chloride containing electrolyte. This is explained by the higher dissolution rate and increased hydrogen evolution. However, as the OCP increases with increased amount of indium, the current efficiency decreases. An optimum content of In $(0.02 - 0.05 \%)$ must be selected in order to achieve good performance of the anode [38].

The activating process is illustrated in Figure 12. Indium will act as an anode in a galvanic cell with the oxide layer. Initially, active dissolution of the In-rich segregated phase will occur at a fast rate due to the big area differences (In-phase:Oxide layer). The dissolution continues until the oxide layer destabilizes, exposing the aluminum matrix. A new galvanic cell will arise with the aluminum matrix and the oxide layer, Al_2O_5, causing dissolution of the Al-matrix. The In-rich phase will then become a cathode, and hence stop dissolving. Over time, detachment of the In-rich segregate will occur as the aluminum matrix around continues to dissolve [38]. Only small amount of alloyed Indium is needed to activate the surface, as studies have shown that they segregate easily and enrich the surface. However, a synergy effect takes place between indium and chlorides so that an activation process only can occur in a chloride containing solution [39].
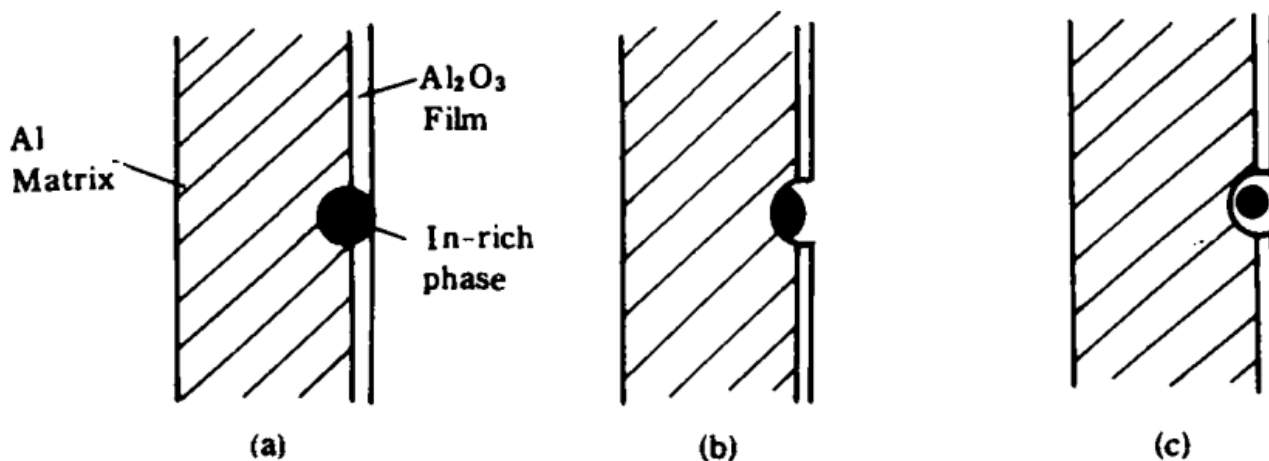
Figure 12 Activation process of In-rich segregated phase on aluminum anode [38].

The Role of Zinc

The role of Zinc as an alloyed element in Aluminum is not fully understood. However, it is believed that its affect lies in decreasing the reduction reactions at the surface, and that in small amounts it be beneficial against pitting corrosion [22], as it moves the pitting potential in the cathodic direction. The effect of Zinc-ions alone, in an electrolyte have little effect, but in combination with In-ions, a synergic interaction appears, illustrated by the potential-time plot in Figure 13. The authors, Breslin and Friery, proposed that the mechanism for this interaction is caused by a higher rate of cracking and rupture of the oxide layer as Zinc deposits on the surface. This was thought to be caused by the formation of $ZnAl_2O_4$ spinel, contributing to stress corrosion cracking of the oxide layer due to its higher molar volume. Further, accelerated deposition of Indium occurs in the exposing areas of bar aluminum, reducing the time of activation [39].
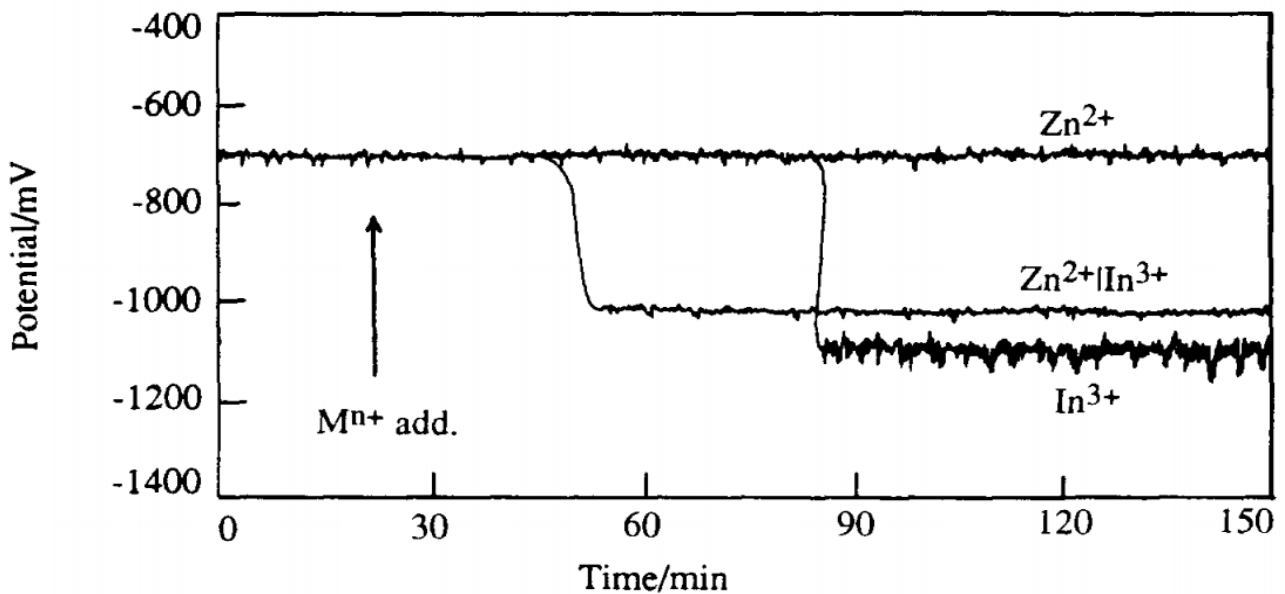
Figure 13 Open circuit potential-time plot for pure aluminum recorded in 0.5M NaCl solution on addition of 0.01 M $ZnSO_4$; 0.005 M $In_2(SO_4)_3$; 0.005 M $ZnSO_4$ and 0.0025 M $In_2(SO_4)_3$ solution following a 25-min immersion period. The time of activator addition is shown by the arrow. A more effective attack occurs when addition of Zn, destabilizes the oxide film [39].

2.3.3 Effect of Deep Water

As exploitation of offshore oil fields are rapidly moving into deeper water depths, greater than 300 meters, studies have been conducted to investigate the anodes behavior. Absent of oxygen may promote growth of sulphate-reducing bacteria which may influence the pH at the surface, and hence influence the electrochemical behavior of the anode material. In addition, the protective potential may increase due to the presence of sulphide, increasing the current density demand [40].

The electrochemical behavior of Al-Zn-In based anodes have been studied in natural seawater simulating deep ocean environments in order to understand the effect of increased hydrostatic pressure. The results suggested that the dissolution of the anodes are non-uniform at low temperature and that

the potential is 5-20 mV more positive at 50 atm. compared to 1 atm. In addition, the anode capacity were in the order of 7-10 % less at 50 atm. [41]. Similar tests were conducted with the use of Al-Zn-In-Ti anodes, showing that an increased amount of anode is needed at deep water environments, at least 22% [42].

2.3.4 Cathodic Protection of Steel

Low alloy steel are the most used engineering materials due to low cost and adequate mechanical and physical properties [43]. The disadvantage is that they have poor corrosion resistance in relatively mild service environments, thus good CP is essential for long term and safe operations subsea. For bare steel exposed to seawater, a potential of -800 mV$_{Ag/AgCl}$ is generally recommended to achieve full protection according to DNV-RP-B401. This is called the protection potential of the material, E$_P$. [7, 17].

In order to obtain this potential, an applied current density is required, which is influenced by the environmental conditions like temperature and water depth. The recommended mean current density requirement is listed in Table 5. The initial and final current density is higher due to lack of a protective oxide layer. But, under CP at -0.9 to -1.4 V$_{SCH}$, dissolved oxygen from seawater is reduced on the metal surface, producing hydroxide [44]. Increased pH adjacent to the steel surface contributes to the formation of calcareous deposits, which plays a crucial role for CP systems of steel in seawater. A dense calcareous layer is formed on the steel surface, reducing the diffusion rate of oxygen to the metal surface, and therefore reduced oxygen reaction, Equation (2.3). Hence, the corrosion rate of the steel surface is reduced which contributes to a reduced current density requirement needed from the anodes in order to protect the steel surface. This is why CP systems are often used in combination with organic coatings, which reduces the amount of anode needed [3]. In addition, it should be noted that for surfaces where the operating temperature exceeds 25℃, the current density shall be increased with 1 mA/m^2 for each ℃ above the recommended DNV standard [7].

Table 5 Recommended mean design current densities (A/m^2) for seawater exposed bare metal surfaces, as a function of depth and climatic region based on water temperature [7].

Depth [m]	Tropical (>20℃)	Sub-Tropical (12-20℃)	Temperate (7-11℃)	Arctic (<7℃)
0-30	0.070	0.080	0.100	0.120
>30-100	0.060	0.070	0.080	0.100
>100-300	0.070	0.080	0.090	0.110
>300	0.090	0.100	0.110	0.110

2.3.5 **Cathodic Protection of Aluminum**

For aluminum structures, the amount of anodes can be reduces substantially compared to carbon steel due to that the current demand is 10 times less for achieving full protection [26]. The main reason for this is because the cathodic reactions are localized at small areas around intermetallic particles whereas for steel it's dependent on the properties of the matrix. In other words, the whole steel surface is cathodic compared to only small intermetallic areas on the aluminum surface due to the protective oxide layer. This layer is an amphoteric oxide layer and is unstable in both acid and alkaline environments making cathodic protection different compared to when conducted on steel [23].

For steel, cathodic protection is performed by bringing the potential closer to the immune area, whereas for aluminum protection is achieved by increasing the potential into the passive region where the oxide layer is stable. This kind of protection is called anodic protection. In practice, this means that the corrosion rate of aluminum cannot be eliminated completely, but a significant reduction in the order of 80-90 % is possible.

The potential should in this case be less than the critical pitting potential at −0.85 V_{SCE}[3], but should not exceed −1.2 V_{SCE} due to formation of alkalis, which as mentioned will destabilize the oxide film [26]. These values are for alloy 5086, see Figure 4. The alloying elements will influence the critical pitting potential.

In the beginning of submerging the required current density of aluminum will increase due to dissolution of the oxide layer. More of the matrix will be exposed, increasing the corrosion rate. The increased corrosion of the matrix will expose more off the intermetallic particles (Fe, Cu) which are nobler than aluminum. The result is localized pitting corrosion around these particles, as described in section 2.2.1. Over time, detachment of the particles may occur, causing re-passivation of the pits by corrosion products, $Al(OH)_2$ and possible calcareous deposits [26]. The result is a reduction of cathodic and anodic reactions, which reduces the pH to a more neutral value and hence stabilizing the oxide layer. The oxide layer contribute to an exponential reduction of the current density requirement in order to achieve full protection of the material. See Figure 14 for a schematically description of the process.

At potentials higher than the pitting potential, pitting corrosion initiate and continue to grow according to equation 2.1. However, for TSA coatings the mass loss as a function of time is of more interest. P.O. Gartland polarized TSA (AlMg5) to −870 mV and −770 mV_{SCE}. The results showed that polarizing over the pitting potential, the corrosion rate increased from 5 μm/year to 200 μm/ year. This significant

---

[3] The potential against a saturated calomel electrode (SCE) can be converted to silver chloride electrode (Ag/AgCl) by adding +45 mV.

increase will rapid consume the coating, and in months exposing the substrate material [19]. Both over- and under protection must hence be avoided when CP is used for aluminum components or TSA coated surfaces.

In DNV-RP-B401 for CP design it states [7]:

> For aluminum components, or those coated with either aluminum or zinc, a design current density of 0.010 A/m2 is recommended for initial/final as well as mean values. For internally heated components, the design current density shall be increased by 0.0002 A/m2 for each °C that the metal /seawater is assumed to exceed 25°C.

TSA coatings have proven to provide long-term corrosion protection, both acting as a barrier and provide cathodic protection to bar steel exposed by damage to the coating under atmospheric conditions. However, for subsea systems, corrosion protection have typically been provide by the use of sacrificial anodes in combination with an organic coating in order to reduce the total anode mass. By using TSA as an alternative to organic coatings, studies have shown that the total anode mass needed to protect a structure covered by 90 % Al-based coating is less than 20 % than for a bare steel structure [4][17]. The current drainage by the coating is an important parameter, as lower drainage contributes to a reduced number of anodes needed for a full lifetime protection.
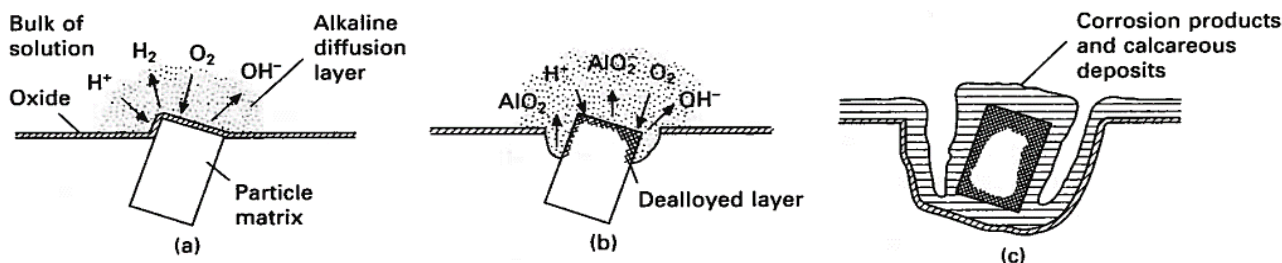
Figure 14 Schematic description of the mechanism of cathodic protection of aluminum alloys in seawater. (a) Development of alkaline diffusion layer. (b) Pitting corrosion around the intermetallic particles and (c) repassivation of the surface [23].

2.4 Calcareous Deposits

Under cathodic protection systems, the formation of calcareous deposits on the cathode is of great importance as it contributes significantly to the effectiveness of CP systems. It is generally believed that calcareous deposit are acting as a barrier to oxygen reduction, like an organic coating which electrically insulates the substrate, protecting the surface against corrosion, thus decreasing the current density (the anode consumption rate). In this chapter, the basic for calcareous formation will be presented, followed by the influence of environment.

2.4.1 **Formation**

During corrosion of iron and steel in seawater, the anodic dissolution is predominant supported by oxygen reduction at potential less negative than -950 mV$_{SCE}$, Equation (2.3). At potential more negative than -1100 mV$_{SCE}$, hydrogen evolution caused by the reduction of water molecules may also be present, Equation (2.4) [45]. This can be seen from the Pourbaix diagram in Figure 4, showing the cathodic reaction's equilibrium potential as a decreasing straight line with increased pH. Nevertheless, in both cases production of hydroxide occurs, increasing the pH adjacent to the polarized surface. The hydroxide ions contributes to increased concentration of carbonate ions at the surface interface, allowing inorganic deposition of calcium carbonate, magnesium hydroxide and small amounts of magnesium carbonate according to Equation (2.10), (2.11) and (2.12), respectively [46]. These solid products are known as calcareous deposits.

$$Ca^{2+} + HCO_3^- + OH^- \rightarrow CaCO_3 + H_2O \tag{2.10}$$
$$Mg^{2+} + 2OH^- \rightarrow Mg(OH)_2 \tag{2.11}$$
$$Mg^{2+} + HCO_3^- \rightarrow MgCO_3 + H_2O \tag{2.12}$$
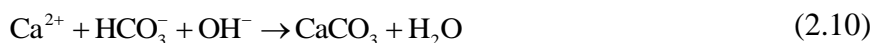
The formation of calcareous deposition is highly influenced by the level of alkalinity at the metal/seawater interface, which in turn is dependent on the applied potential and the flow conditions. Deposition generally forms at pH levels between 8 and 10 [47]. With increasing pH the growth and precipitation rate of $CaCO_3$, which is supersaturated in surface seawater, will increase. Deposition of $Mg(OH)_2$, which is unsaturated in seawater, will only occur at a pH higher than 9.5. Thus, for a freely exposed steel surface in seawater at a pH of approximately 8.2, $Mg(OH)_2$ will not depose at the surface. As that the pH adjacent to the steel surface gradually increases due to polarization, deposition of calcium carbonate should theoretically occur first followed by magnesium hydroxide. However, studies have shown that in the present of corrosion products, iron hydroxide, $Mg(OH)_2$ might precipitate together at a pH as low as 2.26 [45]. This is due to the kinetics for $Mg(OH)_2$ precipitates at a much faster rate than $CaCO_3$, forming a thin layer in the presence of corrosion, as illustrated in Figure 15 [48, 49]. Since the thickness of the layer only is in the micrometer range in addition to its level of porosity, it does not play a significantly roll in corrosion protection alone [44, 50].

Further, it has been shown that the formation of calcareous deposit varies as a linear function of Mg^{2+} concentration. Increased concentration of magnesium ions reduces the formation of $CaCO_3$, favoring a unstable porous layer which is believed to be $Mg(OH)_2$, hence the anodes consumption rate will increase as the corrosion rate increases [44].
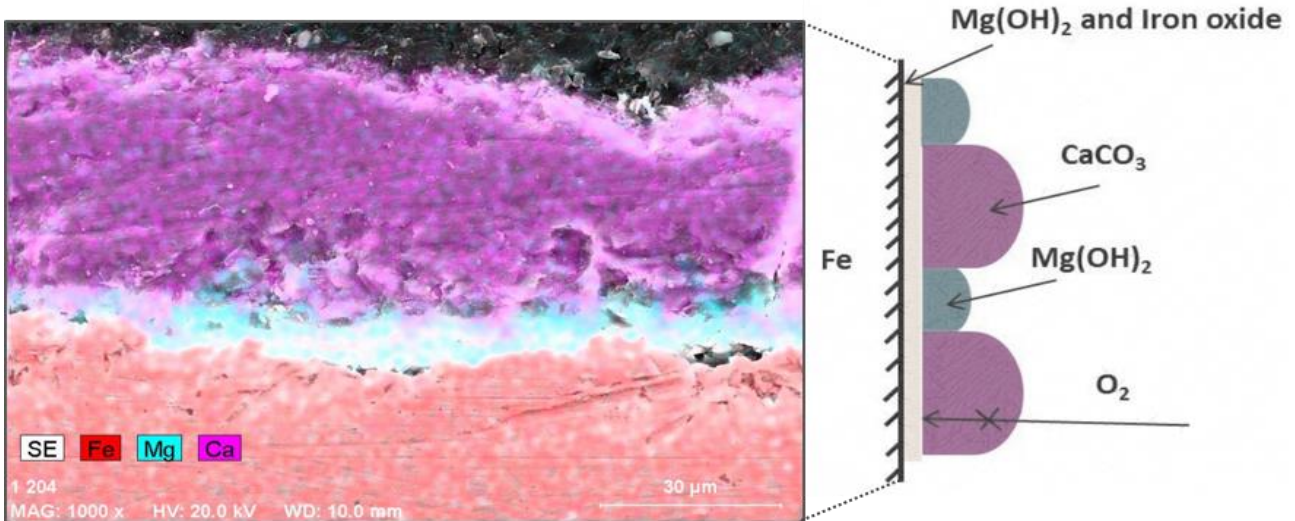
Figure 15 SEM micrograph and corresponding EDX element distribution maps for Mg and Ca, cross-section of calcareous, showing a thin film of $Mg(OH)_2$ deposits between $CaCO_3$ [49].

The Ca/Mg ratio degreases with decreasing potential, which contributes to an increased pH and a high driving force for precipitation of $Mg(OH)_2$ [48]. Barchiche et al showed that in artificial seawater at 20 ℃ and at a potential between −0.9 and −1.1 V_{SCE}, only $CaCO_3$ in the form of aragonite was formed. Further lowering the potential to −1.2 V_{SCE}, brucite precipitated together with aragonite. At potential lower than −1.3 V_{SCE}, only brucite was formed [44]. This is illustrated in Figure 16, which shows that at high potential the curves has an initial decreasing slope as a result of $CaCO_3$ deposition. At lower potential, the curve starts with a plateau as a result of precipitation of $Mg(OH)_2$. In addition, hydrogen evolution will be the dominant reduction reaction at low potential, inducing cracks in the deposits which will prevent total coverage [51].
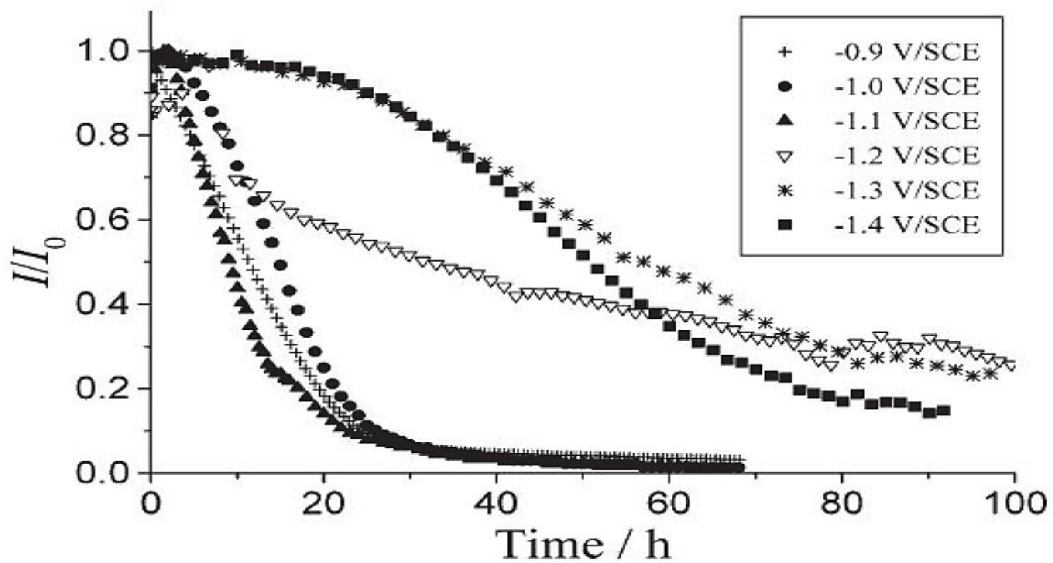
Figure 16 The effect of potential on the deposition at 600 rpm on a steel surface in artificial seawater. The steep curve represents CaCO3 deposition while at -1.2 VS SCE the curve has an initial stage before decreasing which represents $Mg(OH)_2$ [44].

At increasing flow the oxygen content increases at the metal surface, which again increases the corrosion rate. An accelerated production of hydroxide ions will occur. However, the pH will decrease with increasing flow rate due to a more effective mass transfer of OH$^-$ away from the surface. This contributes to that precipitation of $CaCO_3$ increases with a more negative potential as the flow rate increases, which can be seen in Figure 17 [48]. The combination of increased flowrate and oxygen content will hence increase the CP demand for the steel substrate. For example at stagnate conditions with oxygen content of 6 ppm, the CP current demand is 60 mA/m^2 whereas at a flow rate of 4 m/s and an oxygen content of 10 ppm requires 350 mA/m^2, according to estimation conducted for North Sea water at 7 ℃ [49].
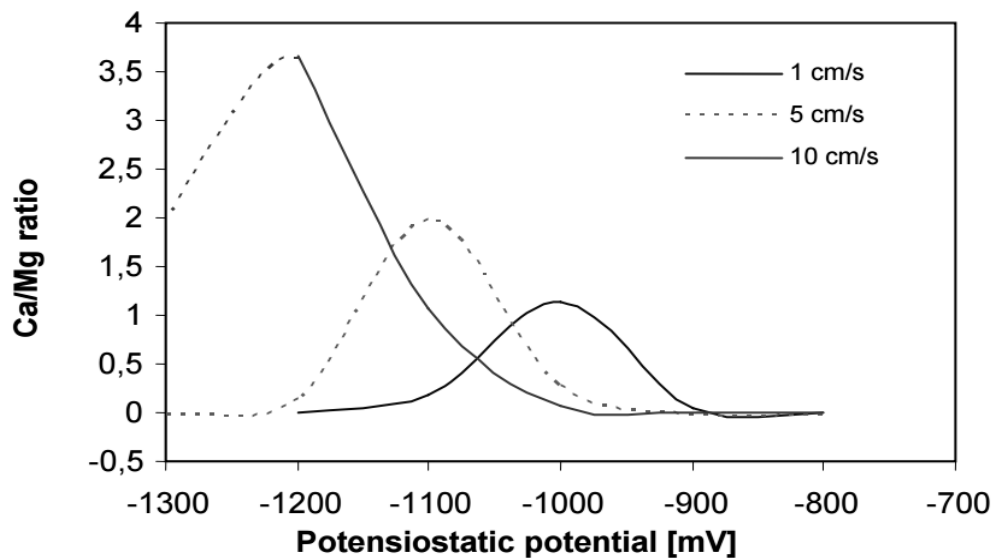
Figure 17 Ca/Mg ratio for calcareous deposit as a function of applied potential and flow rate [48].

Temperature is one of the most important factors that influence the deposition since most chemical and physical properties of seawater depends on it [52]. Both the diffusion coefficient of oxygen and hydroxide in addition the cathodic reactions, oxygen reduction and hydrogen evolution, are sensitive to the temperature. With increasing temperature, studies have shown that the protective performance of the calcareous deposits will increase exponentially, as a higher temperature leads to a faster, more dense and coherent deposition [51, 52]. The main contributor for this is the solubility limit. As the temperature increases, the solubility of $CaCO_3$ decreases, which means that calcium carbonate will form more easily in warm seawater. For $Mg(OH)_2$, the opposite effect occurs. The solubility increases with increasing temperature, inhibiting its formation. However, at low potential ($E \leq -1.2$ V$_{SCE}$) the temperature has no influence on the kinetics of the deposition. In this case, deposition of $Mg(OH)_2$ increased with increasing temperature which is in contrast to what's expected as the solubility increases. This is caused by a higher pH at the metal-seawater interface at low potentials as mentioned earlier, facilitating the formation of both $CaCO_3$ and $Mg(OH)_2$ so that the solubility variation of the compounds have a negligible effect [51].

2.4.2 **Microstructure**

The formation of calcium carbonate in calcareous deposits can take two forms, calcite or aragonite [53]. By examination in SEM, they can easily be identified. Calcite has a characteristic rhombohedral crystal shape and are often incorrectly identified as a cubic. The crystals are usually spread over the surface with large caps between them where hydrated iron (rust) is formed. The aragonite deposits however, covers and protects the surface more effectively and can be identified as a flower shape structure caused by its orthorhombic crystallinity. Both calcium carbonate forms are clearly illustrated in Figure 18.
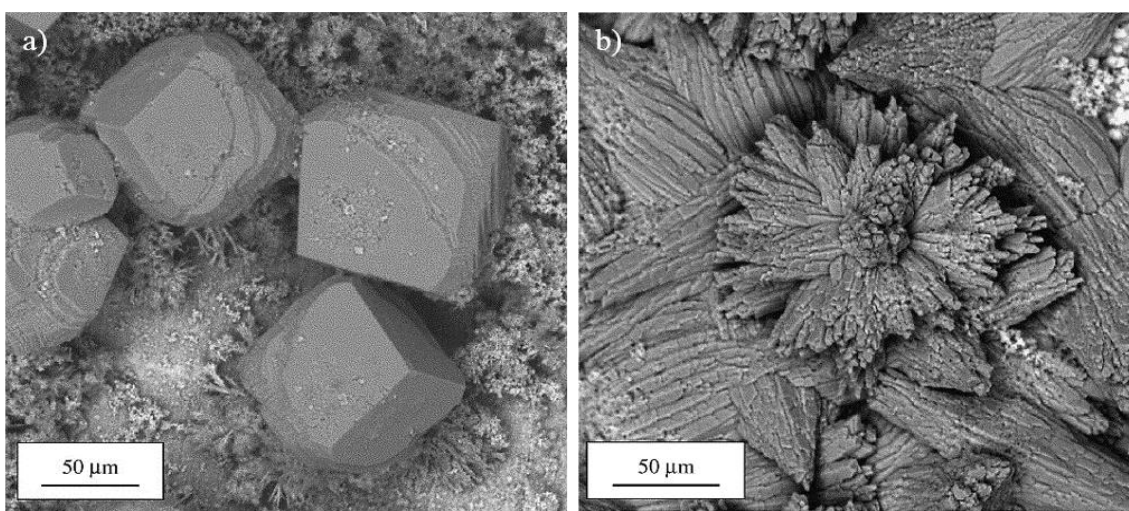
Figure 18 Calcareous deposit on steel surface: a) calcite precipitates formed during immersion for 21 days in a Mg^{2+} - free solution and b) aragonite deposits during 21 days in a Mg^{2+}-containing solution [53].

As mentioned, the Mg^{2+} has an inhibiting effect on the calcareous deposit, as it inhibits nucleation and growth of calcites. However, once aragonite is formed, Mg^{2+} ions will not have any further effect on the growth. The formation of $Mg(OH)_2$ under cathodic protection is deposited in the crystalline form of brucite [53]. Brucite has a crystallinity of hexagonal platelets where the size of the crystal is much smaller than calcium carbonate, in addition to a more loose and porous structure. See Figure 19.
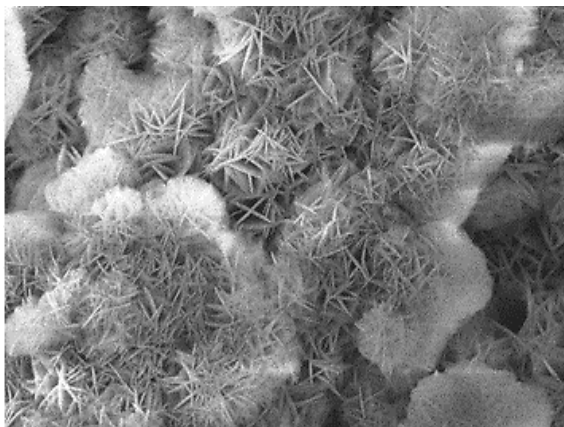
Figure 19 Precipitation of brucite on steel surface in natural seawater at 25℃, galvniostatic polarization at 200 mA/m^2 over a period of 168 hours [52].

3   Literature Review

A lot of research regarding the use of TSA as a corrosion protection strategy have been conducted during the past 40 years. However, studies regarding the electrochemical properties, especially the anodic properties of TSA are limited. In this chapter, some of the most important studies will be presented in order to evaluate DSA with respect to TSA later on.

In 1974, J. Bland published a report of the corrosion protection achieved by thermally sprayed aluminum and zinc coatings, applied by flame spray technique [54]. Thermally sprayed panels with a coating thickness between 80 and 150 µm were exposed to seawater immersion, marine and industrial atmosphere over a period 19 years. The overall conclusion was that thermally sprayed aluminum and zinc coatings are recommended in order to protect iron and steel surfaces. It was also discovered that where the TSA coating had been damaged, corrosion did not progress as the substrate was galvanic protected by the coating. The CP effect from TSA was also confirmed by H.D. Steffens, who observed that TSA applied by flame spray produced a free corrosion potential of -855 mV$_{Ag/AgCl}$. However, for a cold surface with 50% holiday protection achieved by TSA was adequate but less than what was provided by flame sprayed zinc (TSZ). The conclusion was that TSA will provide a long service life but with large coating damages, CP achieved from the coating would be limited [5].

In 1985, W. H. Thomasson published an article regarding the use of TSA for corrosion protection offshore [2]. Laboratory and field studies were conducted, where the focus were on the electrochemical properties and the effect of corrosion fatigue service in seawater for TSA coated steel applied by flame spray. The results indicated that holidays as high as 50% could be cathodic protected by the TSA coating for a few years. It was further estimated that a 200 µm thick coating could protect a 5.7 % holiday for 30 years. See Table 1. The corrosion potential for TSA specimens with 8% holiday were approximately -895 mV$_{Ag/AgCl}$. For the corrosion fatigue test, the result showed that for a cylinder shaped specimen coated with TSA experienced no disbanding after 2 million cycles. In fact, the coated specimens provided a longer fatigue life than for specimens protected by sacrificial aluminum anodes.

The electrochemical performance of flame sprayed aluminum coatings on steel in natural seawater was studied by Fischer et al. The overall conclusion was that TSA performed excellent in both splash- and immersed environments. It was further claimed that the use of a silicon sealer will increase the service life of the coating by function as a barrier, filling the pores of the coating. However, the sealer will reduce the anodic capacity of the coating, as mentioned in section 2.1.3. A current density output of around 30 to 200 mA/m^2 was estimated, while for unsealed TSA the output could be up to 500 mA/m^2. The high current density will consume the coating within months [55].

In June 1984, the Hutton Tension leg platform (TLP) was installed in the North Sea. The tethers, risers and flare boom were coated with TSA by flame spray technique. A two coat vinyl seal was applied on the tethers and a silicon on the risers. The adhesion of the coating was measured to be 6.9 MPa. No external CP system was applied to the submerged components. After 8 years in service, Fischer et al investigated the coatings performance [1]. Blistering was detected on the tethers, whereas the risers were in excellent conditions. No corrosion of the substrate was observed underneath the blisters. The studied documented the importance of the use of a proper sealer. The corrosion potential of the coated tethers ranged from −880 to −910 mV$_{Ag/AgCl}$. The good results contributed to increased use of TSA at North Sea platforms during the later years.

Fischer et al. studied the effect on steel pipe spools coated with TSA, exposed to seawater temperature from 70 and 100℃. Besides the initial low OCP found at higher temperature mentioned in Section 2.2.3, a pipe spool with a 10% holiday did not experience any corrosion attack on the CS substrate. White areas around the holiday showed that the coating had provided adequate CP to the steel surface. A silicon sealer was applied to some the test spools, while some were left unsealed. A clear difference was observed in their blistering behavior. Sealed spools experienced no blistering during 14 months of exposure at both 70 and 100℃, while for 14 out of 17 spools without sealer blistering was detected.

The properties of TSA based coatings under both anodic and cathodic polarization was investigated by Gartland and Eggen in 1990 [4]. Several coatings (Al99.6, AlMg5, AlZn) applied by both flame spray and arc sprayed were exposed to seawater for up to 18 months. In addition, an organic sealer was applied to distinguish its affect. The results showed that the cathodic current density requirement decreased with time for all coatings, and after 16 months to a value of 5 mA/m^2 and 1 mA/m^2 for un-sealed and sealed, respectively. The polarization level was −1030 mV$_{Ag/AgCl}$. However, it was stated that higher values should be expected at large depths (600 m), above 30 mA/m^2. For freely exposed specimens, the OCP development as a function of time were in the range between −1000 and −900 mV$_{Ag/AgCl}$, see table Table 2. The corrosion rate for the aluminum based coatings were initially 10 µm/year, but decreased with time to a value between 2 and 3 µm/year. For the Zn-based coating, the corrosion rate were approximately 3 times large. At anodic polarization to −870 mV$_{Ag/AgCl}$, the corrosion rate of AlMg5 increased significantly from 3 to 200 µm/year. At higher potential, −770 and −670 mV$_{Ag/AgCl}$, an increased corrosion rate was also observed for TSA. It was concluded that the thermally sprayed coatings should not be anodically polarized for a long period of time due to the high consumption rate. Applying a silicon sealer would however improve the barrier effect of the coating, thus reducing the corrosion rate at OCP by a factor of 2-3. The effect at higher potential was small.

In 1995, Heidrum TLP was installed. Large amount of TSA were used for risers, tethers, deck underside etc. Sacrificial anodes were mounted on the TLP hull and the seafloor templates, thus

providing CP also to the risers and tethers [56]. After only four years of service, severe coating degradation in the splash zone area was observed on three export risers, which were the hottest risers with temperature at around 50℃. The degradation was highest on the seawater impact side. For the submerged part of the risers, blisters and white ring shaped deposits were discovered. The failures are believed to be caused from a combination of wrong coating thickness, insufficient sealing and that the sealing may have been washed out when stored outside. In addition, high thermal cycling contributing to increased stress cycling between the coating and the substrate may have accelerated the rate of disbandment and blistering. A TSA coating thickness of 400-450 µm was found to be highly susceptible to blistering, while 200 µm gave optimal performance.

The performance of TSA in saline subsea mud without CP was investigated by S. L. Wolfson in 1996 [3]. Four- and 12-month exposure test was conducted in the Gulf of Mexico in order to quantify the ability for TSA coated steel surfaces to protect different degree of coating holidays. The results showed that TSA can provide cathodic protection to 5 % steel coating holidays, and that small holidays will have a significant longer service life time in saline mud compared to seawater environments. This is due to the current demand for bar steel was found to be lower than in seawater. The conclusion was that a 254 µm thick TSA coating with a 5 % coating damage, the steel area can be protected over a period of 25 years with CP achieved from the coating alone.

In the period 1999-2004, Shell Malaysia applied TSA on 3 offshore structures [6]. TSA (AlMg5) was applied on splash zone structures on a 4-legged jacket, F23K-A, in 1991. Months after installation, several rust stains were observed. The cause was believed to be from uneven coating thickness, where the damage areas experienced very low thickness. In 2000 and 2002, TSA was applied on two other jackets. This time, prior steps were taken to enhance the properties of the coatings. However, inspection in 2004 showed some rust stains with insufficient thickness. It was determined that the most critical factor in order to achieve adequate TSA performance is the applicator/operator. Even though factors like the quality of the surface preparation, the quality of the wire, the thickness of the coating, application and final thickness of the sealer etc. are all performed correct, the end product will be diminished if an unexperienced operator is used.

In 2004, W.T. Young and J. R. Repp studied and evaluated different surface preparation and application parameters of TSCs with respect to the corrosion performance of the coating [57]. For corrosion testing, CS plates thermally sprayed with aluminum and zinc, were exposed to alternating wet-dry seawater (simulating tidal action) and fully immersion test for 1 year. Holidays at 26.7% were made on some test specimens to evaluate the CP performance of the coatings. Results showed that blistering exacerbate more by wet-dry cyclic compared to immersion, and that TSZ was more susceptible to blistering than aluminum. However, applying a sealer will minimize blistering. In addition, less blistering was observed in specimens with holidays. This was believed to be caused by

a more rapid passivation of the coatings when providing CP to the defect, which reduced the activity within the pores of the coating.

In 2014, H. Wilson published his master thesis regarding TSA used for subsea heat exchangers [58]. Over a period of 60 days, UNS S31245 stainless steel pipes coated with TSA were exposed to slow flowing seawater at different temperatures ranging from 30 to 90℃. The pipes were connected to a CP system with a potential of -1050 mV$_{Ag/AgCl.}$ The corrosion rate of freely exposed specimens were also investigated. The results showed that the initial corrosion rate of TSA were quite high at all temperatures, but decreased with time. The corrosion rate were approximately 8 µm/year and 2 µm/year at the end of exposure, for respectively 90℃ and 10℃. At high temperatures, the initial OCP were lower than the anode potential, contributing to a shift in the current direction i.e. the TSA coating protected the anode. However, the corrosion potential increased with time and the current density stabilized in the range of 3-5 mA/m^2 for temperatures between 50 and 90℃.

O. Ø. Knudsen published an article regarding TSA exposed to saline subsea mud under cathodic protection in 2015 [59]. The main issue when it comes to TSA exposed to saline subsea mud under cathodic protection is the possibilities for alkalization at the TSA surface due to overly effective polarization. In flowing seawater, the produced hydroxides from the cathodic reactions will be removed by diffusion, maintaining the pH in the passive region. But, in mud where there is no water flow, this diffusion will be limited. The combination with TSA and CP in seawater mud may therefore not be suited, as it may in fact decrease the lifetime of the coating.

Recently, the department of engineering design and materials at NTNU was engaged by Statoil ASA to execute a research project regarding the properties of TSA under CP in seawater, applied for subsea cooling applications [60]. Thermally sprayed CS without sealer were exposed at 20, 50 and 90℃ over a period of 9 moths. In addition, painted CS and titanium Gr. 2 specimens were also tested. All specimens were cathodic protected to a potential of −1050 mV$_{Ag/AgCl}$. The results showed that the initial potential of TSA were lower than the anode potential at 90℃, i.e. TSA acts as a sacrificial anode protecting the anode. However, after 100 days of exposure the current density stabilized to a positive value below 10 mA/m^2, independent of temperature. Higher coating degradation was observed on specimens exposed at 50℃ and 90℃ compared to does at 20℃.

From these studies and experiences, it can be concluded that TSA works excellent for corrosion protection, acting as a barrier. However, with a damage in the coating, the protection properties may be limited. TSZ has shown to provides high protective properties, but with the cost of high consumption rate and increased possibilities for blistering, reducing the service life of the coating. DSA may be a solution in order to bridge the gap between TSA and TSZ coatings, providing a coating with adequate barrier -and anodic properties.

4   Experimental procedure

In this study, the preparation -and electrochemical test procedure for the new concept with distributed sacrificial cathodic protection is presented. The main purpose of the tests are to determine if the electrochemical properties of DSA are similar to those of conventional sacrificial anode and if they are greater than for TSA, where the anodic properties as well as the OCP and current density development will be of most importance. Firstly, manufacturing of the anode wire and the thermal spray process is described, followed by the preparation of the different test specimens used for the experiment. Secondly, the experimental test-setup is described for the different conditions. Then, electrochemical measurement which were conducted during the exposure period is described, followed by the surface characterization technique used for both post -and prior exposed specimens in order to determine the/if degradation of the coating have initiated during the exposure period of 30 days.

4.1   Re-casted conventional anode to DSA

Conventional Al-Zn-In anodes were re-casted into bars with a dimeter of 100 mm and pressed through an orifice forming wire-die with Ø5 mm. The re-casted anode bars were made of CORAL A High Graded alloys delivered from Skarpenord Corrosion. Technical data for this alloy can be found in Appendix A. These alloys are according to NORSOK standard M-503 and ISO 15589-2, and certified according to DNV Type Approval Program Three bars were hot pressed, where the maximum applied force was measured to be 2815 kN with an average piston speed at 0.7 mm/s. The die was placed in an oven where the bars were heated up to approximately 506℃ during the extrusion process. The bar with 100 mm diameter was reduced to a 5 mm wire in one stage through the extrusion process. Data for the process can be found in Appendix B – First stage of the extrusion process. Further, the 5 mm extruded wire needed to be subsequently reduced to a diameter of 2 mm in order for it to be used by thermal spray equipment. The wire was drawn with 8-20 % area reduction for each step. After 20 successfully reductions, one Ø100 mm bar had been extruded to a 300 meter long wire, ready for coating deposition. The described process was performed by NTNU/SINTEF, and is illustrated in Figure 20.

The wires were sent to Total Coating in Drammen [61], where 7 carbon steel plates with dimension $300 \times 300 \times 6$ mm were coated by a 300 µm thick conventional TSA (Al99.5) layer followed by a 700 µm thick sacrificial layer made from the extrude anode wire, distributed sacrificial anode (DSA). In addition, 3 plates were only coated by a 300 µm thick TSA coating. The carbon steel surfaces were grit blasted to Sa ½ according to ISO 8501-1 before electric arc spraying. In addition, sharp edges and corners were rounded by grinding or disc sanding to a min of 2 mm radius. Both coatings were applied using electric arc thermal spray technique, Osu Hessler 300A with a modified pistol for smooth surfaces, see Figure 21. A 9.5 mm die and a pressure of 7 bar was used under the cleaning process with

an oil/water separator to secure that the air was free from oil and water. Surface dust was controlled with the use of pressure sensitive tape method according to ISO 5202-3 and salts and chlorides were controlled using Bresle Test according to ISO 8502-6. The roughness was determined by using comparator according to ISO 8503. No sealer was applied on the coating. After application the thickness of each plate was measured, see Table 6, before the plates were sent to NTNU in Trondheim for electrochemical testing.

Figure 20 Illustration of the extrusion process: a) An ingot of re-melted traditional flush-mount anode with Ø100 mm, b) The ingot is hot pressed through an orifice forming wire-die with Ø5 mm. c) The hot pressed wire is produced and cooled and d) The wire is subsequently reduced to Ø2 mm for thermal spraying.

Table 6 Result of film thickness measurement achieved from 6 measurements on each thermally sprayed DSA plates, performed by using electrophysik minitest 730 FN5.

Plate number	1.	2.	3.	4.	5.	6.	7.
Min. film thickness [µm]	1062	1084	1054	984	1014	1206	1008
Max. film thickness [µm]	1210	1398	1374	1248	1374	1272	1190
Avg. film thickness [µm]	1140	1225	1191	1138	1213	1247	1093

Figure 21 Coatings applied using electric arc spray.

4.2 Test specimens

In this chapter, the preparation of the tests specimens is described. The dimension of the samples vary depending on the experimental test program. However, manufacturing of the samples were performed in the same procedure.

Freely Exposed Specimens

For OCP measurements and specimens for measuring the electrochemical properties of the materials (LPR and polarization curves), test specimens with a dimension of 50×50 mm were prepared. Four different materials were used, see Table 7. For practical reasons, the length of the wire-specimens were cut to approximately 78 mm (half of the exposed areas as for the plates). Further, a two component polyamine cured epoxy mastic coating, type Jotun Jostamastic 87 std 038 was applied on the sides that were not thermally sprayed, see Figure 22. The cast anode specimens were also coated to ensure that the exposed areas were equal. For exposure at 40℃, only DSA and TSA specimens were freely exposed. It should be noted that some specimens were only freely exposed without measurements, which were used for surface examination after 30 days and shall be used for later examination (not in this report).

Table 7 List of materials used for the different measurements at both 10℃ and 40℃.

Test specimens	Number of specimens prepared				
	OCP 10℃	OCP 40℃	LPR and Pol. Curves 10℃	LPR and Pol. Curves 40℃	Area [cm²]
DSA	6	2	4	1*	25
TSA	3	2	4	1*	25
Cast Anode Piece	2	-	4	-	25
Wire piece (Ø5 mm)	2	-	4	-	12.5

*Polarization curves at 40℃ were obtained on one of the two freely exposed specimens after 30 days.
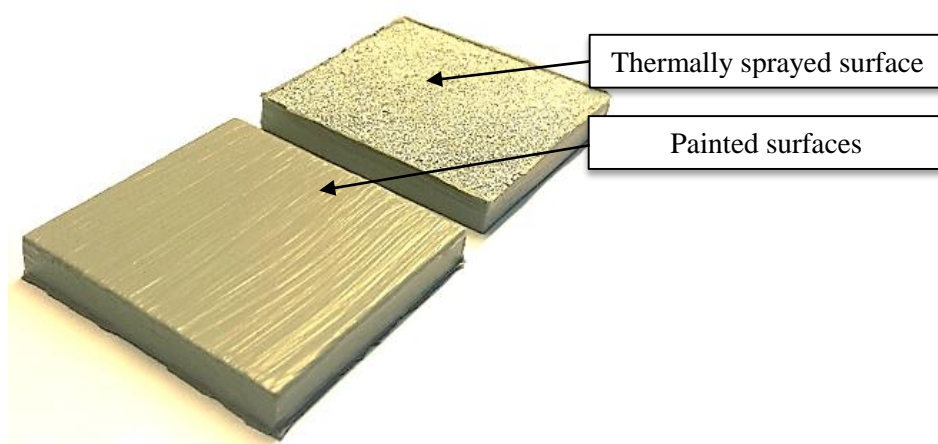
Figure 22 Thermally sprayed carbon steel specimen with area 50×50 mm, coated with Jotun Jostamastic 87 std 038 to ensure that only the DSA or TSA surface were exposed.

In order to achieve stable electrical connection to the test specimens, M3 threads were made such that a 3 mm conductive threaded rod could be fixed into the test specimens. To avoid galvanic corrosion between the wire and the test specimen, a heat-shrinkable tubing was applied to the rod and silicone around the connection, see Figure 23.

Figure 23 DSA specimens connected to a 3 mm insulated threaded rod, ready for exposure (the painted sides of the specimens are shown). Notice that the specimens are called TSA Al-Zn-In. This was before it was decided to name the new coating system for DSA.

Galvanic Couplings

To simulate a defect in the coating, i.e. a holiday, and to determine the performance of DSA compared to conventional anodes and TSA, galvanic couplings between DSA, TSA, conventional anodes and CS were conducted. The area ratio between the anode and cathode (A-C) were 1:1, 10:1 and 100:1. A limited number of couplings were tested at 40℃, see Table 8.

In order to manufacture the small specimens with more accuracy, a milling machine was used. However, some deviation in the lengths of $\pm$ 0.25 mm were seen. Otherwise, the same procedure of applying the electrical connection and coating the surrounding surfaces was followed as described earlier. The specimens which were not thermally sprayed, i.e. cast anode piece and CS, were mechanically fine grinded with SiC paper to P500 to ensure a uniform surface with no contamination. Two parallel couplings of each were made in order to have one exposed over a longer period.

Table 8 Galvanic couplings to investigate the protection efficiency of DSA, TSA and commercial Al-anode in natural seawater at 10±2℃.

Couplings (A-C)	Area Ratio	Area A [mm]	Area C [mm]
DSA-CS*	10:1	100×100	40×25
DSA-CS	100:1	100×100	10×10
DSA-TSA**	10:1	100×100	40×25
DSA-TSA	100:1	100×100	10×10
TSA-CS	10:1	100×100	40×25
TSA-CS	100:1	100×100	10×10
Anode-CS*	10:1	40×40	1.265×1.265
Anode-DSA	1:1	40×40	40×40
Anode-DSA	1:100	10×10	100×100
Anode-TSA	1:1	40×40	40×40

*   Similar coupling was <u>also</u> exposed to natural seawater at 40℃
**   Similar coupling was <u>only</u> exposed to natural seawater at 40℃

The specimens were mounted on a plank, where for the galvanic couplings the distance between each drilled mounting hole were 5 cm. In order to achieve uniform current distribution from the most active to less active metal, the specimens were placed with the exposed surfaces in the center of each other, i.e. the un-coated (not painted) surfaces are facing each other, see Figure 24.

All specimens, both freely exposed and galvanic coupled were degreased in acetone and rinsed in ethanol before exposure.

4.3 **Experimental conditions**

The experiments were performed on SEALAB located at Brattøra, Trondheim. All the specimens described above, were exposed to natural seawater pumped from 80 m deep from the Trondheimsfjord. Fresh seawater entered the vessels at a replacement rate of 0.1 l/min, contributing to nearly stagnate conditions with a constant pH of approximately 8.1. Most of the specimens were exposed to natural seawater at temperature 10±2℃. Later on, freely exposed and galvanic couplings were also exposed at 40±5℃ as presented in Table 7 and Table 8, respectively. The exposure time was initially set at 30 days but was increased for some test specimens.

Two separate containers were used. The galvanic couplings were placed in one and the freely exposed samples for OCP measurements and for potentiodynamic polarization curves were placed in another container as illustrated in Figure 24. For exposure at 40℃, a third similar container was used. Two electrical heating elements in two pipes made from titanium with internal diameter 80 mm and connected to two Variac's were used to heat seawater from the inlet temperature to 40℃. MEG was used as heating medium inside the pipes.
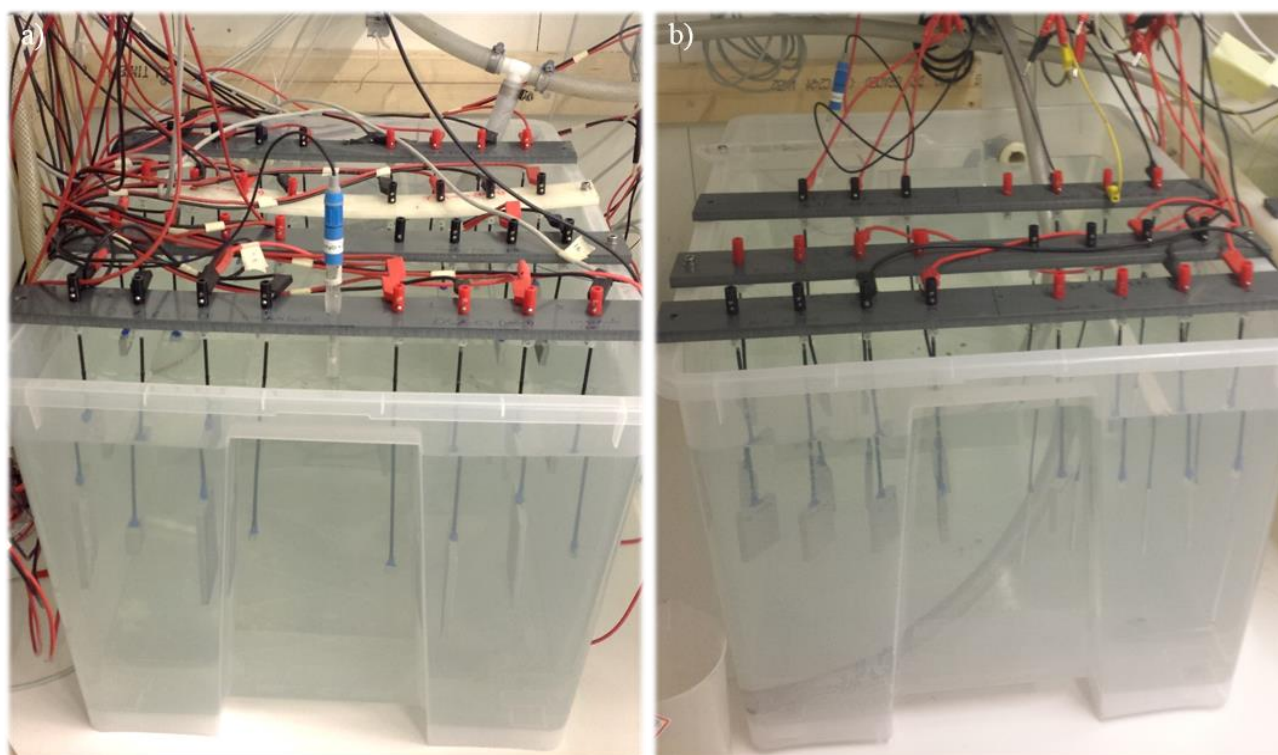
Figure 24 Experimental setup a) galvanic couplings and b) freely exposed specimens

The potential development for the freely exposed specimens and the galvanic couplings, from her on called the OCP and coupling potential respectively, were monitored by using a logging equipment vs. a reference electrode. An Ag/AgCl saturated KCl reference electrode was used for all measurements, which has a potential of +0.230 V_{SHE}. The OCP and the coupling potential were recorded every 10

minutes by a Data Management System (DMS). In addition, the current for the different couplings were measured every 5 min. This was done by measuring the potential drop over a fixed resistance from the most active metal to the less active metal (anode-cathode), followed by applying ohm's law. Depending on the potential differences for the coupled metals, a resistance of 1, 10 or 100 ohm was used in order to keep the potential drop less than 1 mV. A simplified illustration of the setup can be seen on Figure 25.
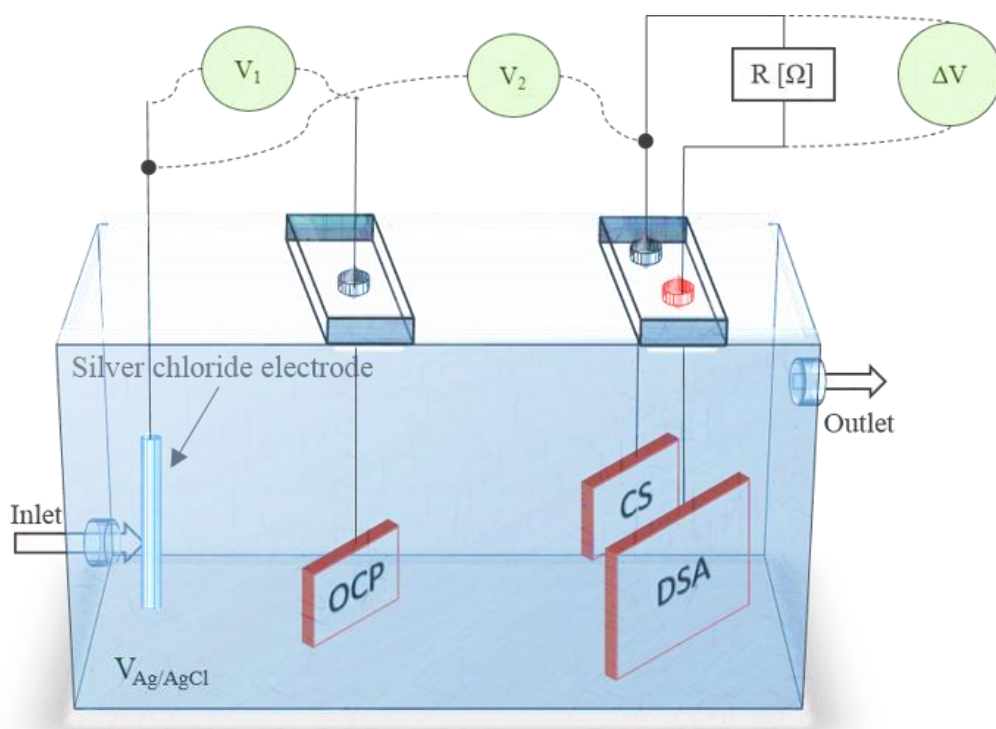
Figure 25 Simplified illustration of the setup showing the OCP -and coupling potential measurement (V_1 and $V_{2)}$ with respect to an Ag/AgCl reference electrode. In addition, the potential drop over the couplings is measured to determine the current density.

Due to a reduced numbers of channels for the DMS, the corrosion potential for some of the couplings were measured manually 2-3 times a week.

4.4 Electrochemical measurements

Corrosion rate measurements were conducted on the freely exposed specimens. After 1, 8, 15 and 30 days of exposure, LPR measurements and polarization curves were obtained on the same specimens, but on new (not prior polarized) specimens at each time. The following materials were included:

- DSA coated specimen without damage
- TSA (Al99.5) coated specimen without damage
- Cast anode piece
- Anode wire (Ø5 mm) after stage one of the production process

These metals were chosen in order to evaluate the anodic properties for the DSA coating and comparing the result with conventional CORAL A anode. The wire piece is also tested to determine if the metal composition is changed after the extrusion process, which hence will change the electrochemical properties. In addition, TSA is tested to determine if there are any benefits by replacing TSA with DSA, regarding anodic capability and the dissolution rate.

A three electrode system consisting of the working electrode for testing, a platinum counter electrode and an Ag/AgCl reference electrode were used for the electrochemical measurements. Before obtaining the polarization curved for the different specimens, LPR measurements were conducted. The LPR measurement was obtained as following: The OCP was first measured and noted on the exposed specimens. Then the freely exposed specimen was polarized 20 $mV_{Ag/AgCl}$ in cathodic direction by using a potensiostat. The potential was held for 2 minutes before the current was measured as a potential drop across a fixed resistor. The potensiostat was then put in standby for 10 minutes in order for the test specimen to recover and stabilize back to its OCP. Then, the same procedure was conducted in the anodic direction, and the current was measured after 2 min. Stern-Geary's equation (2.8) was used to calculate the corrosion rate.

After LPR measurement and when the specimen had recovered to its OCP, the polarization curves were obtained. This was done by polarizing the sample in cathodic direction from OCP in several steps, with 25 mV for each step, down to -1600 $mV_{Ag/AgCl}$. For stabilization, the potential was held for 2.5 min before the current was noted. After the cathodic polarization curves were obtained, the potensiostat was put on standby for 4 hours or until reaching OCP[4]. Then, the same procedure was conducted in anodic direction up to -600 $mV_{Ag/AgCl}$ or longer until one decade (i.e. one order of magnitude) in increased current was reached. By plotting the data, the anodic and cathodic Tafel constants was obtained and the corrosion rate calculated. The calculated corrosion rate from the LPR measurements and the polarization rates were compared.

4.5 Surface Characterization

In this chapter, the surface characterization analysis will be described. The chapter is divide into two sub-chapters, prior- and post exposure analyses.

4.5.1 Prior Exposure Analysis

Adhesion Test

Before exposure, an adhesion pull-off test on a "special" thermally sprayed CS plate was performed according to ASTM D4541 standard [62]. The plate was divided into three parts as illustrated in

---

[4] In some cases, the anodic polarization curves was obtained the day after due to slow recovery rate.

Figure 26. The whole plate was coated with a 300um thick TSA layer, where the middle and bottom part were coated with a 300 µm and 700 µm thick DSA layer, respectively.

Dollies were glued perpendicular to the coated surface, which was grinded with a P500 to ensure acceptable adhesion to the coating, according to ASTM D4541 [62]. The applied glue was a 3M Scotch-Weld™ epoxy DP 490. After cured (24h), a cutting device was used to cut around the circumference of the dollies to the substrate. A testing apparatus was attached, and aligned in order to apply normal tension to the coating. The force was gradually increased until detachment of the coating encountered. The setup can be seen in Figure 26.
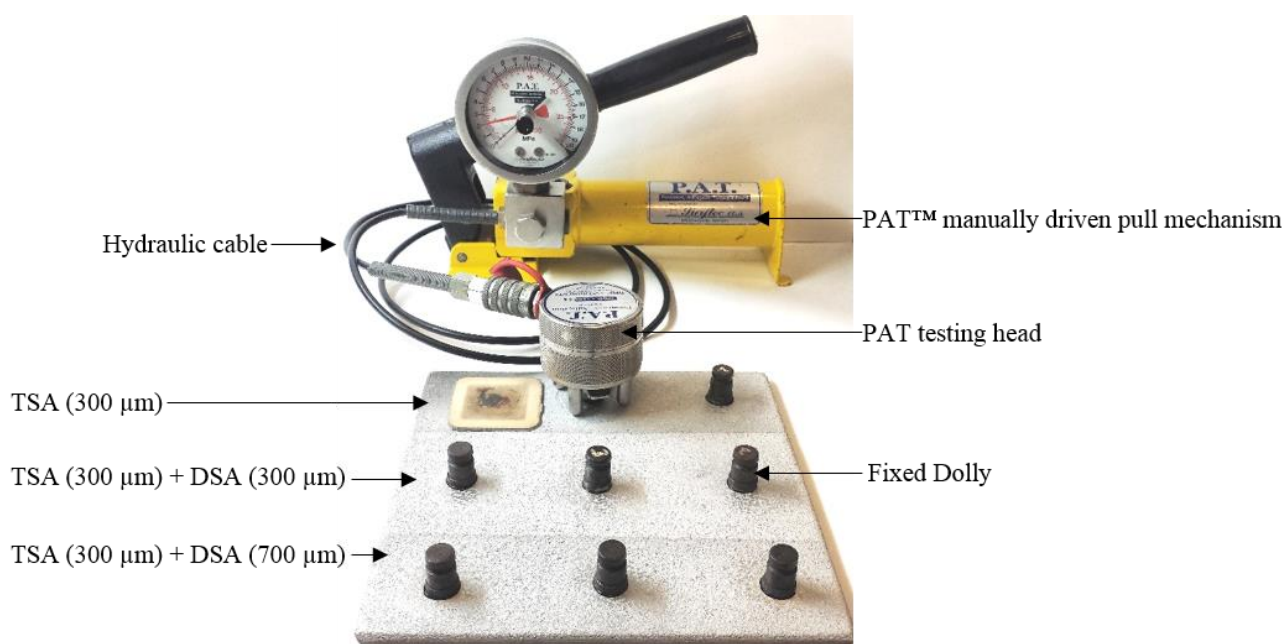
Figure 26 The adhesion pull-off setup used for this experiment.

Adhesion pull-off test were also conducted on individual thermally sprayed plates used for this experiments, both DSA and TSA plates. This will be used as reference values in order to determine if the adhesion between the substrate and the coating is reduced after exposure.

Cross Section Analysis

Before exposure, cross section analysis were conducted for DSA and TSA specimens in order to evaluate the coating thickness as well as the composition of the surfaces. Also, the examination would be a reference, together with the average coating thickens listed in Table 6, for evaluation of the corrosion attack after 30 days of exposure to natural seawater. The microstructure of the coatings were examined by using a scanning electron microscope (SEM) coupled to an Energy-dispersive spectroscopy (EDS). In this thesis two types of SEM were used, Hitachi S-3400N where EDS was needed and Quanta FEG 650 where higher resolution images were desired. The SEM images were taken with different magnification at 20kV and a working distance of 10 mm.

The specimens were cut into smaller pieces using Struers Accutom-50, with a diamond cut-off wheel MOD13. In order to avoid rounding of the edges during grinding and polishing, the pieces were imbedded in a phenolic hot mounting resin with cabon filler, Poly-fast. Afterwards, the cross-sections were mechanically fine grinded using SiC paper from 320P to 2400P, then polished to a mirror like surface using Struers MDDac plates with diamond grain sizes from 3 µm to 1 µm. The specimens were cleaned in ethanol before analyzed in the SEM.

4.5.2 Post Exposure Analysis

After 30 days of exposure, following specimens were examined in SEM:

Freely Exposed Specimens
- DSA at both temperatures
- TSA at both temperatures

Galvanic Couplings
- DSA-CS (10:1) at both temperatures
- TSA-CS (10:1) at 10℃
- DSA-TSA (100:1) at 10℃
- DSA-TSA (10:1) at 40℃

Cross-section analysis were conducted in the same way as for prior-exposure. The cross-section examinations was done in order to evaluate the coating degradations and determine if there are any significant differences between DSA and TSA.

The TSCs surfaces were examined in order to determine if there were any pits or cracks in the coating exposing the CS substrate. Before examination, the specimens were immersed in 65% HNO_3 for 3 minutes in an attempt to remove any corrosion products. After immersion, the specimens were thoroughly rinsed in distilled water.

The calcareous deposition on the CS surfaces were also investigated in SEM. Both, surface and cross section examination was conducted. Since calcareous deposits are non-conductive, only the white areas were further investigated with EDS to determine the compositions of the deposits.

Adhesion pull-off test was performed on DSA and TSA coupled to CS with area ratio of 100:1, after 30 days of exposure. This test was performed in the same manner as for the prior exposed specimens.

5   Electrochemical Results

In this chapter, the electrochemical results obtained from continuously monitoring the test specimens during exposure to natural seawater at both 10±2℃ and at 40±5℃ are presented. Some temperature variation were observed during the exposure period, however when referring to a temperature condition, 10℃ and 40℃ will be used from her on.

5.1 Open-circuit potential

Freely exposed at 10℃

In Figure 27, data for the open-circuit potential (OCP) development for DSA, TSA, Al-Zn-In anode, and the corresponding extruded anode wire is presented. The OCP for all the specimens dropped rapidly the first days of exposure. After approximately 5 days, the OCP for DSA decreased to a very low value, from −900 mV$_{Ag/AgCl}$ to −1110 mV$_{Ag/AgCl}$. The potential then gradually increased with time, and after 60 days of exposure the potential stabilized around −1000 mV$_{Ag/AgCl}$.
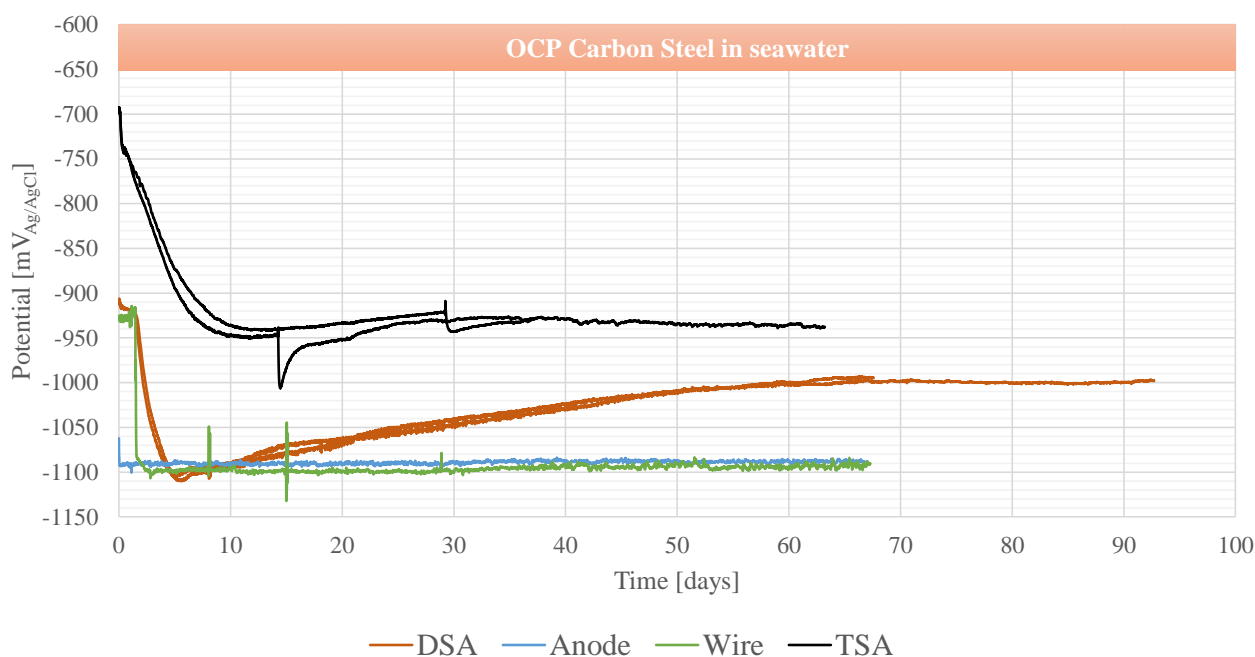
Figure 27 Open-Circuit potential development for DSA- and TSA coated steel specimens, and conventional Al-Zn-In anode alloy and a corresponding extruded wire specimen exposed to natural seawater at 10±2℃. The OCP for carbon steel in seawater is also marked.

The potential for TSA decreased from −700 mV$_{Ag/AgCl}$ to approximately −950 mV$_{Ag/AgCl}$ after 10 days of exposure. This is the same value as Gartland and Eggen measured for arc sprayed Al after 11 months of exposure, Table 2. The time until activation, i.e. the time until the most negative potential was reached, was doubled compared to the DSA specimens. From there on, the potential slowly increased with time reaching a stable value of −935 mV$_{Ag/AgCl}$ after 40 days of exposure.

For the conventional Al-Zn-In anode alloy and the extruded wire specimens, the OCP development followed the same trend. Only one of each specimens are shown in Figure 27. After 1-2 days, the potential dropped significantly from -925 mV$_{Ag/AgCl}$ to -1090 mV$_{Ag/AgCl}$ and -1100 mV$_{Ag/AgCl}$ for anode alloy and wire respectively. The potentials stabilized at these value throughout the exposure period.

Freely exposed at 40℃

In Figure 28, data for the OCP development for DSA and TSA specimens, freely exposed to natural seawater at approximatly 40℃ are presented. In addition, the temperature is plotted with a secondary axis. During the first days, the temperature was kept between 32 and 35℃ due to another ongoing project. However, as the temperature was increased to approximately 40℃, some instability can be observed. The drop at day 12 was due to increased water replacement rate, to 0.1 l/min, as the flow had nearly stopped. Due to reduced amount of heating medium (MEG) in one of the titanium pipes, caused by evaporation, the temperature had to be reduced at day 28. From a temperature-OCP point of view, it can clearly be observed that all specimens are affected by the temperature changes. Increased temperature contributed to decreasing potential, and vice versa.
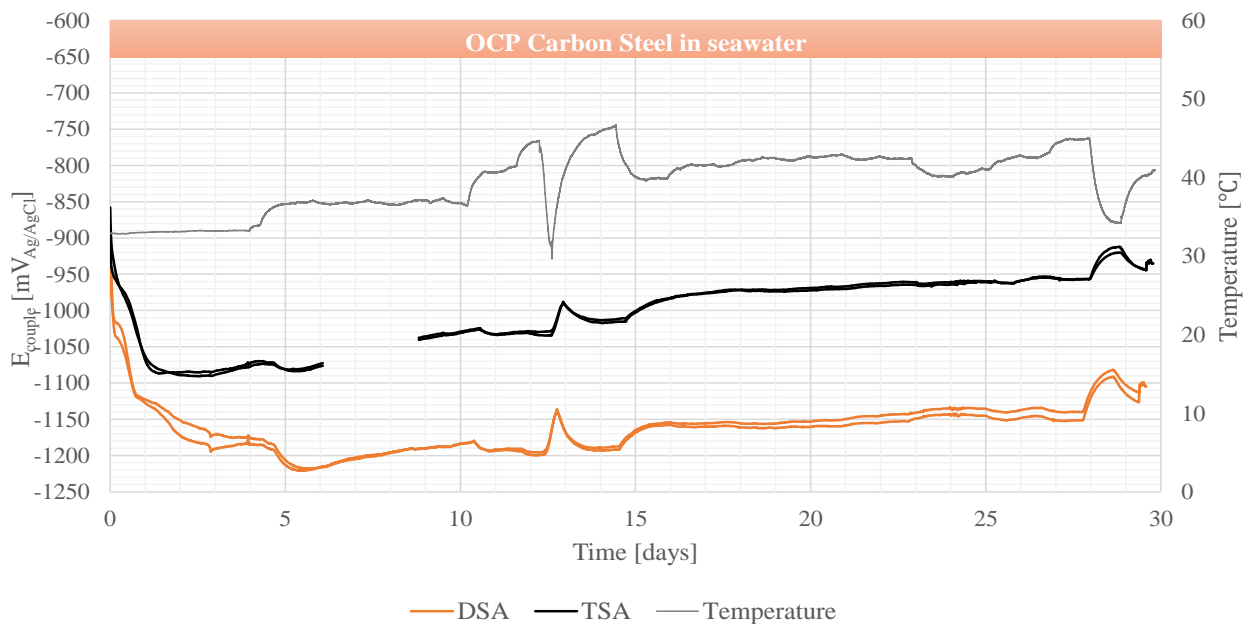
Figure 28 Open-Circuit potential development for DSA and TSA coated steel specimens exposed to natural seawater at 40±5℃. The OCP for carbon steel in seawater is also marked.

The potential for DSA decreased substantially during the first 5 days of exposure, from -950 mV$_{Ag/AgCl}$ to -1218 mV$_{Ag/AgCl}$. In the period from day 16 to day 25, where the temperature was approximately at the desired value (40℃), the potential appeared to reach it steady state value around -1150 mV$_{Ag/AgCl}$. However, as the temperature was decreased subsequently at day 28, the potential seemed to still increase at day 30, ending at -1098 mV$_{Ag/AgCl}$.

The OCP of TSA is more positive than for DSA, as can be seen in Figure 28. The initial potential drop during the first days was lower, reaching a value of −1088 mV$_{Ag/AgCl}$ at day 3. From this point on until the end, the potential increased, moving towards a steady state value. After 30 days of exposure, the OCP was −935 mV$_{Ag/AgCl}$, which is the same steady state value observed for TSA at 10℃. Due to software problems, data from day 6 to 9 were lost.

5.1.1 **Open Circuit Potential Summary**

A summary of the OCP development for the test specimens at both 10℃ and 40℃, can be seen in Table 9. The initial potential, i.e. the lowest potential observed during the first days for exposure, is quite low for DSA and TSA at both temperatures. With time, the potential increased and reached a steady state value independent of the temperature. This can be seen for the TSA specimen where the potentials stabilized at −935 mV$_{Ag/AgCl}$ for both temperatures. DSA at 40℃ did not reach a steady state value during 1 month.

Table 9 Open-circuit potential development for test specimens at 10 and 40℃.

	OCP development [mV$_{Ag/AgCl}$]					
	Temperature 10±2℃			Temperature 40±5℃		
Specimen	Initial	1 Month	2 Months	Initial	1 month	2 Months
DSA	-1110	-1040	-1000	-1218	-1098	-
TSA	-950	-940	-935	-1088	-935	-
Anode	-1090	-1085	-1090	-	-	-
Wire	-1100	-1095	-1095	-	-	-

5.2 **Galvanic Couplings Potential**

In this chapter, the galvanic couplings potential development are presented. Firstly, the couplings whom have been exposed to natural seawater at 10℃ will be presented, followed by those exposed at 40℃.

Galvanic couplings at 10℃

In Figure 29, the galvanic coupling potentials as a function of time for DSA and TSA coupled to carbon steel specimens with area ratio of 100:1 and 10:1 are presented. In addition, coupling potentials between traditional sacrificial Al-Zn-In and CS with area ratio 10:1 are shown. Two of each galvanic couplings are plotted, where one was stopped after 30 days of exposure for surface examination. Some couplings were only measured periodically, 2-3 times a week, and therefore the corresponding graphs consist of non-fluctuating potential.

Figure 29 Couplings potential development for different couplings with area ratio 10:1 and 100:1, exposed to natural seawater at 10±2℃ under nearly stagnant conditions. The OCP for carbon steel in seawater is also marked.

The coupling potential for DSA-CS (10:1) experienced a drop from approximately −900 mV$_{Ag/AgCl}$ to −1075 mV$_{Ag/AgCl}$ after 5 days of exposure. With time, the potential slowly increased and stabilized at a value of −1000 mV$_{Ag/AgCl}$ after 60 days. The coupling potential development for DSA-CS (100:1) is the same as for 10:1. However, the initial potential drop after 5 days was higher, reaching −1102 mV$_{Ag/AgCl}$. With time, the potential increased to a higher value than couplings with area ratio 10:1, stabilizing at −975 mV$_{Ag/AgCl}$ after 60 days.

TSA-CS (10:1) couplings potential were initially high, −700 mV$_{Ag/AgCl}$, but decreased to −930 mV$_{Ag/AgCl}$ after 7 days. The potential than increased to approximately −820 mV$_{Ag/AgCl}$ after 42 days with a steeper slope compared to the DSA couplings. The potential stabilized at this value throughout the exposure period. TSA-CS (100:1) experienced a bit higher potential drop during the first days of exposure, to −976 mV$_{Ag/AgCl}$. Thereafter, the potential gradually increased at approximately the same rate as for the 10:1 couplings, ending at −890 mV$_{Ag/AgCl}$ after 62 days.

The couplings potential for Anode-CS (10:1) were stable around −1090 mV$_{Ag/AgCl}$ the entire period of exposure.

In Figure 30, the galvanic couplings potential as a function of time for DSA and TSA coupled to anode specimens where the exposed area are equal, i.e. area ratio 1:1, are plotted. In addition, couplings between DSA-TSA (100:1) and Anode-DSA (1:100) are presented. The test for Anode-DSA (1:100) was performed later than the other couplings, hence the exposure time is shorter.
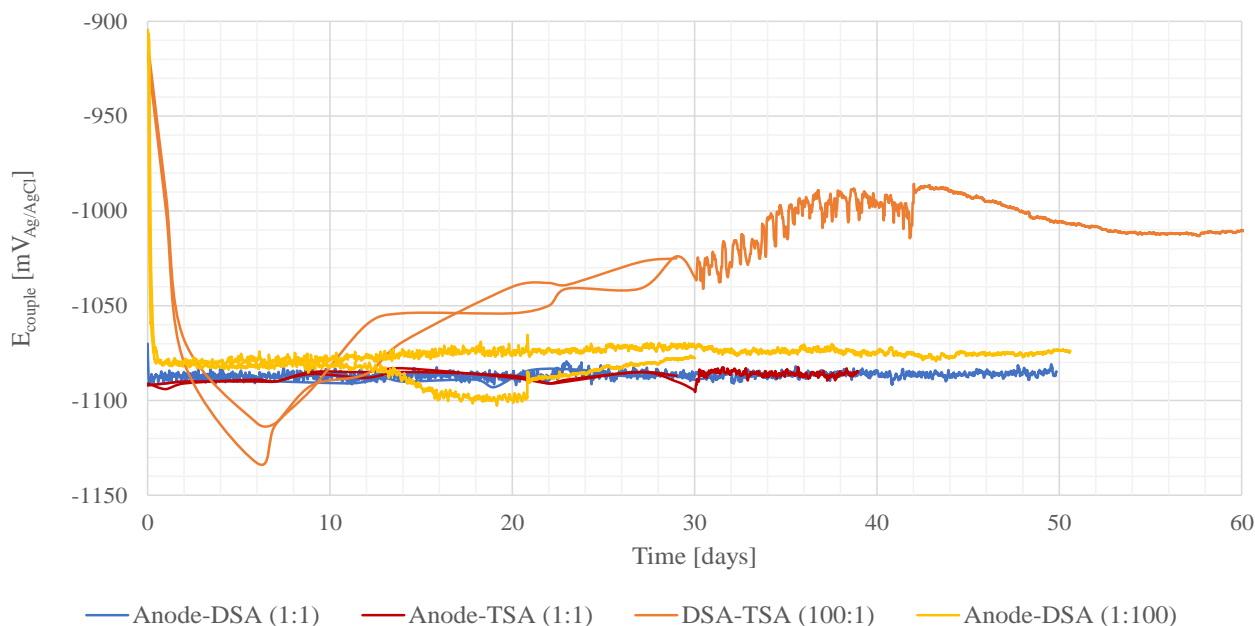
Figure 30 Couplings potential development for different couplings with area ratio 1:1 and 100:1, exposed to natural seawater at 10±2℃ under nearly stagnant conditions.

For both anode (1:1) couplings, the potential was stable between −1080 and −1090 mV$_{Ag/AgCl}$ the entire period.

The galvanic coupling potential for DSA-TSA (100:1) experienced a significant steep drop during the first 6 days of exposure, from approximately −900 mV$_{Ag/AgCl}$ to −1133 and −1112 mV$_{Ag/AgCl}$ for both couplings. Thereafter, the potential increased at a high rate. At day 30, one coupling was disconnected, and the other was connected to DMS which is the result of the potential fluctuation due to high frequent monitoring, every 5 min. However, higher degree of fluctuation can be observed in comparison to the anode couplings. The coupling potential continued the inclining pattern, reaching −990 mV$_{Ag/AgCl}$ after 40 days of exposure. From this potential, some instability can be observed with a sudden (vertical) increase in the potential followed by a declining pattern. After 54 days, the coupling potential appeared to have stabilized at approximately −1010 mV$_{Ag/AgCl}$.

For Anode-DSA (1:100) the coupling potential experienced a similar drop as for the other anode couplings, down to −1080 mV$_{Ag/AgCl}$. Some, but little fluctuation in the potential can be observed. The potential slowly increased with time for both couplings. However, one coupling experienced declining pattern at day 14, suggesting that the OCP for the DSA specimen is higher than the Anode. This is most likely not the case. It was discovered some bad connection between the threaded rod and the anode specimen, which may be the cause. At day 21, the potential suddenly increased again, moving towards the other coupling potential. The potential stabilized between −1070 and −1075 mV$_{Ag/AgCl}$.

Galvanic couplings at 40℃

In Figure 31 , the galvanic couplings as a function of time for DSA and Anode coupled to CS with area ratio 10:1 are presented. In addition, coupling between DSA-TSA (10:1) and the temperature development (secondary y-axis) during 30 days of exposure is shown. For DSA-CS (10:1) and DSA-TSA (10:1), the coupling potentials have clearly been affected by the temperature fluctuation. Increased temperature contributed to decreasing potential, and vice versa. The effect of temperature is not clearly observed for the anode couplings.

The coupling potential for DSA-CS (10:1) experienced a drop from approximately -900 mV$_{Ag/AgCl}$ to -1060 mV$_{Ag/AgCl}$ during the first 12 hours of exposure. Thereafter, the coupling potential gradually increased and seemed to have stabilized between -1000 and -1020 mV$_{Ag/AgCl}$ in the period where the temperature was approximately stable at 40℃, day 13-25.

For the DSA-TSA (10:1) coupling, a substantial potential drop was observed during the first days of exposure, from -900 mV$_{Ag/AgCl}$ to approximately -1200 mV$_{Ag/AgCl.}$ The potential increased with time, and seemed to have stabilized at -1090 mV$_{Ag/AgCl}$, after 25 days of exposure, when the temperature was 40℃.

For Anode-CS (10:1), the couplings potentials are more or less stable the entire period of exposure, at -1035 mV$_{Ag/AgCl}$ from day 18 until the end. However, a lot of fluctuating was observed, and a filter had to be used in order to remove noise (high and low peaks). This was not observed for the other couplings.

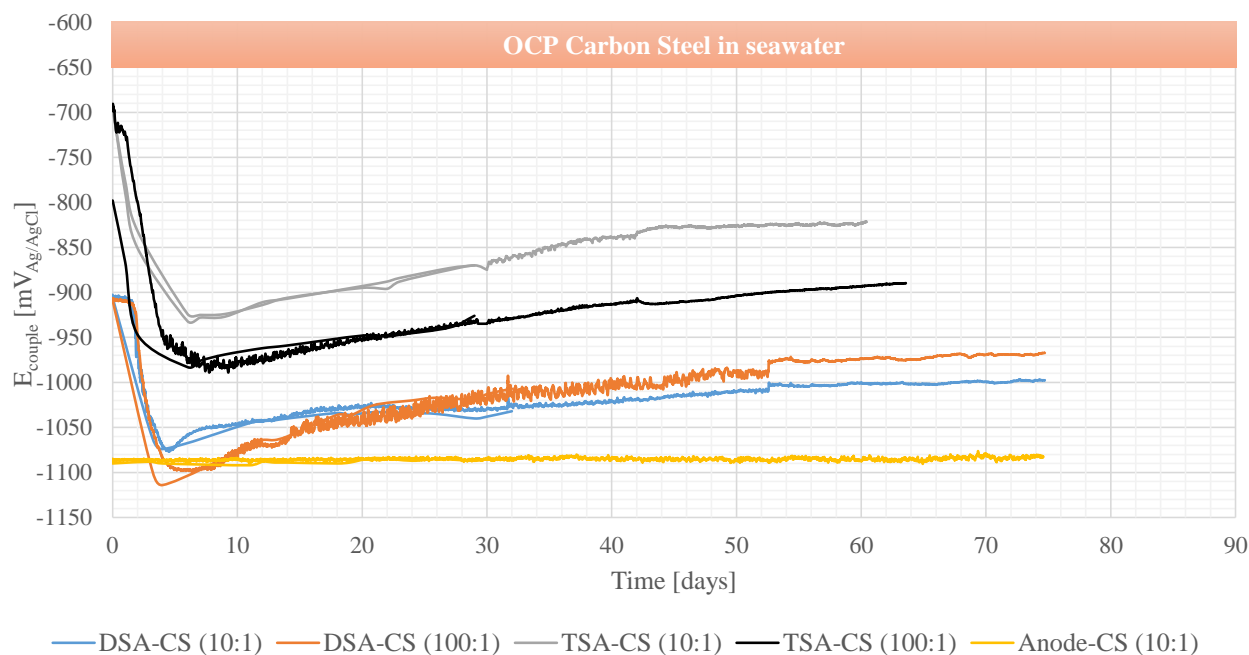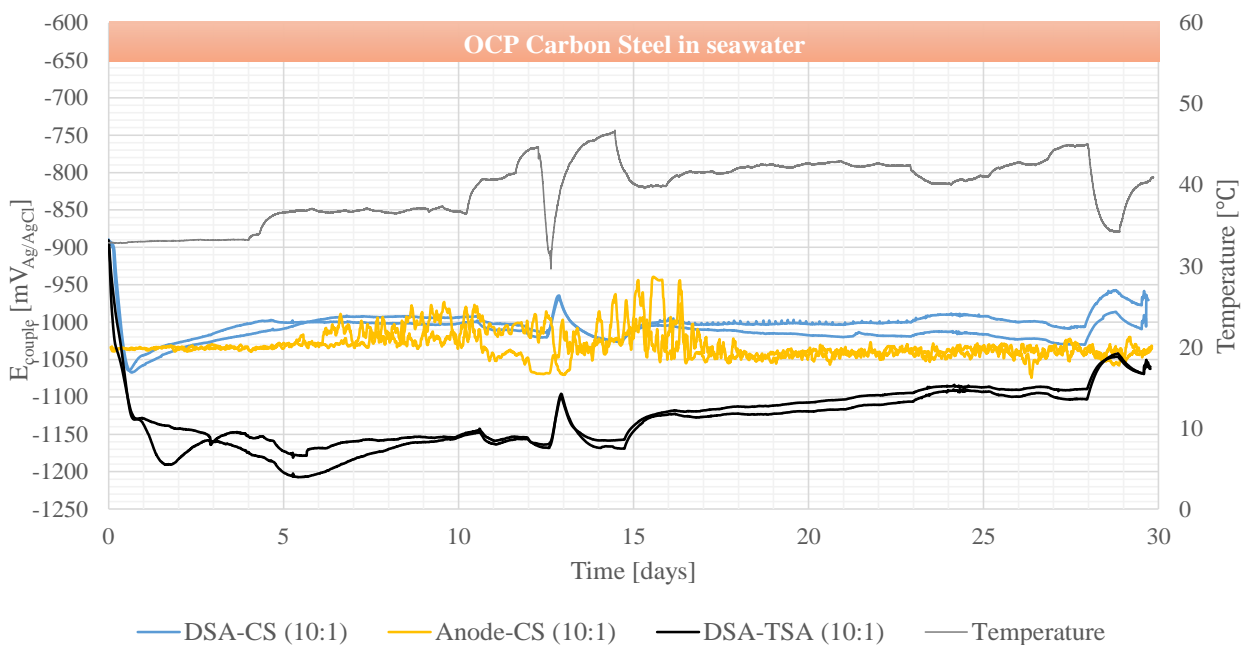**Figure 31** Couplings potential development for different couplings with area ratio 10:1, exposed to natural seawater at 40±5℃ under nearly stagnant conditions. The OCP for carbon steel in seawater is also marked.

5.2.1 **Coupling Potential Summary**

A summary of the galvanic coupling potentials at both 10℃ and 40℃ is presented in Table 10. The initial and 30 day values are based on the average potential of the two couplings. Two months measurements were only conducted on a few couplings. However, for the anode couplings at 10℃, stable values were achieve after 1 month and there were no indication that any change in their coupling potential would occur during the next month. The potential increased with time for all couplings, except for anode couplings whom kept a stable potential from the start of exposure. A close agreement in the coupling potential response between DSA-CS and Anode-CS could be observed at 40℃. The temperature effect is not clear, as the potential was more positive at 40℃ for DSA-CS (10:1) and Anode-CS (10:1) compared to exposure at 10℃.

Table 10 Coupling potential development at both 10℃ and 40℃.

| | Couplings Potential Development [$mV_{Ag/AgCl}$] | | | | | |
| | Temperature 10±2℃ | | | Temperature 40±5℃ | | |
Couplings (A-C)	Initial	1 Month	2 Months	Initial	1 month	2 Months
DSA-CS (10:1)	-1075	-1027	-1000	-1060	-1010	-
DSA-CS (100:1)	-1102	-1013	-975	-	-	-
DSA-TSA (10:1)	-	-	-	-1193	-1090	-
DSA-TSA (100:1)	-1122	-1035	-1010	-	-	-
TSA-CS (10:1)	-930	-875	-822			-
TSA-CS (100:1)	-976	-930	-890	-	-	-
Anode-CS (10:1)	-1090	-1085	-1090	-1035	-1035	-
Anode-DSA (1:1)	-1090	-1085	-	-	-	-
Anode-DSA (1:100)	-1080	-1075	-	-	-	-
Anode-TSA (1:1)	-1090	-1085	-	-	-	-

5.3 **Protection Current Density**

In this chapter, the protection current density measurements between all the different couplings are presented. The most active metal in the coupling has always been used as a reference (Anode-Cathode), hence positive current means that it supplies current to the less active metal. The notation of the coupling (A-C) means that A is assumed to be most active. Negative current density value therefore means a shift in the current direction. It is important to understand that the measured current between each couplings have been re-calculated to current density values by dividing the current with the area of the noble material, the cathode (A-C), i.e. dividing the current with the area of CS, TSA etc. depending on the galvanic coupling. At day 30, one out of two couplings were removed for surface examination.

Galvanic couplings at 10±2℃

In Figure 32, the current density as a function of time for DSA and TSA coupled to CS specimens with area ratio of 100:1 and 10:1 are presented. In addition, couplings between conventional sacrificial Al-Zn-In alloy and CS with area ration 10:1 are shown.

The current density increased substantial the first 5 days for the DSA-CS couplings, both 10:1 and 100:1. For three out of four couplings, the cathodic current density increased from approximately 300 mA/m^2 to around 1050 mA/m^2. For one of the DSA-CS (100:1) couplings a higher value was reached, 1400 mA/m^2. The current density decreased with time, ending up at 54 and 43 mA/m^2 for 10:1 and 100:1 respectively, after 60 days of exposure.

The initial current density value for Anode-CS (10:1) started at a higher value for CS than for the DSA couplings, between 700-1000 mA/m^2, before it gradually decreased with time. After 60 days, the current density was approximately 130 mA/m^2, more than doubled compared to DSA-CS (10:1). However, the current density still decreased and reached 100 mA/m^2 after 70 days.

Both TSA couplings, i.e. both area ratios, experienced much lower current density throughout the exposure period. The development with respect to the different area ratio are negligible. With an initial current density at 150-300 mA/m^2, the values slowly decreased with time. After 60 days, the current density were approximately 46 mA/m^2 and 97 mA/m^2 for TSA-CS (10:1) and TSA-CS (100:1) respectively.
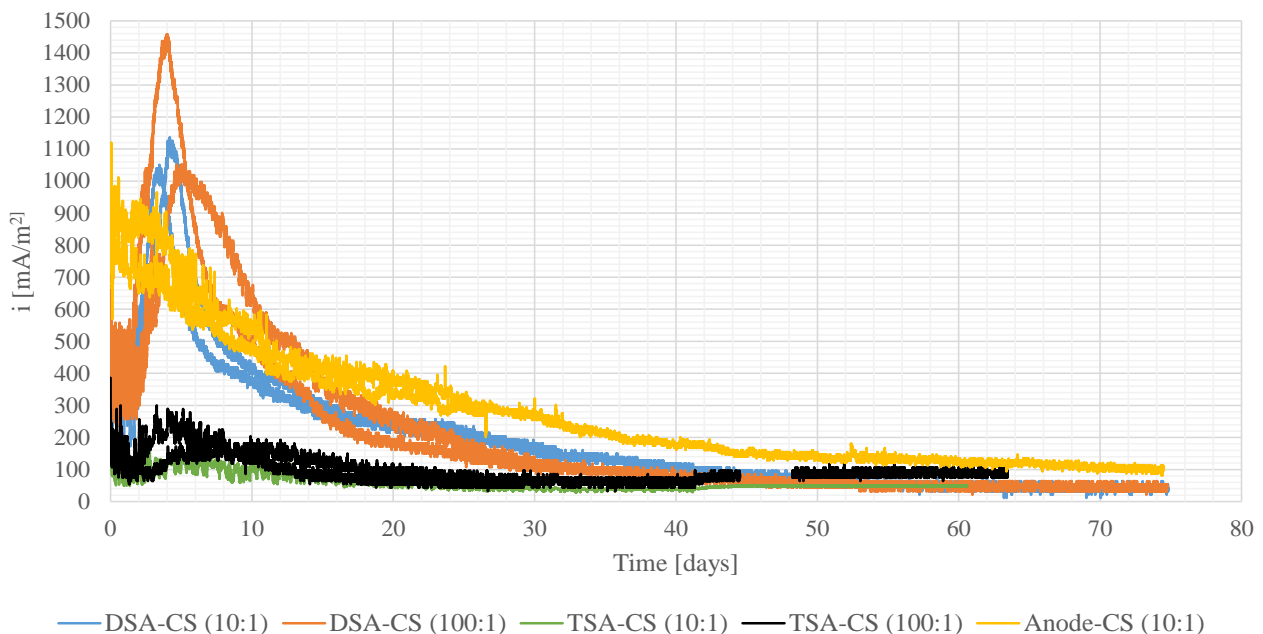
Figure 32 Current density development for CS in different couplings with area ratio 10:1 and 100:1, exposed to natural seawater at 10±2℃ under nearly stagnant conditions.

In Figure 33, both the coupling potential -and the current density development on CS for DSA-CS and Anode-CS with area ratio 10:1 are presented. For the Anode couplings, the potential was as mentioned stable the entire period of exposure. A close agreement in the current density response between anode and DSA can be observed.
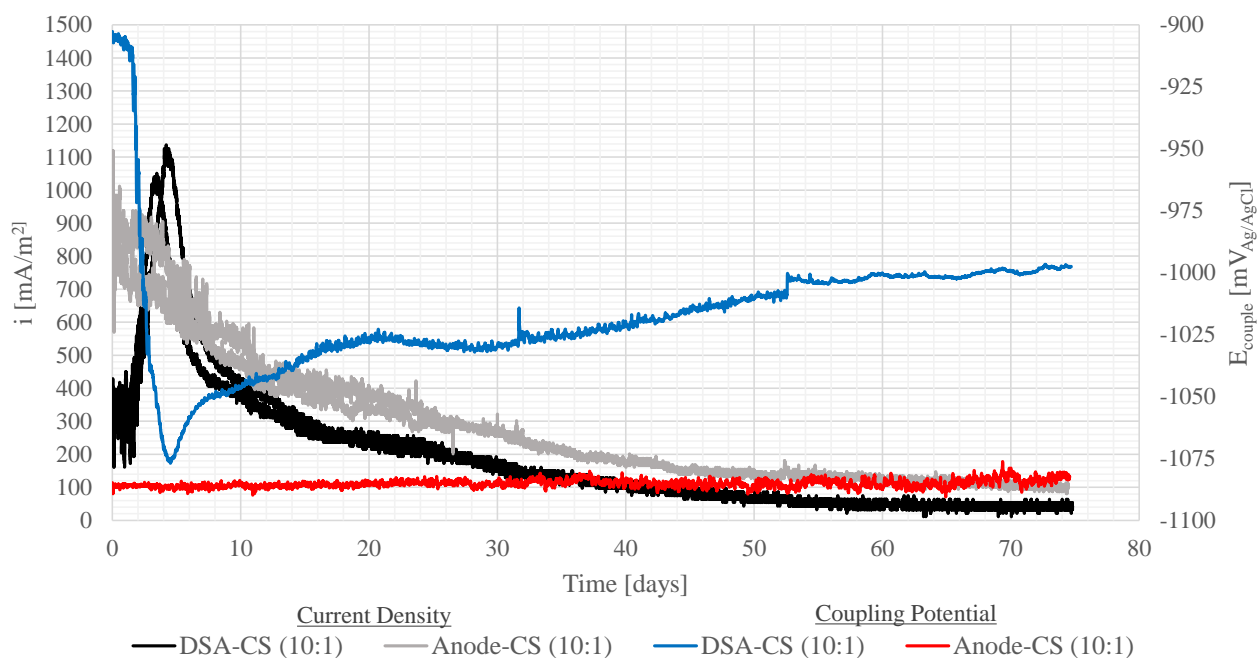
Figure 33 Coupling potential -and current density development on CS for DSA-CS (10:1) and Anode-CS (10:1), exposed to natural seawater at $10\pm2°C$ under nearly stagnant conditions over a period 50 days.

In Figure 34, the current density demand as a function of time for DSA and TSA coupled to anode specimens where the exposed area is equal, i.e. area ratio 1:1, are plotted. In addition, couplings between DSA-TSA (100:1) and Anode-DSA (1:100) are presented.

After 20 days, the current density for DSA in Anode-DSA (1:1) decreased from approximately 80 mA/m^2 to 14 mA/m^2 and 0 mA/m^2 for the two couplings. Further, one coupling continued its decreasing pattern to a negative value, i.e. the polarity was shifted due to DSA becomes more active than the anode specimen. The negative current density lasted for approximately 5 days reaching its lowest value of -7.5 mA/m^2 at day 22, before increasing again. After 31 days of exposure, this coupling was stopped at a current density of 17 mA/m^2. For the other coupling, the current density decreased at slower rate after 20 days of exposure. However, a change in current direction also occurred on this coupling at day 28. The negative current was of a lower value, -2 mA/m^2, and lasted for a shorter period of time as it slowly increased again reaching 6 mA/m^2 after 49 days. For the longest exposed coupling, the average current density demand for DSA was 11.7 mA/m^2. Due to a reduced numbers of DMS channels in the lab, continuously monitoring was cancelled.
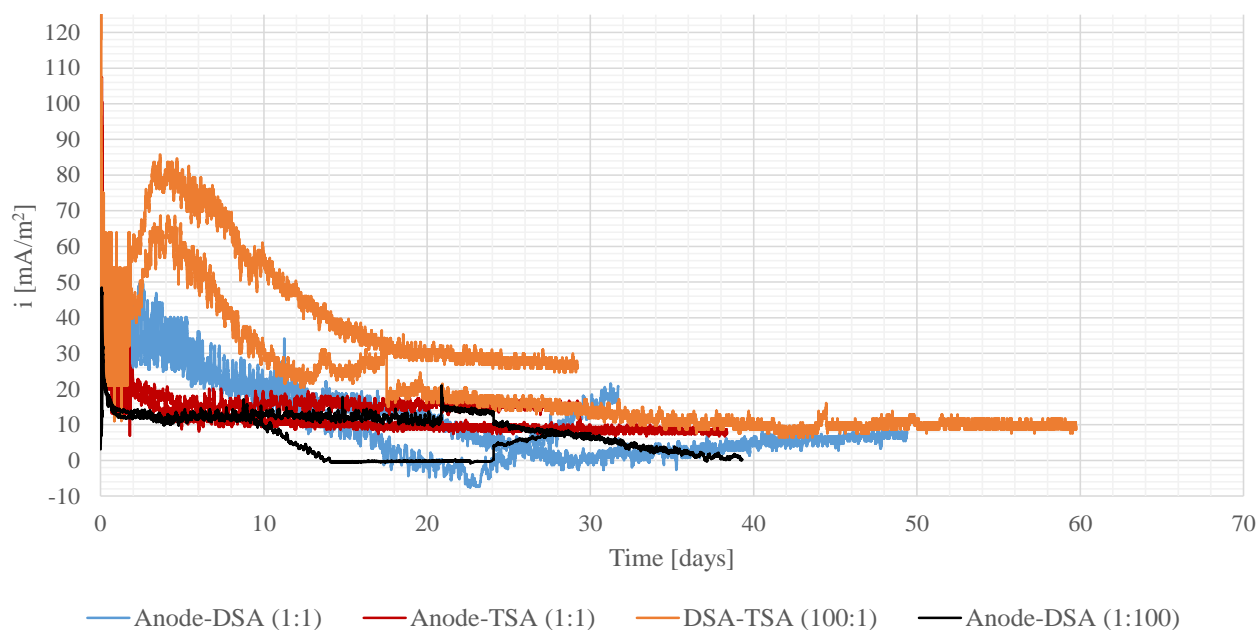
Figure 34 Current density development on DSA and TSA for different couplings with area ratio 1:1 and 100:1, exposed to natural seawater at $10\pm2°C$ under nearly stagnant conditions.

The initial current density for TSA in the Anode-TSA (1:1) couplings were approximately 90 mA/m^2, but decreased rapidly down to a value between 10 and 20 mA/m^2 for both couplings. From this point and throughout, the current density for the longest exposed coupling was approximately stable at 10 ± 2 mA/m^2, while the other coupling was at 15 ± 2 mA/m^2. The average current density for the longest exposed coupling was 10.8 mA/m^2.

DSA-TSA (100:1) experienced a substantial drop in the current density for TSA the first day, before it gradually increased the next 4 days to approximately 60 mA/m^2 and 80 mA/m^2 for both couplings. From this point, the current densities decreased throughout the exposure period, reaching 22 mA/m^2 after 30 days. For the longer exposed coupling, the decreasing rate continued to 11 mA/m^2 after 60 days. The sudden drop at day 17 for one coupling is most likely due to some connection error, and will not be further discussed.

The current density for DSA in the Anode-DSA (1:100) coupling stabilized rapidly to a value between 10 and 15 mA/m^2. On day 10, one of the coupling decreased to 0 mA/m^2, which was most likely caused by poor galvanic connection between the coupled specimens, while the other was stable. The non-current density was held until 24 days of exposure were the current density suddenly increased to 7.5 mA/m^2 before the coupling was removed. The longer exposed coupling experienced a declining pattern after day 24, approaching 0 mA/m^2 at the end.

Galvanic couplings at 40±5℃

In Figure 35 and Figure 36, the current density as a function of time is shown for galvanic couplings exposed at higher temperature, 40℃. Due to very high initial values, the current density development is divided into two figures. Figure 35 shows the total trend during the 30 days of exposure, while Figure 36 presents the last 15 days. Software problems resulted in loss of data between day 6-8 for DSA and anode couplings.

From Figure 35, very high initial values on CS in DSA-CS (10:1) and Anode-CS (10:1) coupling can be observed. The cathodic current density for the DSA couplings, i.e. current density to CS, reached its highest value of 4800 mA/m^2 during the first day, followed by a rapid decreasing trend, ending up below 100 mA/m^2 after 15 days. Some fluctuation in the current density can be observed. After 30 days, the average current density was 37 mA/m^2.

For the Anode coupling, the current density on CS is highest initially at immersion, but decreased fast during the first 15 days, from 3350 mA/m^2 to below 100 mA/m^2. For unknown reasons, a lot of fluctuation and instability was observed for this coupling, and a filter was used in order to remove noice. However, during the end both couplings seemed to have stabilized, ending up between 40 and 50 mA/m^2.

For the DSA-TSA (10:1) couplings, the current density on TSA is low throughout the entire period. The highest value was observed at day 14, at approximately 100 mA/m^2. From this point on, the curve decreased ending up between 30-40 mA/m^2.
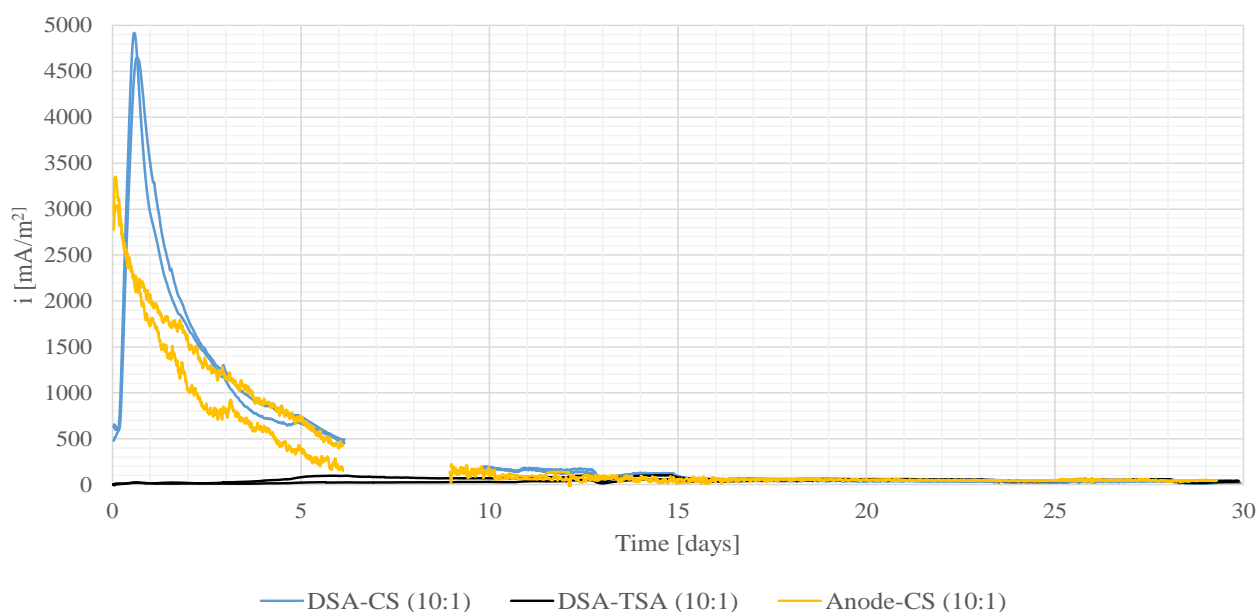
Figure 35 Current density development on CS and TSA for different couplings with area ratio 10:1, exposed to natural seawater at 40℃.
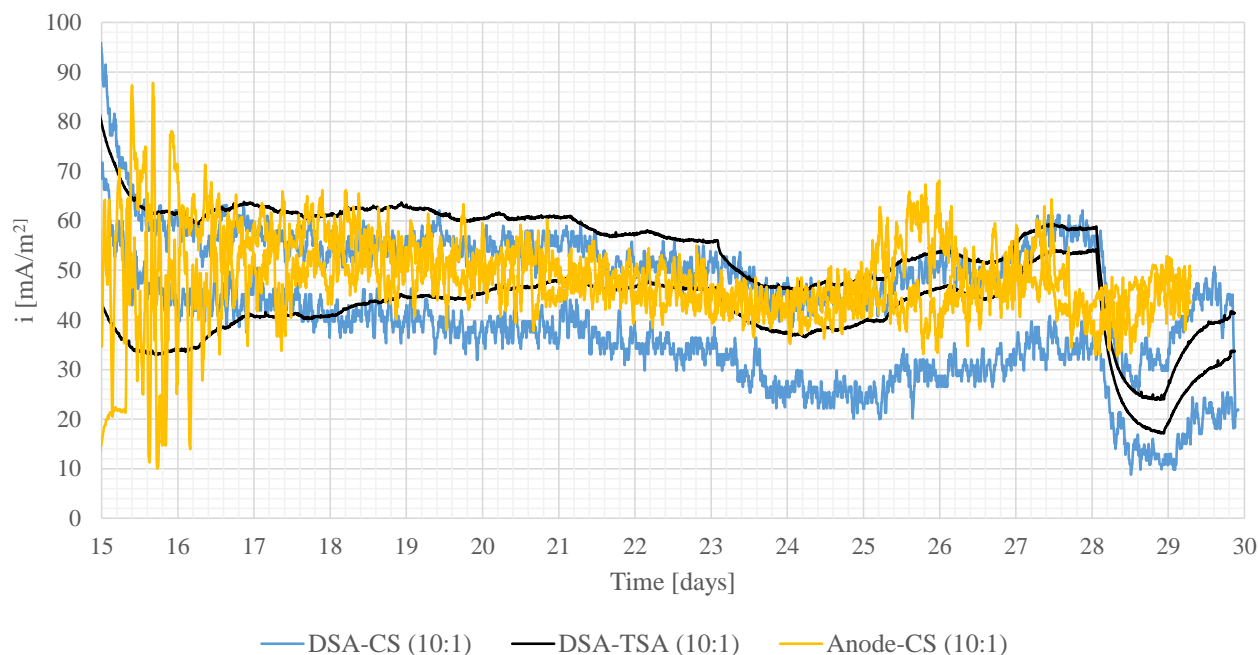
Figure 36 Current density development on CS and TSA for the last 15 days of exposure for couplings with area ratio 10:1 exposed to natural seawater at 40±5℃.

5.3.1 **Protection Current Density Summary**

A summary of the current density development for the galvanic couplings at both 10℃ and 40℃, can be seen in Table 10. The initial and 30 day values are based on the average current density of the two couplings. 2 months measurements were only conducted on a few couplings. It is important to understand that the measured current between each couplings have been re-calculated to current density values by dividing the current with the area of the noble material, the cathode (A-C), i.e. dividing the current with the area of CS, TSA etc. depending on the galvanic coupling. Thus, the summarized values are the cathodic current density.

Table 11 Current density development on the cathodic metal at both 10℃ and 40℃.

	Current density development [mA/m²]					
	Temperature 10±2℃			Temperature 40±5℃		
Couplings (A-C)	Initial	1 Month	2 Months	Initial	1 month	2 Months
DSA-CS (10:1)	1072	172	54	4800	38	-
DSA-CS (100:1)	1239	130	43	-	-	-
DSA-TSA (10:1)	-	-	-	64	37	-
DSA-TSA (100:1)	73	22	11	-	-	-
TSA-CS (10:1)	160	39	46	-	-	-
TSA-CS (100:1)	241	64	97	-	-	-
Anode-CS (10:1)	1035	259	130	3350	45	-
Anode-DSA (1:1)	75	8	-	-	-	-
Anode-DSA (1:100)	35	7	-	-	-	-
Anode-TSA (1:1)	90	12	-	-	-	-

5.4 **Potentiodynamic Polarization Curves**

Potentiodynamic polarization curves were recorded after 1, 8, 15 and 30 days of exposure for all the freely exposed test materials. This was only done for specimens exposed at 10℃, whereas for DSA and TSA specimens freely exposed at 40℃, polarization curves were only obtained at day 30. The result for the 10℃ are presented first, followed by the 40℃. A summary is given in Table 12.

Polarization at 10℃

In Figure 37 the anodic and cathodic polarization curves for traditional sacrificial anode and corresponding extruded wire pieces are presented. For the sacrificial anode, insignificant changes in the polarization curves during 30 days can be observed. The anodic dissolution rate increased with increasing potential, as expected for an active metal. The active dissolution continued in a linear pattern, until reaching a potential of -800 mV$_{Ag/AgCl}$. At this potential until the end at -600 mV$_{Ag/AgCl}$, the slope increased.

At day one, the polarization curves were only obtained to ±300 mV$_{Ag/AgCl}$, as indicated. At this potential, the cathodic current density was lowest at day one compared to the other days. The cathodic curves for day 8, 15 and 30 were almost identical, with a linear decreasing pattern.

The polarization curves for the wire pieces experienced a shift to the left at each day of polarization. This indicated that the corrosion current (i_{corr}), i.e. corrosion rate decreased in some degree with time, or that the exposed area is reduced with time as corrosion products covers the surface. Like the anode, high dissolution rate can be observed as the current density increased significantly with increased potential.

No passive behavior were observed for the anode and the corresponding wire.
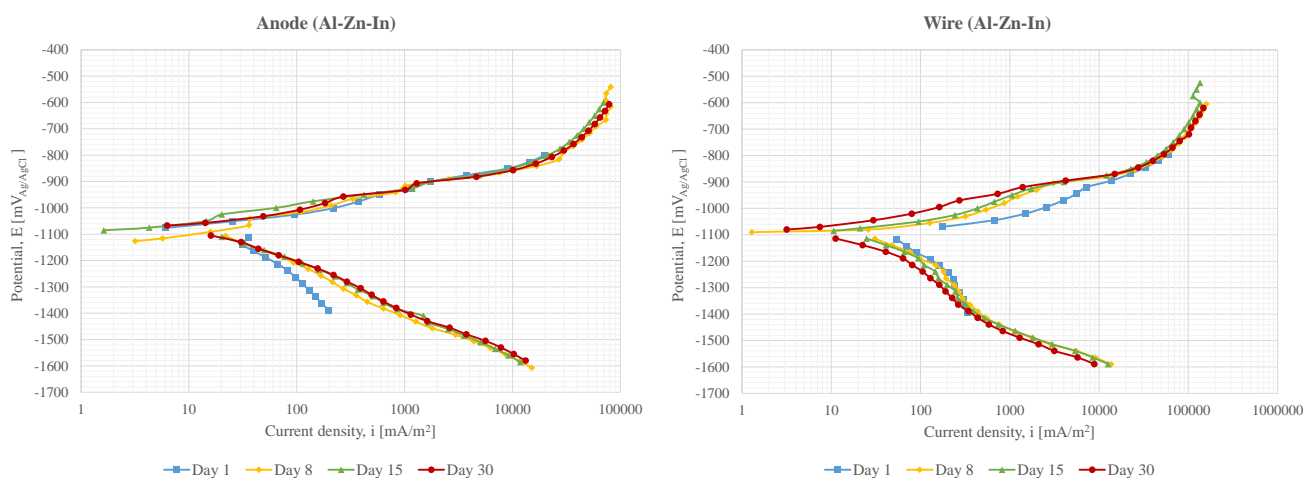
Figure 37 Polarization Curves for traditional sacrificial aluminum anode and the corresponding extruded wire, obtained after 1, 8, 15 and 30 days of exposure to natural seawater at 10±2℃ under nearly stagnant conditions.

Comparing the polarization curves for the anode and the wire piece obtained at day 30, the inequities are small, as shown in Figure 38. The anodic corrosion current density with increased potential for both specimens are similar until reaching a potential of approximately −900 mV$_{Ag/AgCl}$. At this potential and above, the current density for the wire piece was in fact higher.

The opposite change in the cathodic curves can be seen. From OCP to −1200 mV$_{Ag/AgCl}$, both curves are almost identical. At a potential of −1200 mV$_{Ag/AgCl}$, the cathodic curve for the wire specimen experienced a slightly drop, reducing the cathodic current density in comparison to the anode. The current density for the wire increased more at potentials above −1500 mV$_{Ag/AgCl}$, moving towards the anode curve.
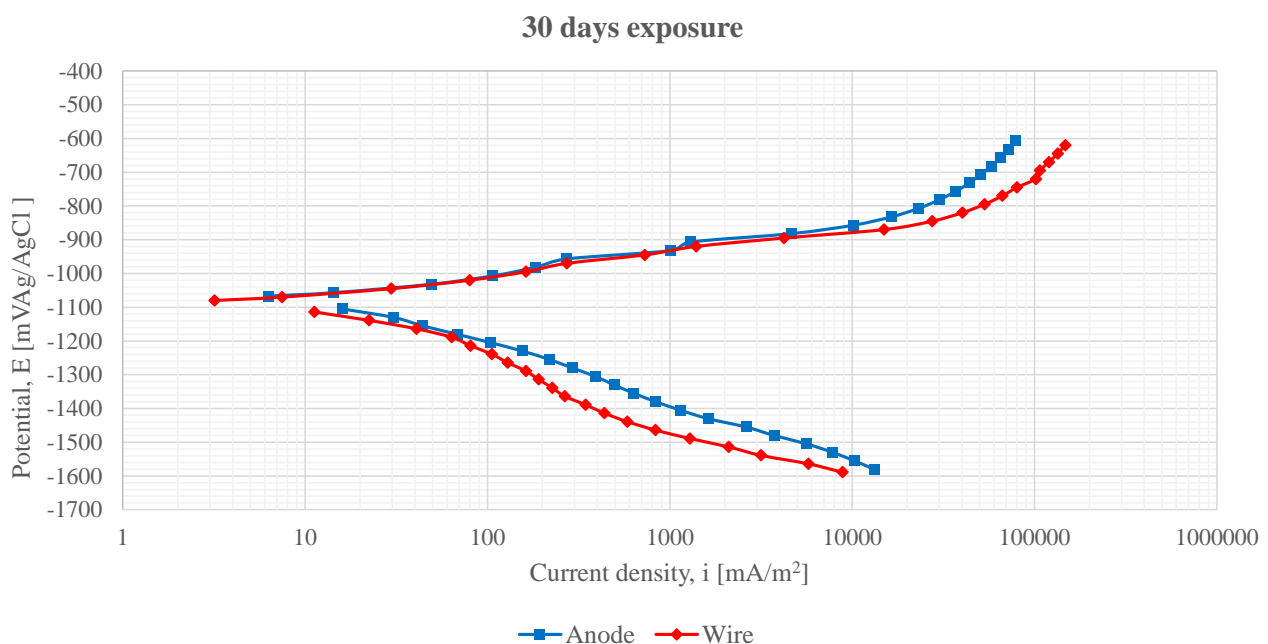
Figure 38 Polarization curves for conventional anode specimen and the corresponding extruded wire piece, obtained after 30 days exposure to natural seawater at 10±2℃ under nearly stagnant conditions.

In Figure 39, the anodic- and cathodic polarization curves for DSA and TSA are presented. At day one, it can be noticed that the OCP for both specimens are quite high due to only one day exposure. A more negative OCP can be observed at day 8 and 15, followed by an increase at day 30.

With increasing potential in a range between 100-200 mV$_{Ag/AgCl}$ from OCP, the anodic curves for DSA experienced a relatively steep slope, i.e. small changes in the current density with increased potential, indicating some passive behavior. At higher potential, −882 mV$_{Ag/AgCl}$ for day 1, the critical pitting potential is reached and more active dissolution occurs as the curve formed nearly a plateau. For day 8, 15 and 30, the critical pitting potential has decreased to −916 mV$_{Ag/AgCl}$.
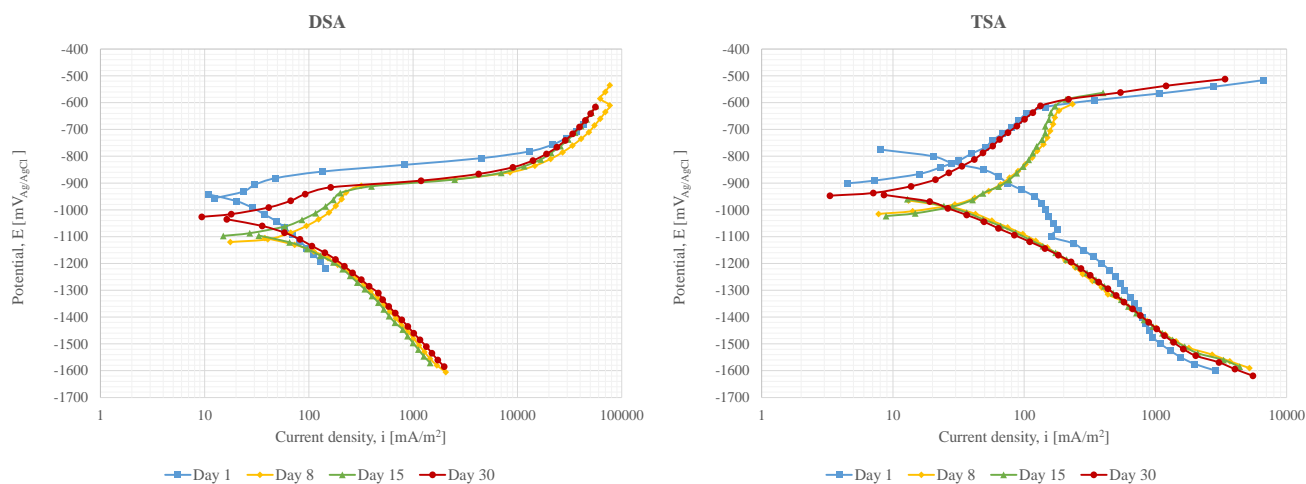
Figure 39 Polarization curves for DSA and TSA obtained after 1, 8, 15 and 30 days of exposure to natural seawater at 10±2℃ under nearly stagnant conditions.

Except for day one, the cathodic development for DSA are approximately identical, except from the higher OCP on day 30. With decreasing potential, each plot moves closer and closer to each other, i.e. with low potential the changes in the current density is reduced. From −1300 mV$_{Ag/AgCl}$, a relatively steep linear curves can be observed.

TSA experienced the same initial steep sloop for the anodic curves as for DSA. However, the sloop continued over a much longer potential range than for DSA. From OCP to −600 mV$_{Ag/AgCl}$, relatively small changes can be observed in the current density from ≈10-100 mA/m². At day 8 and 15, there are clear tendency to passive behavior from −900 mV$_{Ag/AgCl}$ to −600 mV$_{Ag/AgCl}$, i.e. passivation of the surface contributing to low steady state current density value until breakdown of the protective film occurs when reaching a critical potential value, the pitting potential. The pitting potential was approximately −600 mV$_{Ag/AgCl}$ for all days, see Table 12. At this potential and above, the curve flattens and big changes in the current density per mV$_{Ag/AgCl}$ can be observed. Notice, that at day 1 and 30, polarization was conducted up to −500 mV$_{Ag/AgCl}$.

The cathodic curves for TSA followed the exact same pattern with increasing potential, except for day one. Due to some instability, this curve will not be further discussed. The OCP for TSA is at that point very high, −775 mV$_{Ag/AgCl}$, and therefore not valid.

In Figure 40, the polarization curves obtained after 30 days of exposure for DSA, TSA and conventional Al-Zn-In anode are presented. There are clear differences on the anodic curves. For DSA and Anode, the development for the anodic polarization curves are quite similar. However, at potentials from OCP up to −900 mV$_{Ag/AgCl}$, more active dissolution of the anode can be observed, i.e. the current density is higher. At more positive potentials, the deviation is reduced. For TSA, active dissolution does not encounter until reaching a potential of approximately −600 mV$_{Ag/AgCl}$, i.e. the pitting potential.
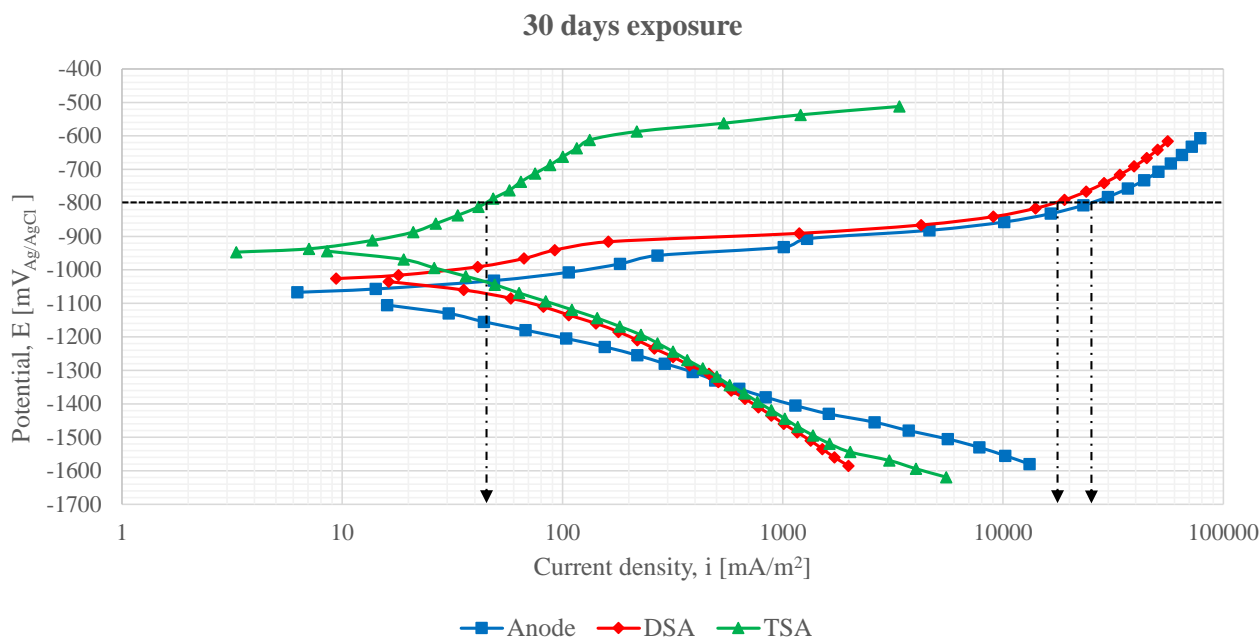
Figure 40 Polarization curves for Anode, DSA and TSA obtained after 30 days of exposure to natural seawater at 10±2℃ under nearly stagnant conditions.

The protective potential for carbon and low-alloy steel is −800 mV$_{Ag/AgCl}$, according to DNV-RP-B401 [7]. At this potential, TSA can only deliver a current density of 50 mA/m² in contrary to DSA and Anode which can supply a current density of 19,000 mA/m² and 23,000 mA/m², respectively according to the polarization curves after 30 days of exposure. This is illustrated in Figure 40.

The cathodic polarization curves for DSA and TSA are almost identical from −1100 mV$_{Ag/AgCl}$ to −1550 mV$_{Ag/AgCl}$. From OCP down to the intersection between the cathodic curves for the anode at −1350 mV$_{Ag/AgCl}$, the current density for DSA and TSA are higher compared to the anode. At lower potential, the slope increased for DSA and TSA, resulting in a lower current density in contrary to the anode which experienced a decrease in the slope, i.e. the curve flattens out (absolute values).

5.4.1 Potentiodynamic Polarization Summary

An overview of the electrochemical properties for polarized test specimens after 1 and 30 days of exposure are presented in Table 12. Decreasing OCP with time can be observed on DSA and TSA, in contrary to Anode –and wire specimen which stabilized at OCP the first day of immersion. The corrosion current density decreased with time for all specimens, except for DSA which increased from 12.07 mA/m² to 28.18 mA/m². A clear passive behavior was only observed on TSA specimens at day 8 and 15 at 100 mA/m², however a tendency was observed on day 1 and 30, and are therefore noted in Table 12. The values for the corrosion current density and the Tafel constants were obtained from the overvoltage curves, which can be found in Appendix C – Corrosion Rate Calculation.

Table 12 Overview of the electrochemical properties for test specimens at day 1 and day 30 at 10℃.

	DSA		TSA		Anode		Wire	
	Day 1	Day 30	Day1	Day 30	Day 1	Day 30	Day 1	Day 30
OCP, E_{corr}[mV$_{Ag/AgCl}$]	−917	−1010	−750	−919	−1088	−1080	−1093	−1089
Corrosion Current Density, i_{corr} [mA/m^2]	12.07	28.18	15.73	14.45	36.31	13.18	53.70	12.58
Anodic Tafel Constant, b_a [mV/dec]	42.86	128.87	299.52	253.34	108.11	86.34	52.63	89.19
Cathodic Tafel Constant, b_c [mV/dec]	−101.0	−216.2	−188.9	-213.9	−406.8	−163.2	−243.9	−268.5
Passive Current Density, i_p [mA/m^2]	≈60	≈60	≈50	≈50	-	-	-	-
Pitting Potential, E_p [mV$_{Ag/AgCl}$]	−882	−916	−600	−600	-	-	-	-

Polarization at 40℃

In Figure 41, polarization curves obtained after 30 days of exposure for DSA and TSA specimens, freely exposed to natural seawater at 40℃ are presented. In addition, the polarization curves obtained at 10℃ are plotted in order to distinguish the influence of increased temperature. It can be observed that during increased temperature, the OCP decreased as mentioned in Section 5.1. Further, increased tendency of passivation for DSA can be observed at 40℃, relatively small change in current density with increased potential from OCP to −888 mV$_{Ag/AgCl}$. Form this point on, the anodic curve for DSA flattens out as active dissolution initiates. The pitting potential increased from −916 to −888 mV$_{Ag/AgCl}$. The same is observed for TSA, where the pitting potential increased from E_{P1} = −600 mV$_{Ag/AgCl}$ to E_{P2} = −550 mV$_{Ag/AgCl}$.
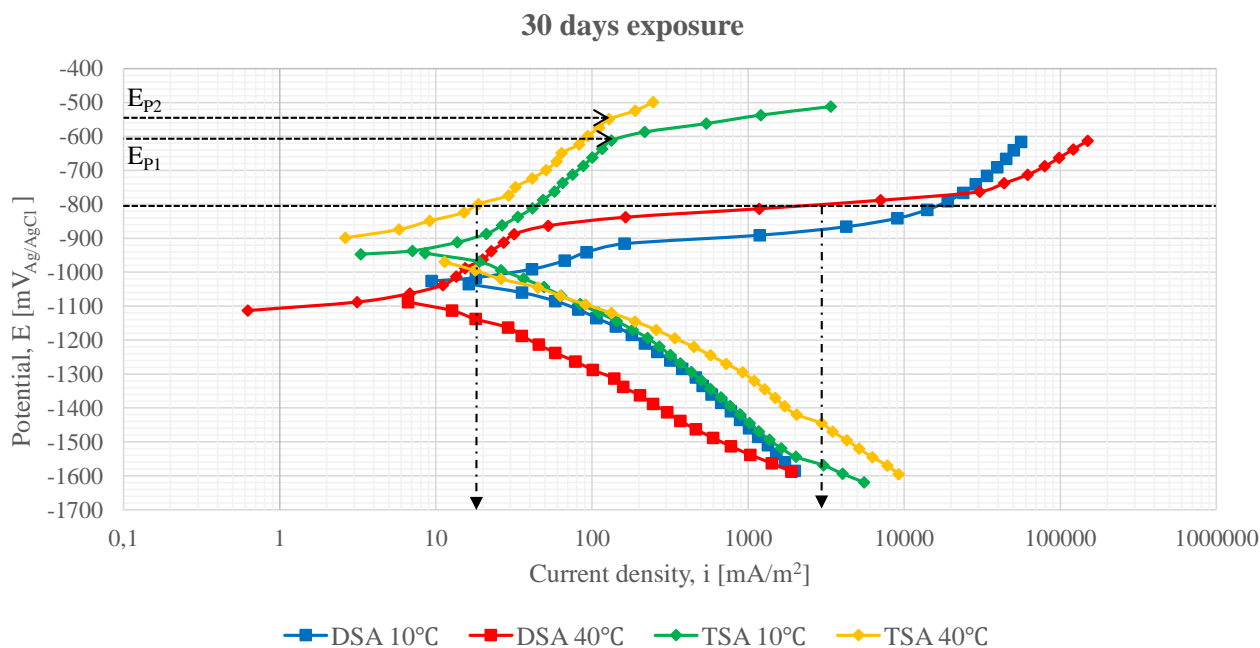
Figure 41 Polarization curves for DSA and TSA obtained after 30 days exposed to natural seawater at both 10 and 40℃, under nearly stagnate conditions.

Overall, the increased temperature shifted the polarization curves to the left, indicating reduced anodic current for protection. At -800 mV$_{Ag/AgCl}$, the protective potential for CS according to DNV-RP-B401, TSA and DSA can supply approximately 19 mA/m^2 and 2500 mA/m^2, as illustrated in Figure 41. The corresponding values at 10℃ are 50 mA/m^2 respective 19,000 mA/m^2.

An overview of the electrochemical properties for DSA and TSA after 30 days of exposure at both 10 and 40℃ can be seen in Table 13. From the table, it can be seen that the corrosion current density, i.e. the corrosion rate, was lower at high temperature, which is the opposite effect according to literature [4, 58]. Also, an increase in the anodic Tafel constant can be observed for DSA at 40℃, whereas the cathodic Tafel is unchanged.

Table 13 Electrochemical properties for DSA and TSA after 30 days of exposure at both 10 and 40℃

	DSA		**TSA**	
	Temperature		Temperature	
	10℃	40℃	10℃	40℃
OCP, E_{corr} [mV$_{Ag/AgCl}$]	-1010	-1063	-919	-945
Corrosion Current Density, i_{corr} [mA/m^2]	28.18	9,33	14.45	7.11
Corrosion rate, CR [μm /year]*	31	11	17	8.6
Anodic Tafel Constant, b_a [mV/dec]	128.87	318.44	253.34	235,49
Cathodic Tafel Constant, b_c [mV/dec]	-216.19	-217.98	-213.87	$-159,92$
Passive Current Density, i_p [mA/m^2]	≈60	≈20	≈50	≈50
Pitting Potential, E_p [mV$_{Ag/AgCl}$]	-916	-888	-600	-550

*From Faraday's Law, with physical data according to Table C. 1

5.5 **Corrosion Rate**

Freely exposed at 10℃

The calculated corrosion rate development over time for the freely exposed specimens at 10℃, are presented in Figure 42. Only measurements obtained by Tafel extrapolation of the polarization curves are shown. The LPR results can be found in Appendic C, Figure C. 1.The calculations were performed as described in Section 2.2.5. Physical data and LPR values can be found in Appendix C – Corrosion Rate Calculation, Table C. 2. The porosity of the coatings (TSA and DSA) was not found. Therefore, a rather conservative value of 10 % was used for both coatings. This implies that the density for pure aluminum (2.7 g/cm^3) and Al-Zn-In anode (2.95 g/cm^3) are reduced to 2.43g/cm^3 and 2.65g/cm^3 for respective TSA and DSA in order to provide more accurate values regarding the corrosion rate.
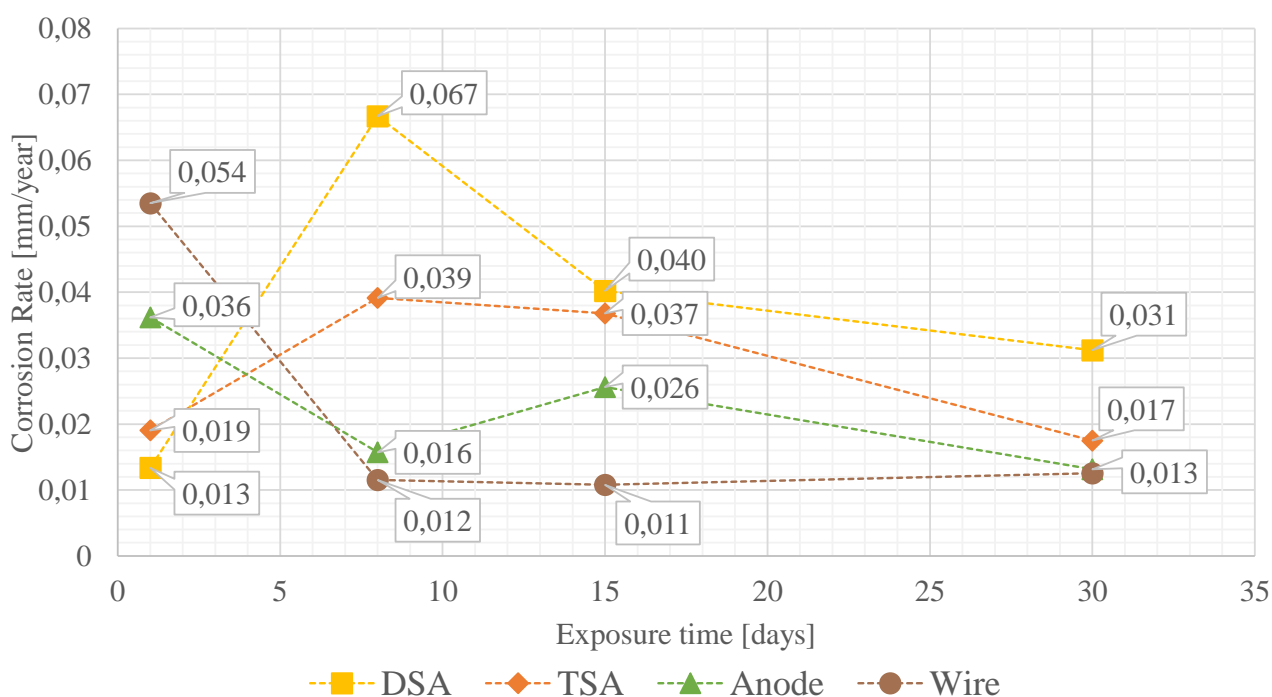
Figure 42 The corrosion rate development as a function of time, obtained from Tafel extrapolation of the polarization curves.

DSA and TSA experienced a low corrosion rate at respective 0.013 and 0.019 mm/year, measured after 1 day of exposure. During the first 8 days of exposure, all specimens experienced their highest corrosion rate values. DSA and TSA reached a value of 0.069 and 0.039 mm/year respectively at day 8. However, the value for TSA at day 1 may not be completely representative due to instabilities in the polarization curves which made it difficult to obtain reasonable Tafel constants. For the anode -and wire specimens, the highest corrosion rates were observed at day 1 with values at respectively 0.036 and 0.054 mm/year.

The corrosion rate for all specimens decreased with time from day 8 until the end of exposure at day 30. DSA and TSA, reached a value of 0.031 and 0.017 mm/year respectively after 30 days of exposure. The corrosion rate for the anode and wire are identical and somewhat lower, at 0.013 mm/year. Some, but small variation can be observed in the two corrosion rate calculation when comparing their results in Figure C. 1.

Freely exposed at 40℃

Corrosion rate measurements were, as mentioned, only obtained for DSA and TSA specimens exposed at 40℃ after 30 days of exposure. The results can be seen in Figure 43, where a) and b) presents the graphical and LRP results, respectively. It can be seen, that the corrosion rate is higher at 10℃ versus at 40℃. This deviates from earlier studies and theory regarding the influence of temperature on the corrosion rate as mentioned in section 2.2.3 [58].
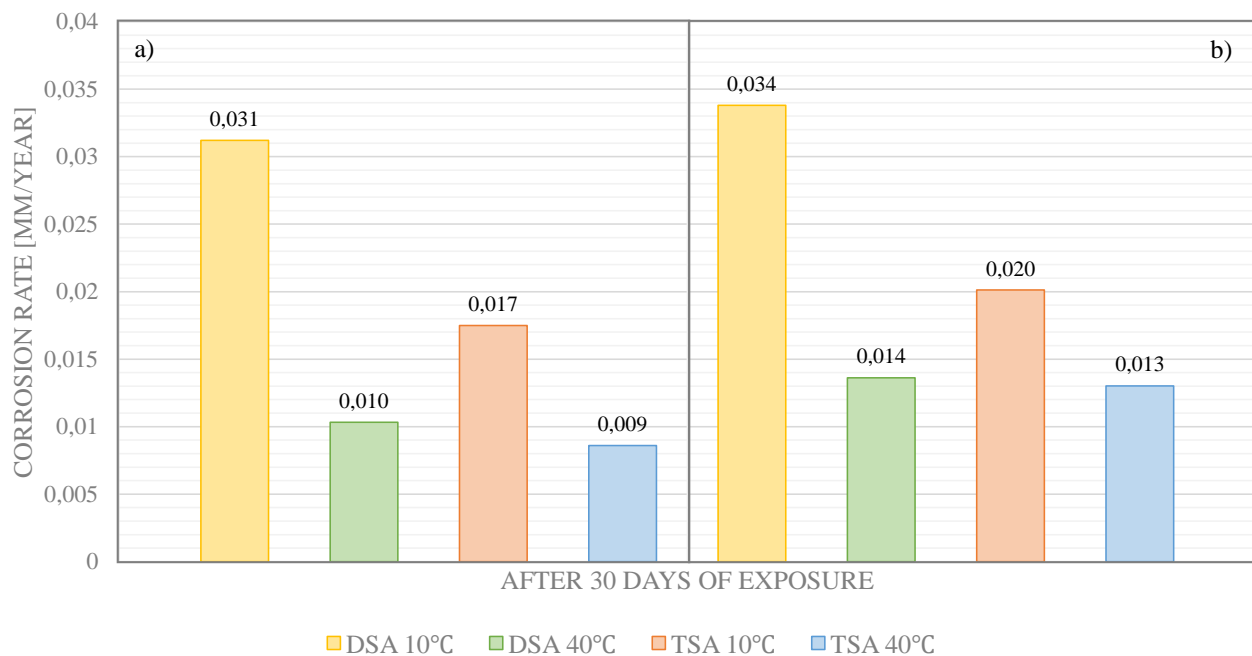
Figure 43 Corrosion rate of DSA and TSA after 30 days of exposure to natural seawater at both 10℃ and 40℃, obtained from a) Tafel extrapolation and b) LPR measurements

6   Surface Characterization

In this chapter, the results from coating adhesion test are presented in addition to SEM and EDS analysis. Firstly, the results from prior exposure analysis are presented. These results will be used as a reference for the coating thickness, as well as the fabrication measurements performed on the DSA plates, Table 6. Secondly, the results from post exposure analysis performed on specific specimens as mentioned in Section 4.5.2 are presented.

6.1 Adhesion Pull-Off test

In this section, the results of the adhesion pull-off test for thermally sprayed DSA and TSA are presented. Both, un-exposed and exposed specimens have been tested in order to determine if any adhesion loss can be observed after 30 days of exposure. For exposed specimen, thermally sprayed specimens which have been galvanic coupled to CS with area ratio of 100:1 were tested. As mentioned in Section 4.5.1, a test was also performed on a special thermally sprayed plate with different thickness of DSA. However, the specified coating thickness achieved from Total Coating was not right. Examination in SEM showed that the coating thicknesses were approximately 1 mm, 1.75 mm and 1.5 mm for top, middle and bottom layer respectively, and not 0.3 mm, 0.6 mm and 1.0 mm as shown in Figure 26. Due to the uncertainties regarding the dual layer ratio, i.e. thickness of TSA vs. DSA, the results from this test can be found in Appendix E – Adhesion Pull-Off Test.

Unexposed Specimens

In Table 14, adhesion test results for un-exposed TSA and DSA are presented. Higher adhesion for single layer of TSA can be observed, with an average applied tensile strength of 13.53 MPa. The mode of failure were cohesive failure for all tests, i.e. fracture in the TSA coating.

For un-exposed DSA, the average tensile strength was 8.82 MPa, 34.8 % lower than what was observed for un-exposed TSA. 7 out of 8 failure modes were 100% adhesive failure between the first and second coating (100% B/C), i.e. fracture in the interface between DSA and TSA. For one test, cohesive failure in the first coating was observed, rupture in the TSA layer.

Exposed Specimens (30 days)

In Table 15, the adhesion test results for DSA and TSA specimens galvanic coupled to CS with area ratio of 100:1, exposed for 30 days in natural seawater at 10℃ are presented. It is obvious that the adhesion strength for both coatings have increased after exposure. The average applied tensile strengths were 12.49 and 18.35 MPa for DSA and TSA respectively. 3 out of 4 fractures for DSA occurred in the interface between DSA and TSA, whereas for one dolly the fracture were approximately 75% in the DSA layer and 35% in TSA, see Figure 44.

Table 14 Results from adhesion pull-off test for un-exposed specimens.

Dollies	DSA MPa	DSA Failure mode	TSA MPa	TSA Failure mode
1.	9.42	100% B/C	14.04	100% B
2.	9.24	100% B/C	13.87	100% B
3.	8.18	100% B/C	12.80	100% B
4.	7.47	100% B	13.87	100% B
5.	10.13	100% B/C	12.80	100% B
6.	8.53	100% B/C	13.33	100% B
7.	7.47	100% B/C	13.51	100% B
8.	10.13	100% B/C	14.04	100% B
Avg.	8.82 MPa		13.53 MPa	

A Cohesive failure of the substrate
A/B Adhesive failure between substrate and first coat
B Cohesive failure of first coat
B/C Adhesive failure between first and second coats

Table 15 Results of adhesion pull-off test for thermally sprayed specimens exposed for 30 days in natural seawater at 10±2℃.

Dollies	DSA MPa	DSA Failure mode	TSA MPa	TSA Failure mode
1.	13,33	100% B/C	17.95	100% B
2.	12.80	100% B/C	19.20	100% B
3.	12,98	100% B/C	19.02	100% B
4.	10.84	75% B /35% C	17.24	100% B
Avg.	12.49 MPa		18.35 MPa	
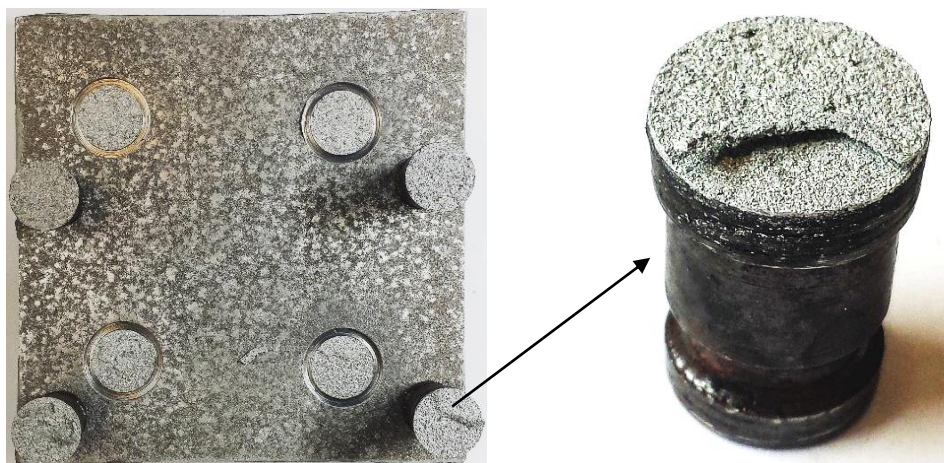
Figure 44 Pull-off test on DSA specimen with dimension 100 × 100 mm, Showing adhesive failure in the TSA-DSA interface, which have been coupled to CS for 30 days

6.2 **Surface Examination**

6.2.1 **Prior Exposure**

In Figure 45, the cross-section of the DSA surface prior to exposure is shown. The degree of zinc distinguishes the TSA layer from the DSA layer. Unevenness in the coating thickness can be seen in Figure 46. However, a thickness of approximately 1000 µm and 300 µm will be used as a reference in order to evaluate the degradation after 30 days of exposure.
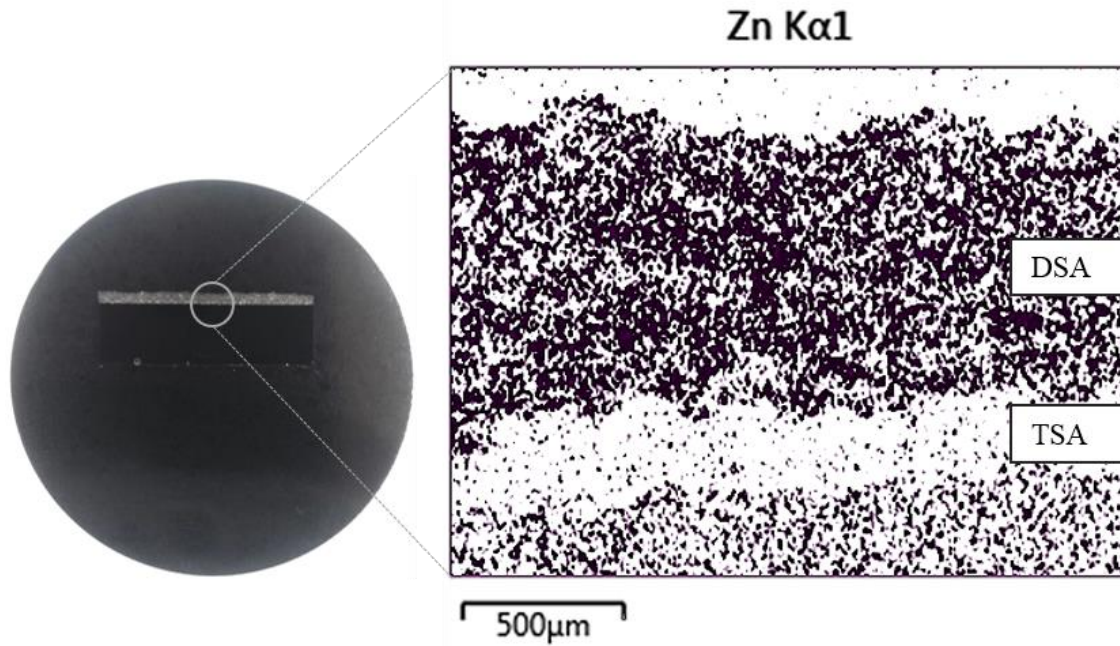
Figure 45 Embedded DSA piece polished to 1 µm with corresponding EDS (only Zn elements) showing the first and second thermally sprayed layer of TSA and DSA respectively.
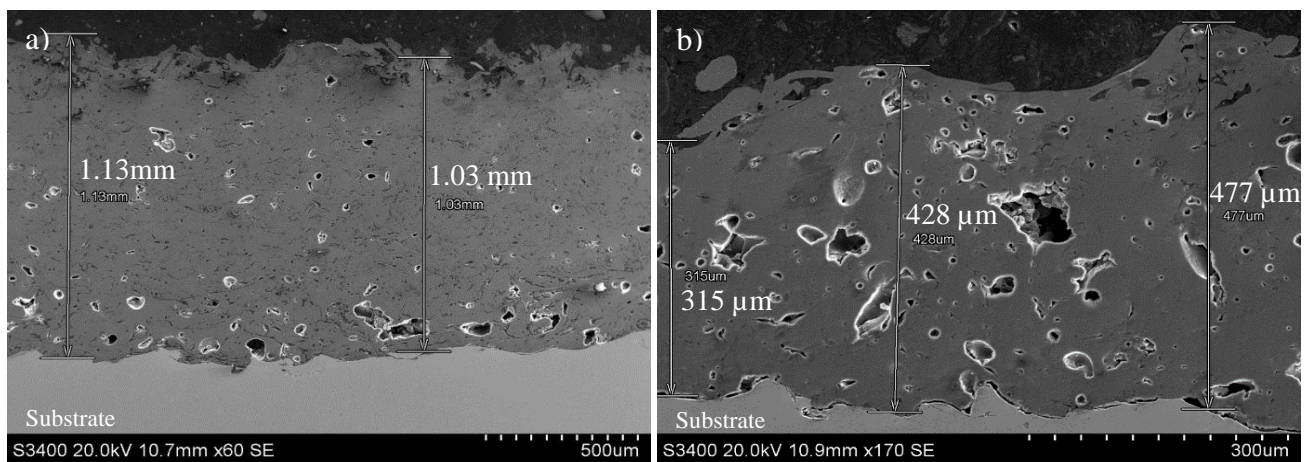
Figure 46 Cross-section of a) DSA and b) TSA, with their coating thickness.

6.2.2 **Post Exposure**

Freely Exposed Specimens at 10℃

In Figure 47, SEM images of freely exposed DSA specimen after 30 days of exposure are shown, both cross-section and surface. No degradation in the coating thickness was observed. However, EDS image with surface mapping showed some areas rich of iron.

Cross-Section   Surface
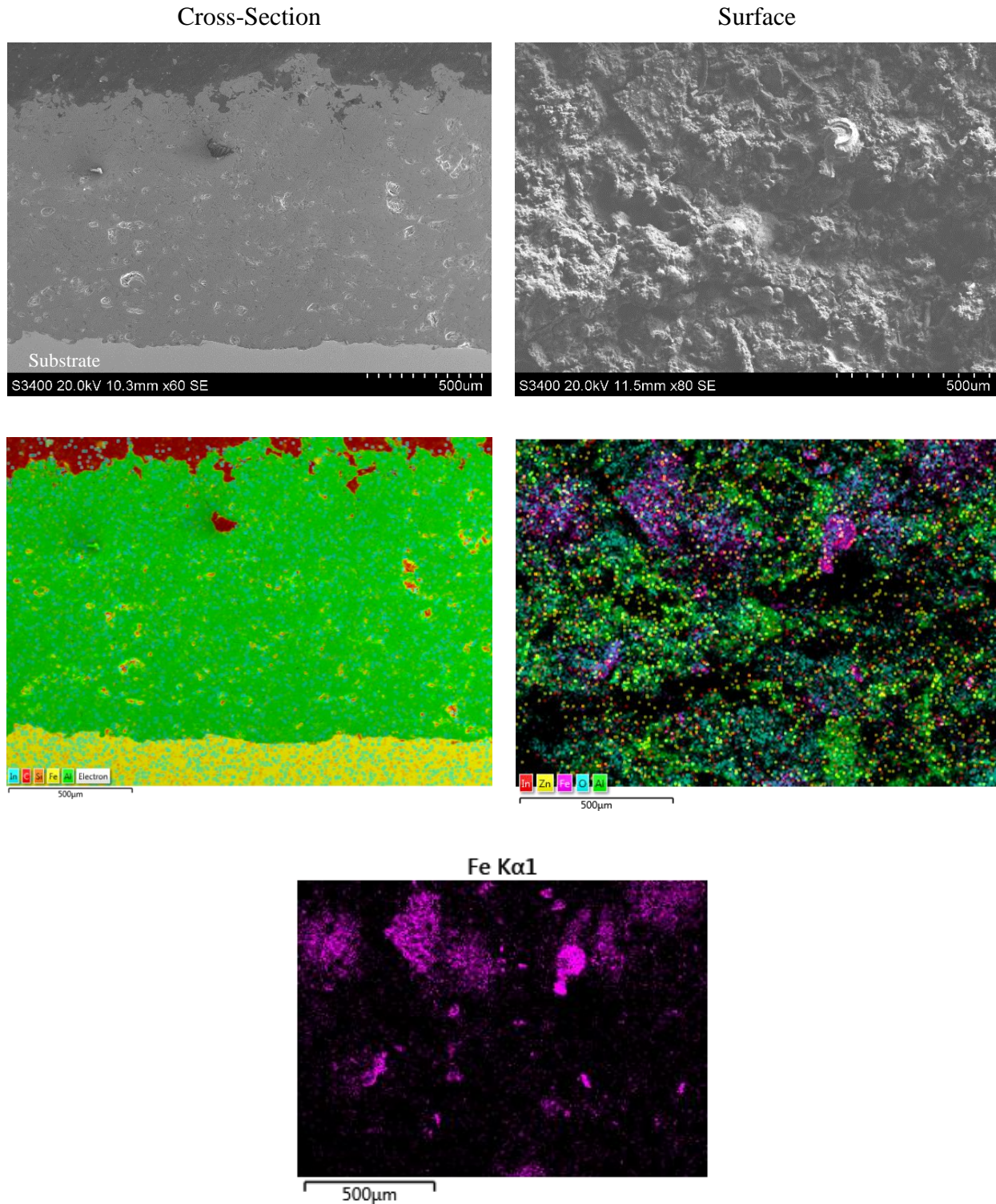
Figure 47 SEM and EDS mapping of DSA specimen exposed for 30 days, showing some iron rich areas. No degradation in coating thickness observed.

72

In Figure 48, SEM and EDS images of the cross-section for freely exposed TSA specimen after 30 days of exposure are shown. Some degradation in the coating thickness can be seen in SEM image a), if using a reference coating thickness of 300 µm. The highest and lowest measured thickness were respectively 315 µm and 201 µm, contributing to an average value of 258 µm. High content of oxygen was detected in the coating-substrate interface with EDS mapping, as marked in image b). Point mapping in this area shows high content of oxygen and iron, as can be seen in the corresponding EDS spectra. In Table 16, the results of point mapping for all marked spectrum in image b) are shown. In addition to high content of iron and oxygen on spectrum 5 and 6, spectrum 10 taken on a particle located in the coating shows similar contents.
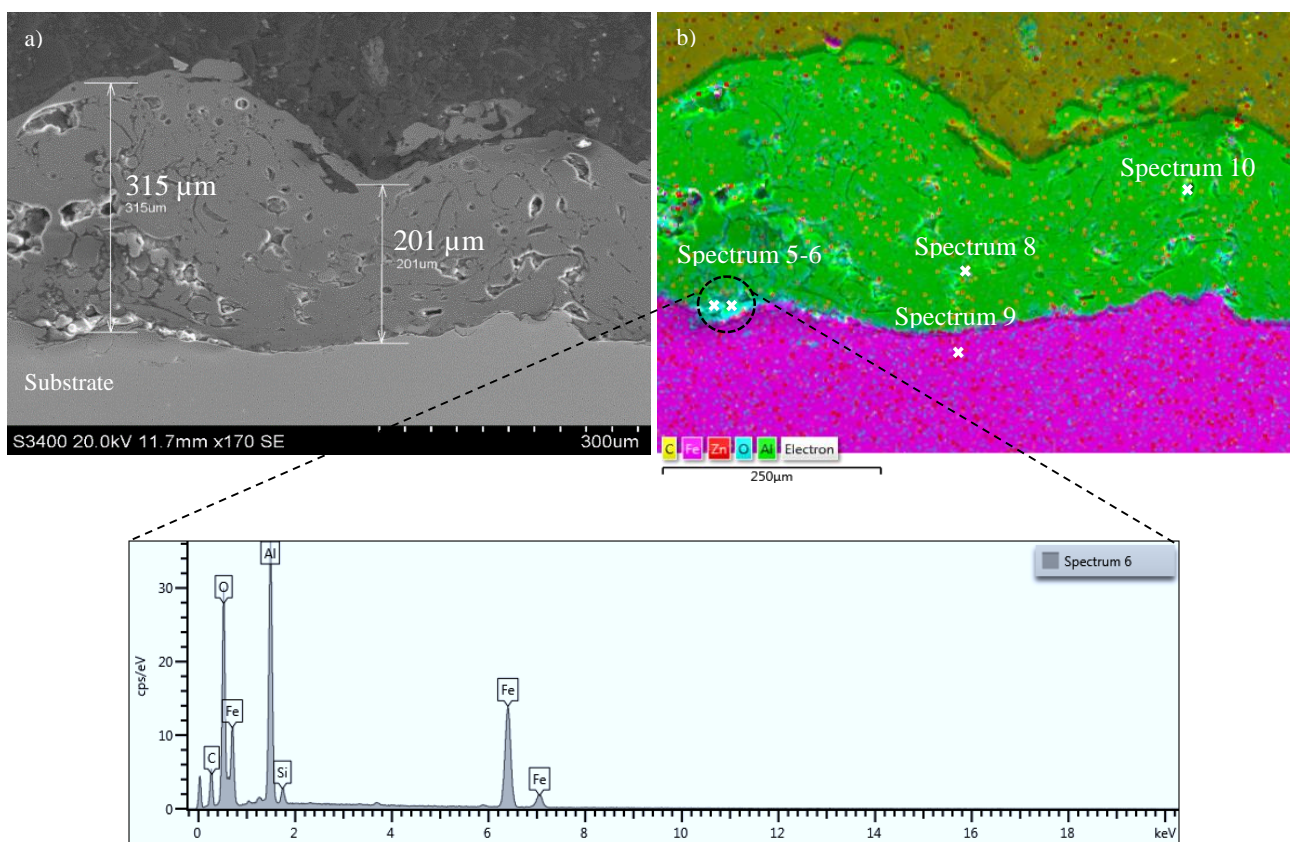
Figure 48 SEM and EDS photo of TSA (cross-section) after 30 days, freely exposed to natural seawater at 10±2℃.

Table 16 Results from EDS point mapping for TSA specimen after 30 days, freely exposed to natural seawater at 10±2℃

Element [wt%]	Spectrum 5	Spectrum 6	Spectrum 8	Spectrum 9	Spectrum 10
C	-	19.17	6.51	4.12	-
O	47.97	32.81	1.57	-	27.83
Al	29.08	18.17	91.2	-	60.06
Si	0.85	1.14	-	0.41	5.53
Fe	21.9	28.71	0.73	95.48	6.59
Other	0.2	-	-	-	-
Total	100	100	100	100	100

In Figure 49, SEM and EDS photos of freely exposed TSA specimen (surface) are shown. It's evidently that corrosion of the substrate has occurred. EDS mapping shows iron rich areas, indicating corrosion of the substrate. Point mapping in these areas shows high content of iron and oxygen (spectrum 1 - 3), see Table 17.
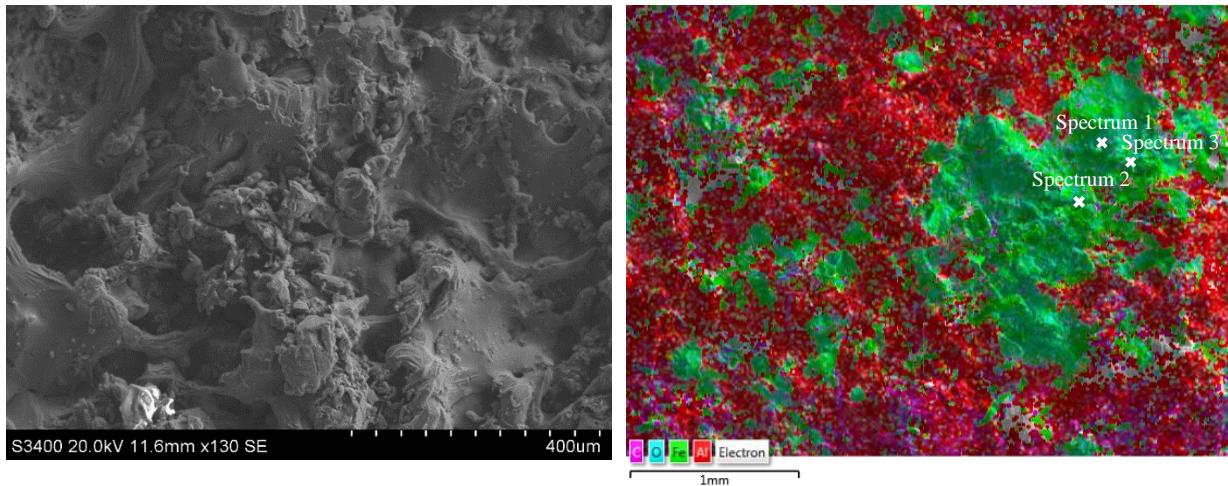
Figure 49 SEM and EDS photo of TSA (surface) after 30 days, freely exposed to natural seawater at 10±2℃, showing major areas of iron rich contents.

Table 17 Results from EDS point mapping on TSA (surface) after 30 days freely exposed to natural seawater at 10±2℃.

Element [wt%]	Spectrum 1	Spectrum 2	Spectrum 3
C	-	11.51	-
O	36.63	7.7	31.26
Al	0.57	-	4.35
Fe	62.8	80.79	64.39
Other	-	-	-
Total	100	100	100

Galvanic Couplings at 10℃

In Figure 50, photos of galvanic coupled specimens between both DSA and TSA coupled to CS with an area ratio of 10:1 and 100:1, exposed to natural seawater at 10℃ for 30 days are presented. The pictures shows clear differences between DSA and TSA. Increased corrosion products (white colored) was found on the DSA surface which has protected the CS surface. A white and dense calcareous deposition is visible for both CS specimens coupled to DSA. For the TSA surfaces, some hydrated oxides (FeO₃), also called brown rust, can be visually observed on the TSA specimens with less white corrosion products. The corresponding CS surfaces experienced a thin, more transparent calcareous layer with some brown areas indicating insufficient CP from the TSA specimen.
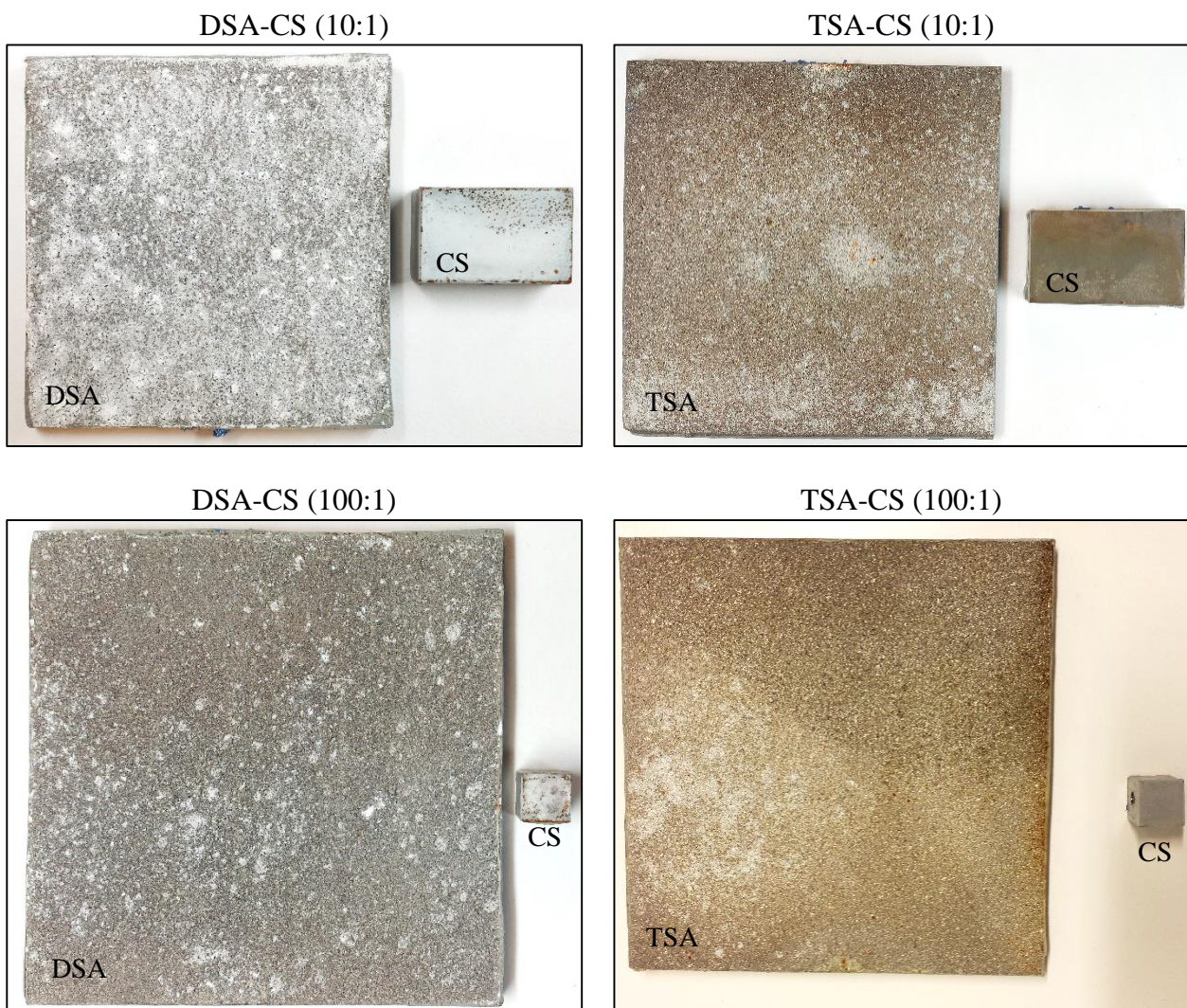
Figure 50 Pictures of galvanic couplings between thermally sprayed specimens (TSA and DSA) coupled to carbon steel with an area ratio of 10:1 and 100:1, exposed to natural seawater at 10±2℃ for 30 days.

In Figure 51, SEM and EDS images of a galvanic coupling between DSA and CS with an area ratio of 10:1, i.e. a 10% defect in the coating, can be seen. Only the DSA specimen is presented, where image a) and b) shows cross-section and surface image, respectively. After 30 days of exposure, acting as a

sacrificial anode/coating protecting the steel surface, the DSA surface shows no noticeable coating degradation where a thickness of 1.25 mm was measured. The coating thickness is in the range of what was measured before exposure, Table 6.
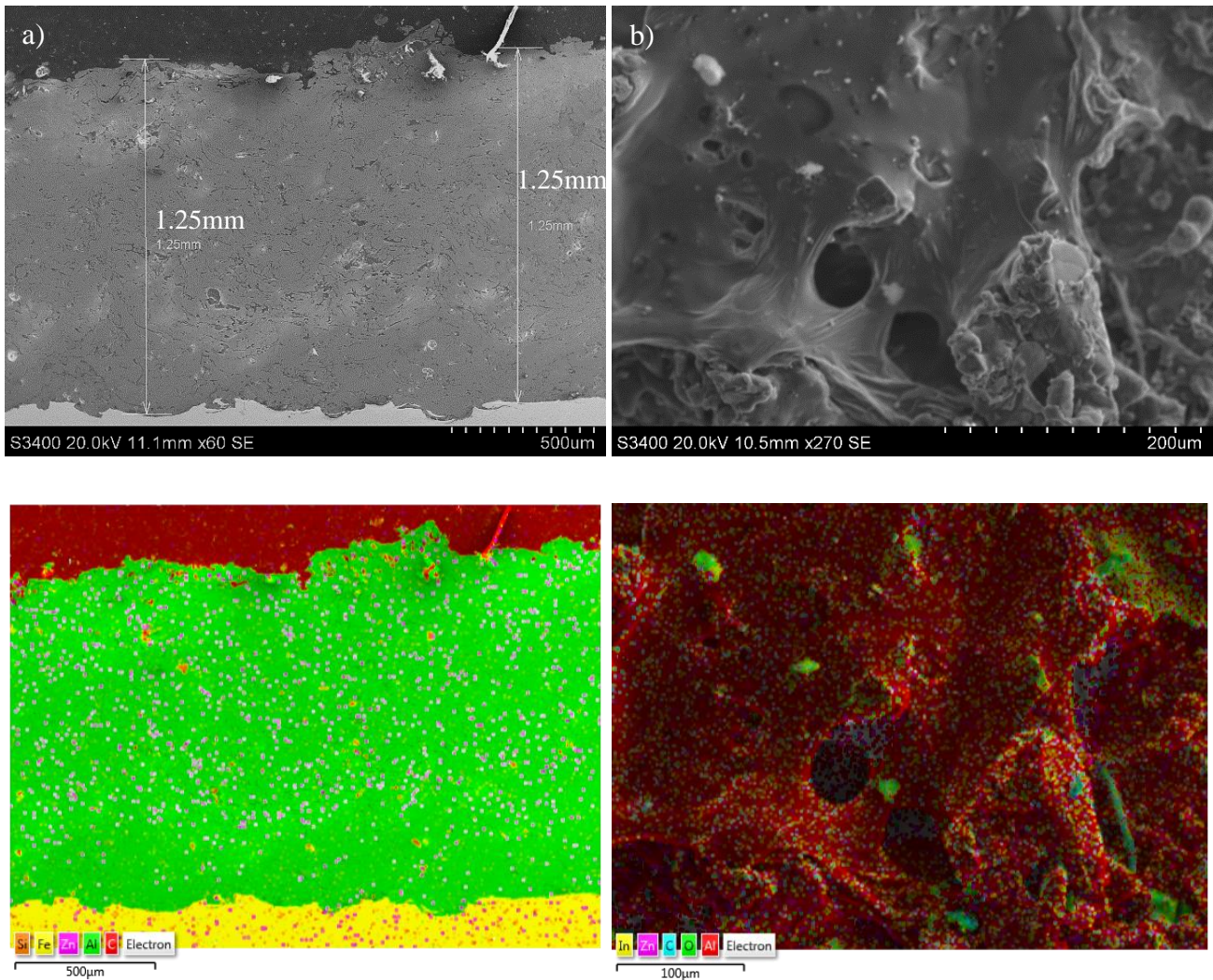
Figure 51 SEM and EDS image of DSA, a) cross-section and b) surface, coupled to CS with an area ratio of 10:1. No degradation in coating thickness can be observed after 30 days of exposure to natural seawater at $10\pm2°C$.

In Figure 52, SEM and EDS photos of a galvanic coupling between TSA and CS with an area ratio of 10:1, i.e. a 10% defect in the coating. After 30 days of exposure where TSA have been the only CP system for the CS, substantial coating degradation can be observed. The thickness was measured to be 146 and 102 µm, contributing to a thickness reduction of 50-75%, assuming a minimum thickness of 300 µm before exposure. Surface analysis showed small circular pits in the coating. EDS point mapping showed some, but small content of Iron (Fe) in these areas, spectrum 1 and 2, see Table 18. In addition, high content of oxygen was detected on most of the analyzed spectrums.
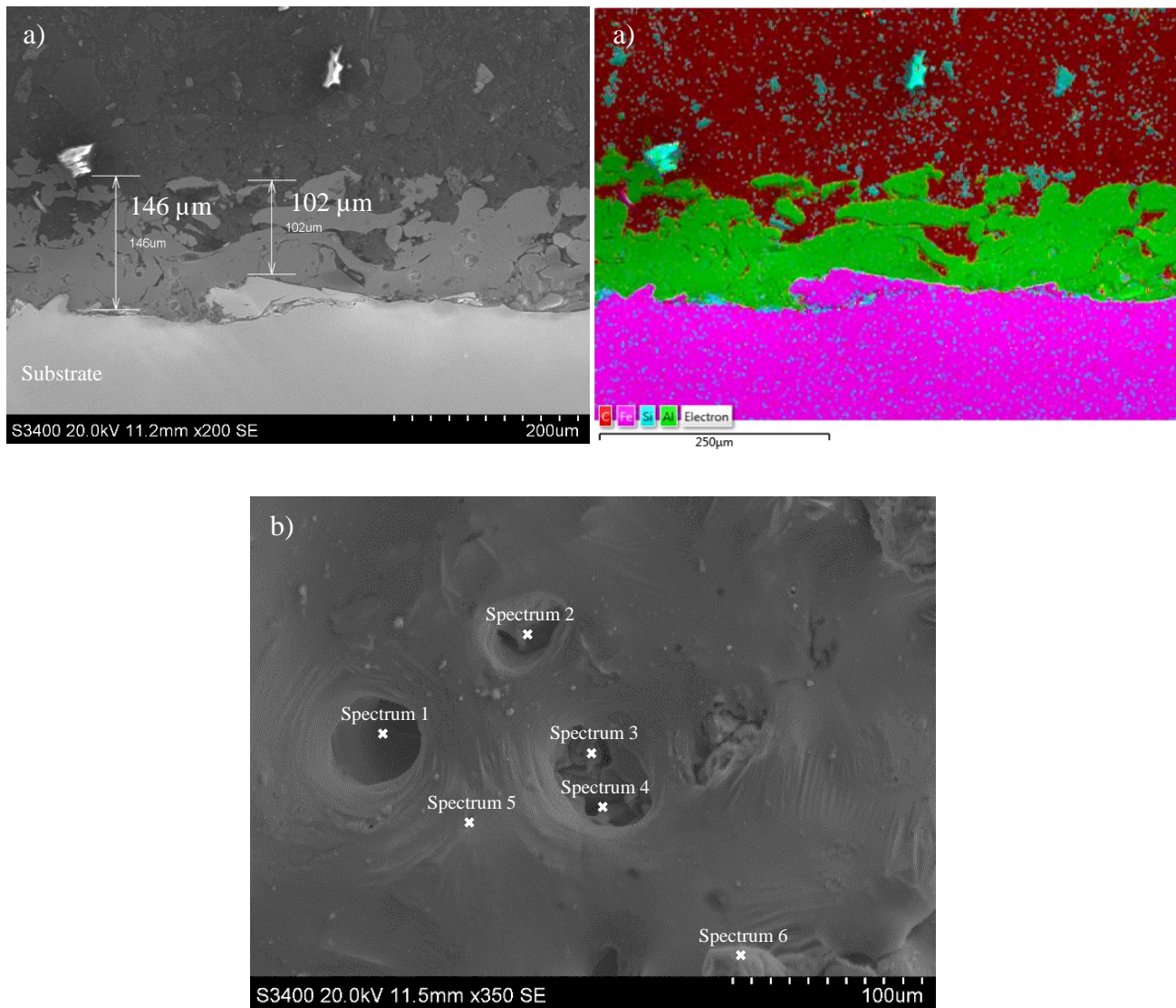
Figure 52 SEM and EDS image of TSA, a) cross-section and b) surface, coupled to CS with an area ratio of 10:1. Substantial coating degradation can be observed as well as small content of iron on some pits on the coating surface.

Table 18 Results from EDS point mapping on TSA (surface) coupled to CS with an area of 10:1, exposed to natural seawater at $10\pm2°C$ for 30 days.

Element [wt%]	Spectrum 1	Spectrum 2	Spectrum 3	Spectrum 4	Spectrum 5	Spectrum 6
C	-	22.17	10.9	19.18	9.38	20.44
O	11.8	9.81	5.63	29.57	4.97	12.22
Al	82.51	65.94	83.47	49.85	85.39	67.04
Fe	5.69	2.08	-	-	0.26	0.31
Other	-	-	-	1.4	-	-
Total	100	100	100	100	100	100

Galvanic Couplings at 40℃

In Figure 53, images of galvanic couplings before and after exposure to natural seawater at 40℃ are presented. SEM and EDS analysis were only conducted on DSA-CS (10:1) and DSA-TSA (10:1), thus only images of these couplings are shown. For Anode-CS (10:1), images can be found in Appendix E – Adhesion Pull-Off Test. It can be seen, that during 30 days of exposure, calcareous deposition is observed on the carbon steel surface and not on the TSA surface. The result from examination of the calcareous deposition can be found in the next sub-chapter, section 6.3.
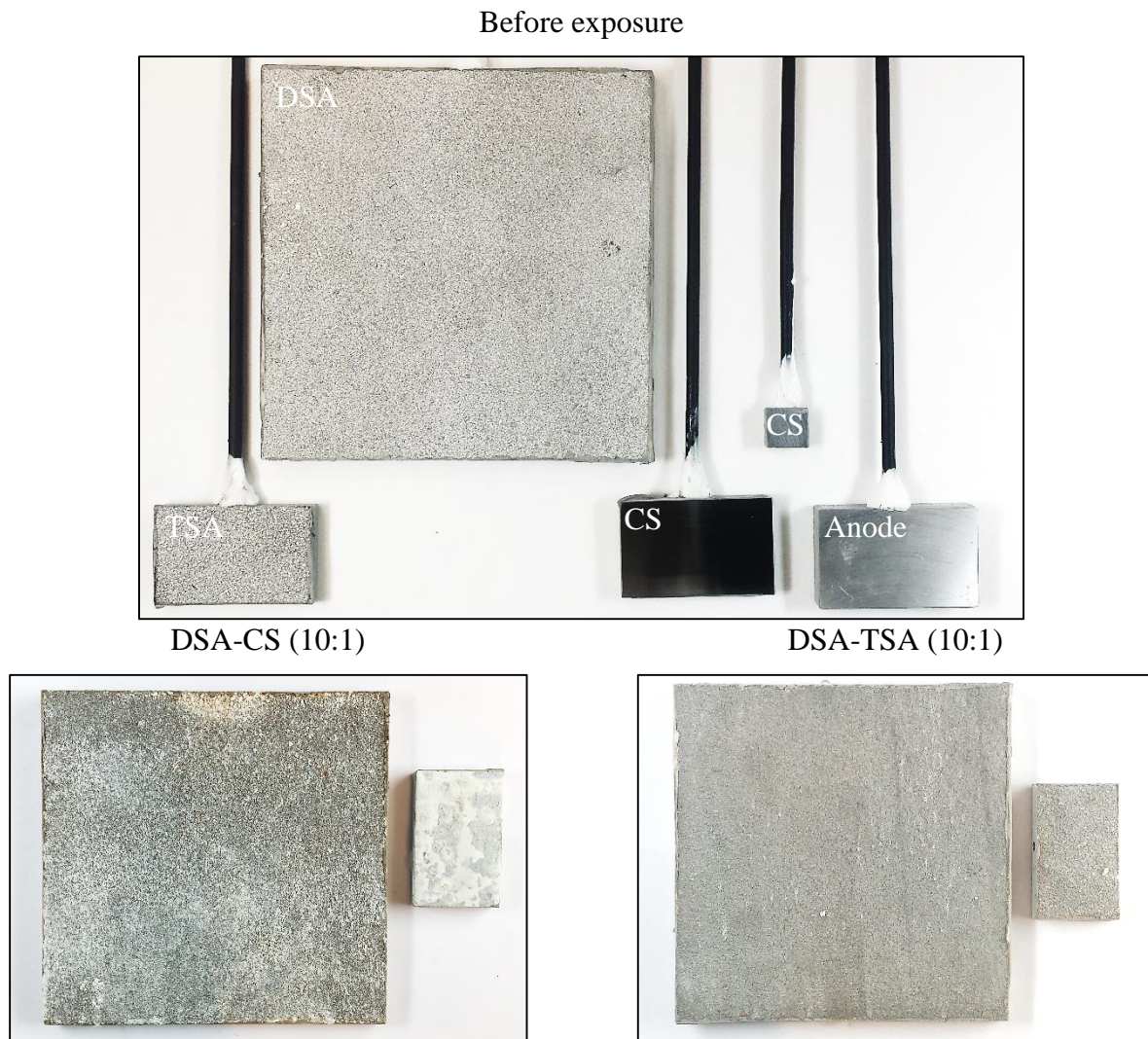
Before exposure

DSA-CS (10:1)   DSA-TSA (10:1)

Figure 53 Images of galvanic couplings before and after exposure to natural seawater at 40℃**.**

In Figure 54, SEM and EDS images of a galvanic coupling between DSA and CS with an area ratio of 10:1, i.e. a 10% defect in the coating, can be seen. Only the DSA specimen is presented, where image a) and b) shows cross-section and surface images, respectively. Coating degradation with respect to thickness reduction was not evident during 30 days of exposure, where measured thickness was 1.15 mm. However, an area rich of oxygen is detected at the interface between the DSA -and TSA layer, spectrum 6. Result from EDS point mapping can be seen in Table 19.
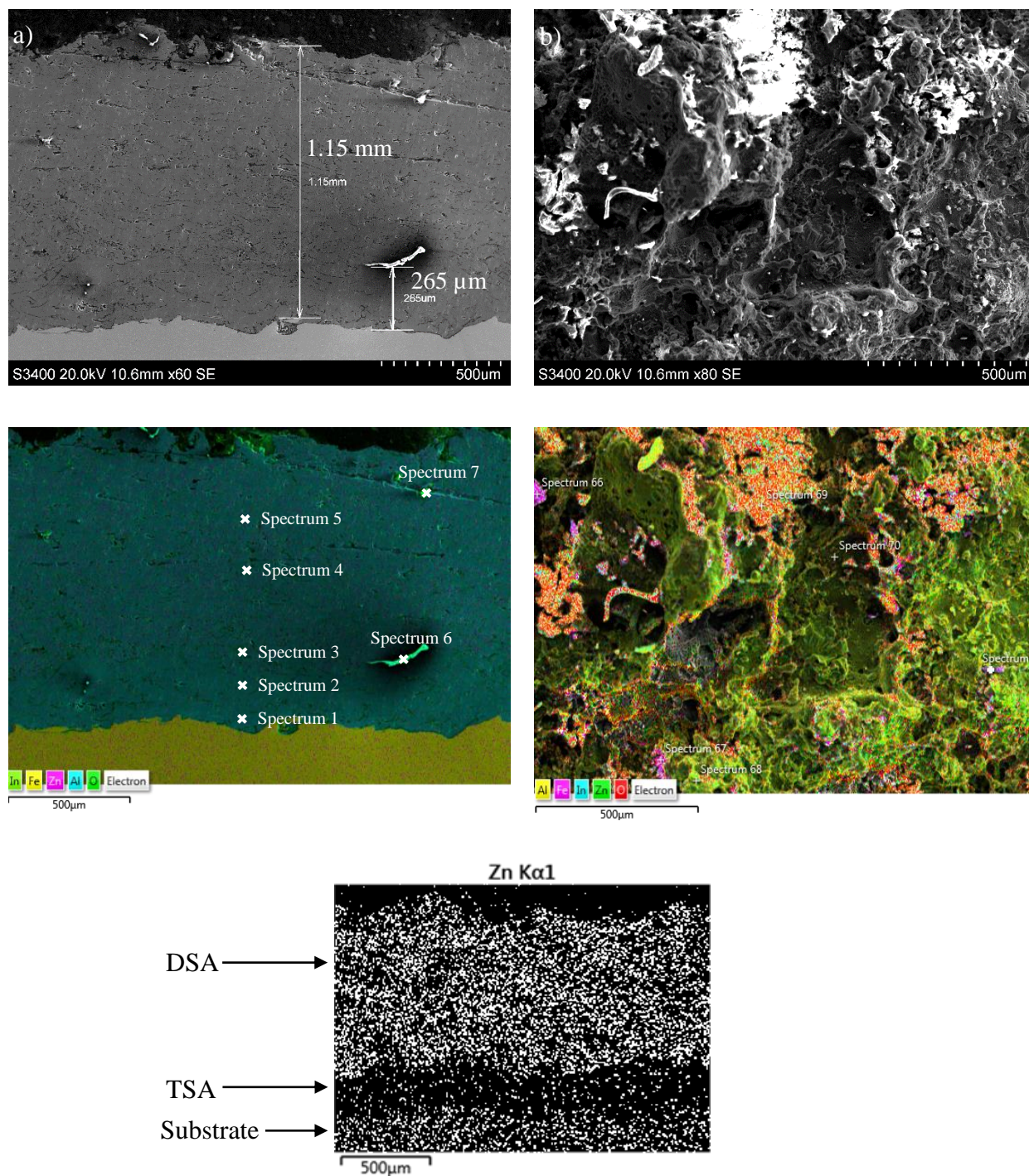
Figure 54 SEM and EDS image of DSA, a) cross-section and b) surface, coupled to CS with an area ratio 10:1. No degradation in coating thickness was observed after 30 days of exposure to natural seawater at 40℃.

Table 19 Results from EDS point mapping on DSA (cross-section)

Element [wt%]	Spectrum 1	Spectrum 2	Spectrum 3	Spectrum 4	Spectrum 5	Spectrum 6	Spectrum 7
O	4.55	0.3	4.67	0.38	8.52	25.34	53.66
Al	94.83	99.8	93.84	97.64	88.79	74.4	44.71
Fe	0.51	0.36	0.21	0.39	-	0.26	1.15
Zn	0.11	0.1	1.28	1.48	2.7	0	0.48
In	0	0.15	0	0.11	0	0	0
Other	-	-	-	-	-	-	-
Total	100	100	100	100	100	100	100

In Figure 55, SEM and EDS cross-section images of DSA and TSA, which have been galvanic coupled with area ratio 10:1 over a period 30 days. It can be observed that DSA (left pictures) still is intact with a thickness between 1-1.1 mm, which is in accordance to the coating applicator measurements in Table 6, and the prior exposure measurement in Section 6.2.1. TSA have some areas where the coating thickness is smaller compared to the reference value of 300 µm. The thickness were measured to be between 139 µm and 282 µm. In addition, some oxygen rich areas can be observed. Results from EDS point mapping on the marked spectrums can be found in Table 20.
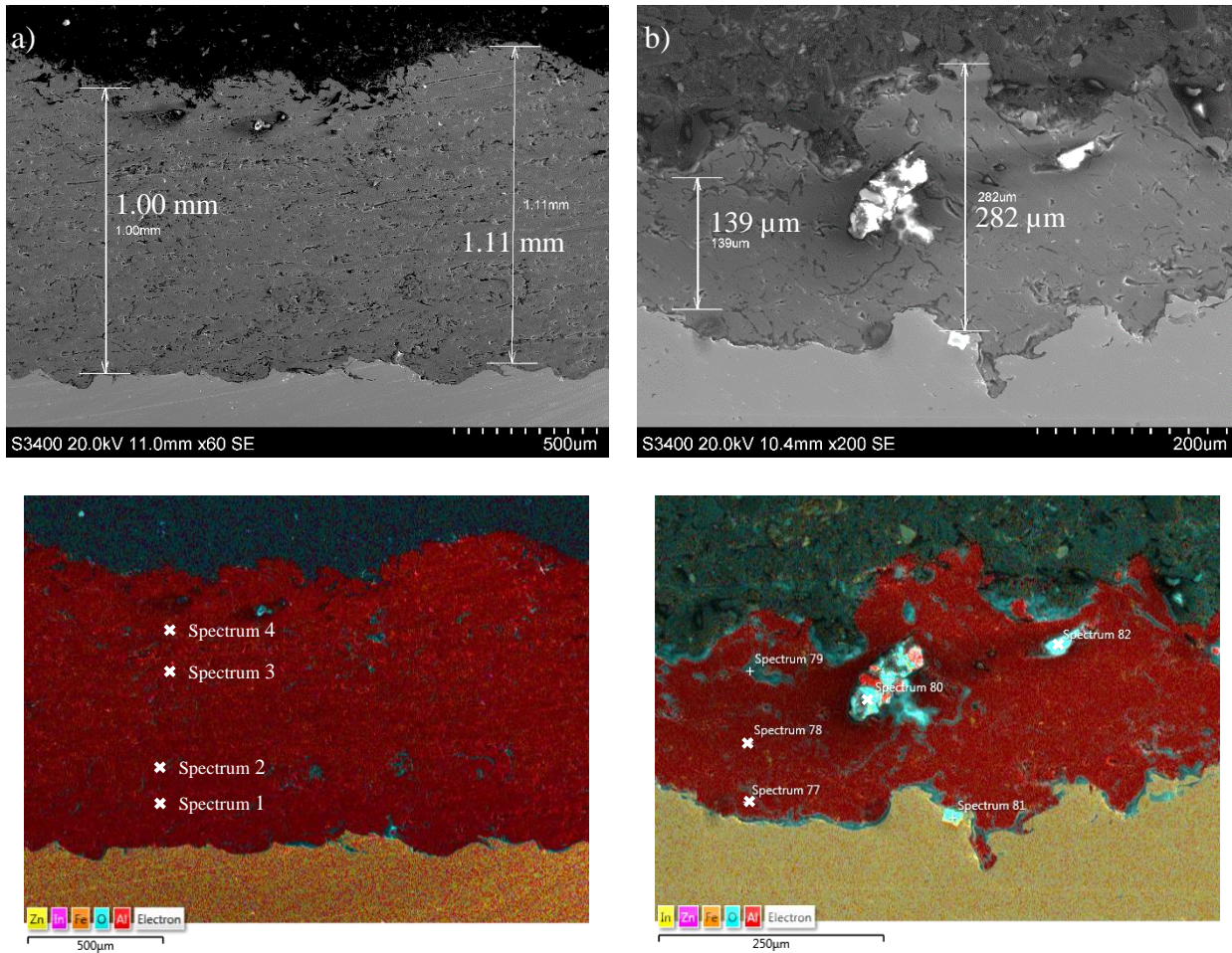
Figure 55 SEM and EDS image of the cross-section for a) DSA and b) TSA, after galvanic coupled with an area ratio 10:1, after 30 days of exposure to natural seawater at 40℃.

Table 20 Result from EDS point mapping on the cross-section of DSA and TSA

Element [wt%]	Spectrum 1	Spectrum 2	Spectrum 3	Spectrum 4	Spectrum 77	Spectrum 78	Spectrum 80	Spectrum 82
O	4.96	1.39	24.91	1.49	0.6	0.12	45.73	52.67
Al	92.83	98.46	73.16	97	95.49	96.49	15.07	21.49
Fe	2.21	0.14	0.18	0.15	1.41	0.38		1.03
Zn	0	0.01	1.59	1.04	0	0.02		0.01
In	0	0	0.15	0.32	0	0		0
Other		-			2.5	2.98		24.8
Total	100	100	100	100	100	100	100	

6.3 **Calcareous Deposits**

In this chapter, results from SEM and EDS analyses of the calcareous deposition on carbon steel specimens coupled to respectively DSA and TSA with area ratio 10:1 are presented.

Carbon steel coupled to DSA

In Figure 56, SEM image of calcareous deposits formed on CS specimen coupled to DSA with an area ratio of 10:1 is shown. A dense first layer followed by round shaped deposition can be observed on the CS surface. The thickness of the deposition made it possible to do a cross-section examination, Figure 57. EDS mapping shows increased content of Mg all over, followed by a high concentration of Ca at the outer surface of the deposit. In addition, increased concentration of O and Al can be observed.

| HV | det | WD | mag ⊞ | HFW | spot | tilt | | 500 µm |
| 20.00 kV | ETD | 9.6 mm | 100 x | 2.07 mm | 3.0 | 0 ° | | NTNU Nanomechanical lab |
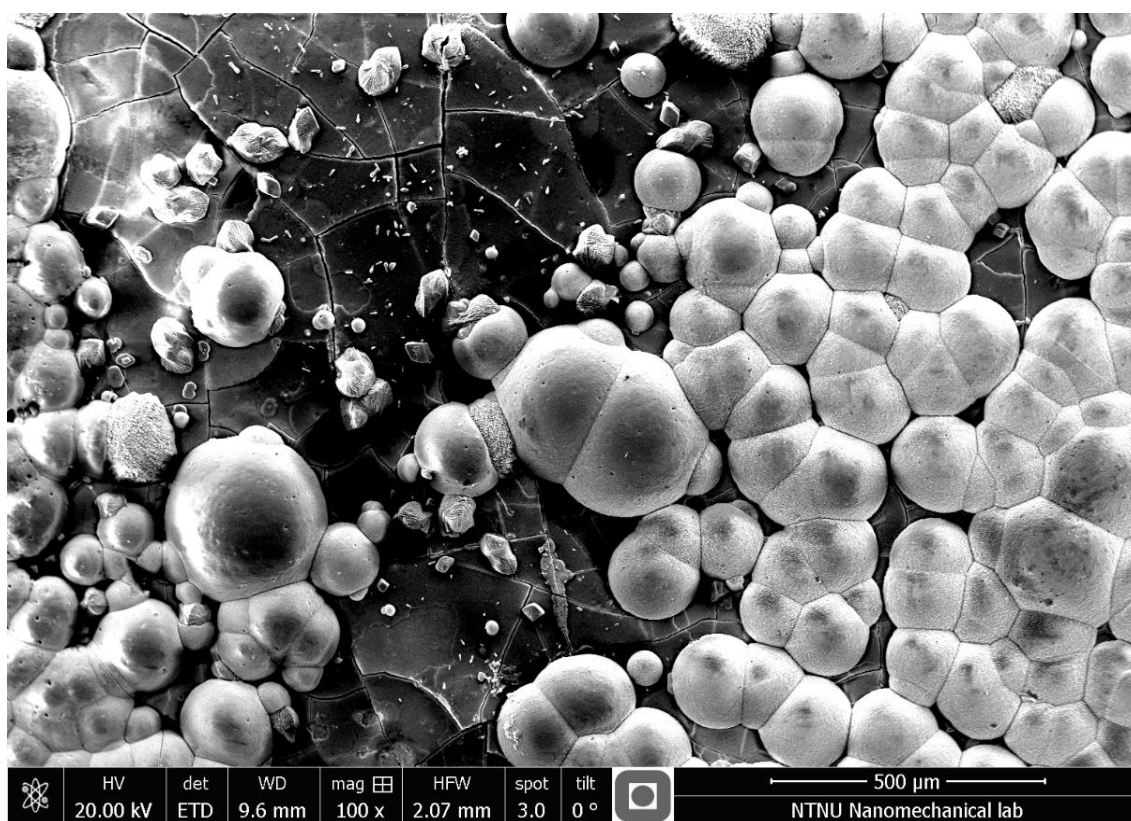
Figure 56 Calcareous deposition on carbon steel surface cathodic protected by DSA for 30 days in natural seawater at 10±℃.

Results from EDS analysis of the cross section Figure 57, can be seen in Table 21. High content of Mg and Ca can be observed.

Table 21 Results from EDS Sum Spectrum on the calcareous deposit on CS at 10℃

Element [wt%]	Map sum Spectrum
O	63.86
Mg	6.58
Ca	15.41
Al	14.14
Total	100
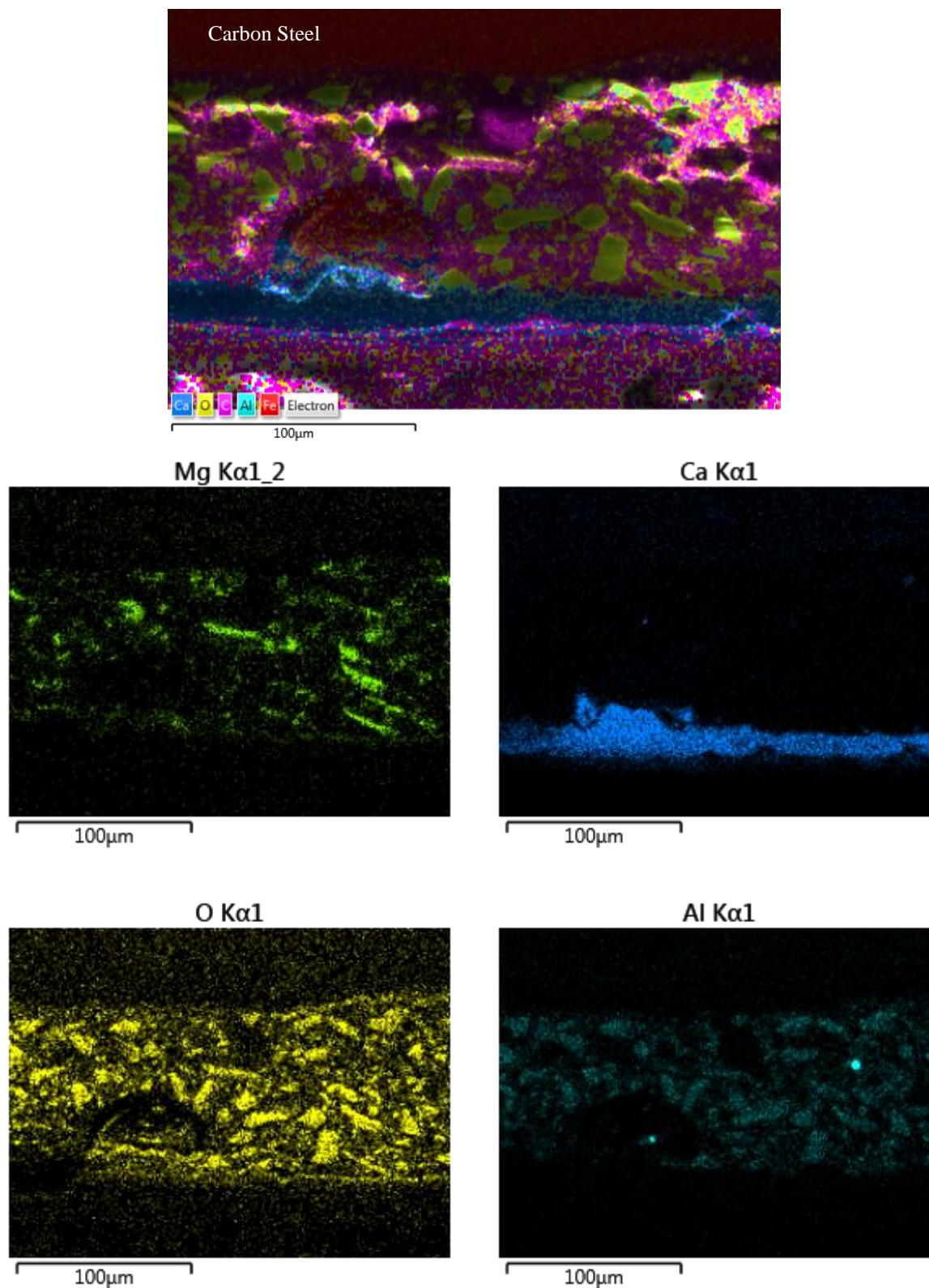
Figure 57 EDS cross-section images of calcareous deposition on carbon steel surface cathodic protected DSA for 30 days in natural seawater at 10±°C.

Carbon steel coupled to TSA

In Figure 58, SEM image of calcareous deposits formed on CS specimen coupled to TSA with an area ratio of 10:1 is shown. Notice, that the magnification is 10 time higher compared to image for the DSA coupling. Due to the thin layer, cross-section examination was not possible. However, a surface mapping was conducted, where the map sum spectrum results i.e. elements of the surface are shown in Table 22. The results shows that the Ca/Mg ratio has increased in comparison to the DSA coupling.
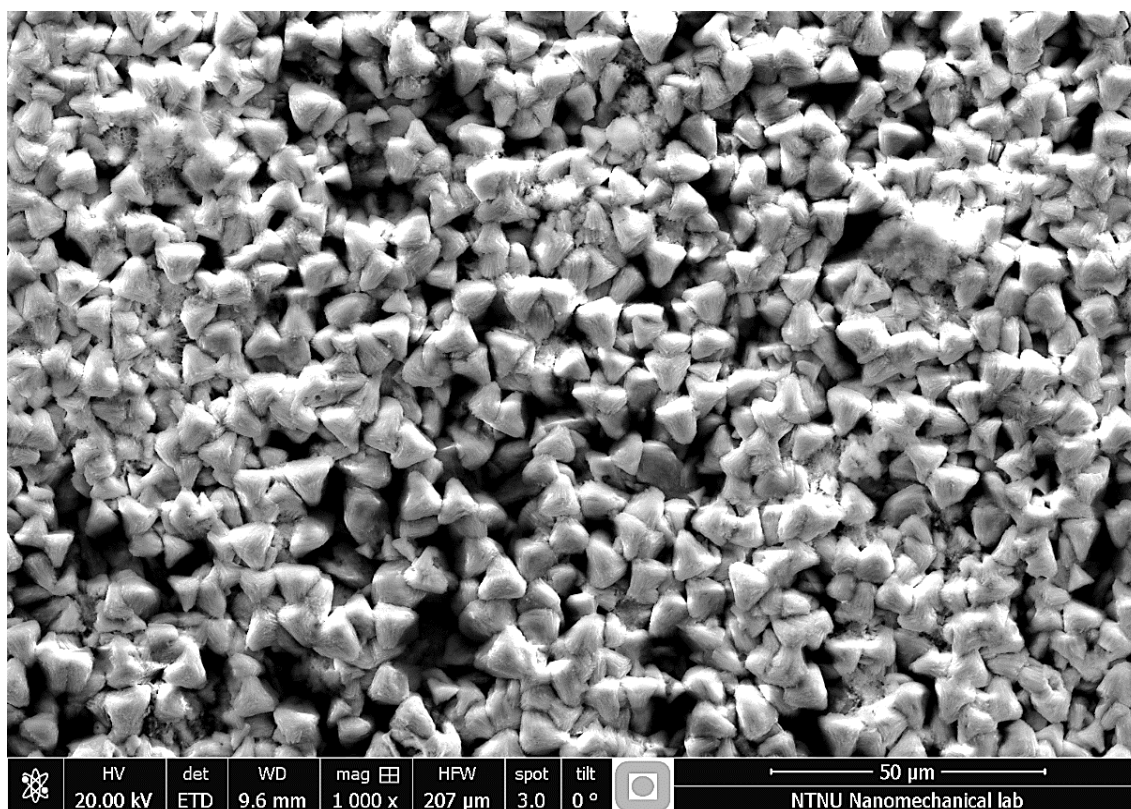
Figure 58 Calcareous deposition on carbon steel surface cathodic protected by TSA for 30 days in natural seawater at 10℃.

Table 22 Results from EDS Sum Spectrum on the calcareous deposit on CS at 10℃

Element [wt%]	Map sum Spectrum
C	14.78
O	49.74
Mg	1.92
Ca	30.85
Fe	2.71
Total	100

A clear difference in their microstructure can be observed in Figure 59. A dense layer with round shaped deposit can be observed on the CS coupled to DSA, while less dense deposition on the CS surface coupled to TSA can be seen.
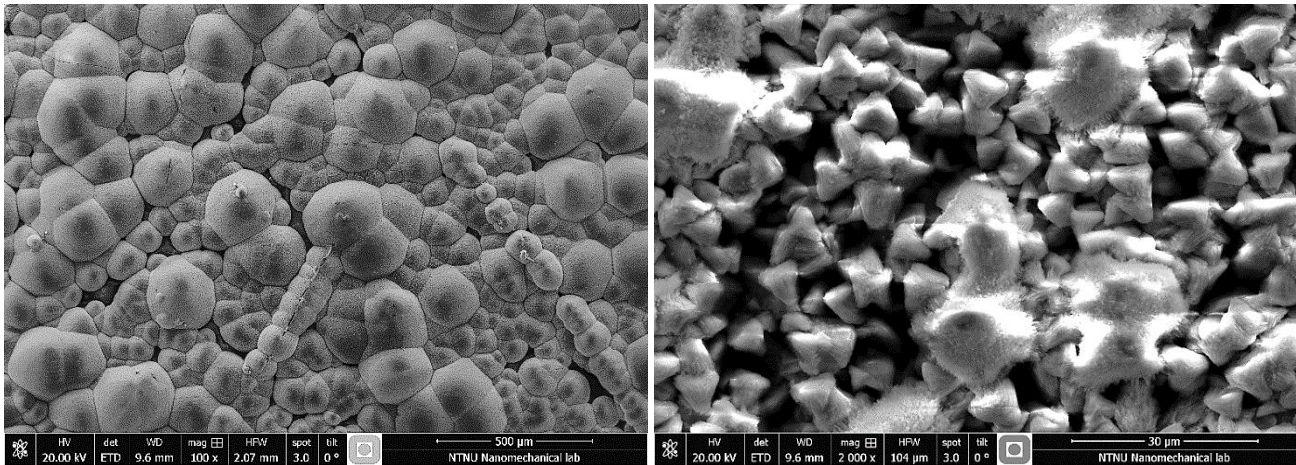
Figure 59 Calcareous deposit on CS surfaces coupled to respectively DSA and TSA for 30 days in natural seawater at 10℃.

Carbon steel coupled to DSA at 40℃

In Figure 60, SEM image of calcareous deposits formed on CS specimens coupled to DSA with an area ratio 10:1, exposed for 30 days in natural seawater at 40℃ is shown. A rather dens layer can be observed.
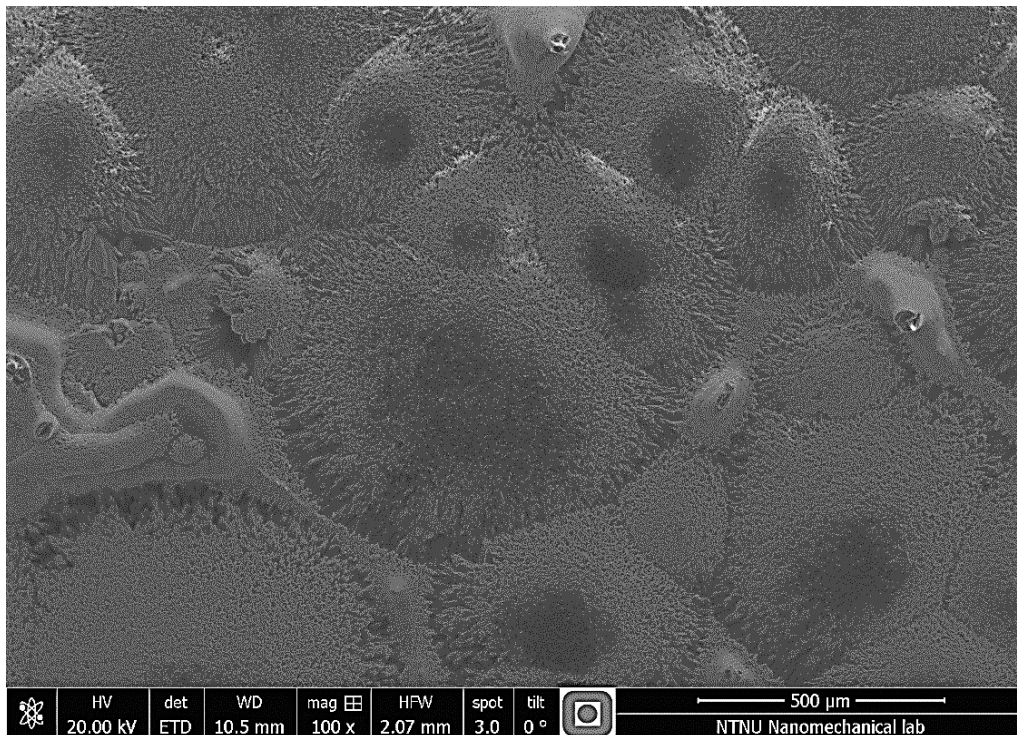
Figure 60 Calcareous deposition on carbon steel surface cathodic protected by DSA for 30 days in natural seawater at 40℃.

In Figure 61, EDS mapping shows increased Ca but reduced Mg concentration with increased temperature. This corresponds to the theory mentioned in section 2.4.1, as calcium carbonate will form more easily in warm seawater, while $Mg(OH)_2$ reduces. Results from EDS analysis can be seen in Table 23.
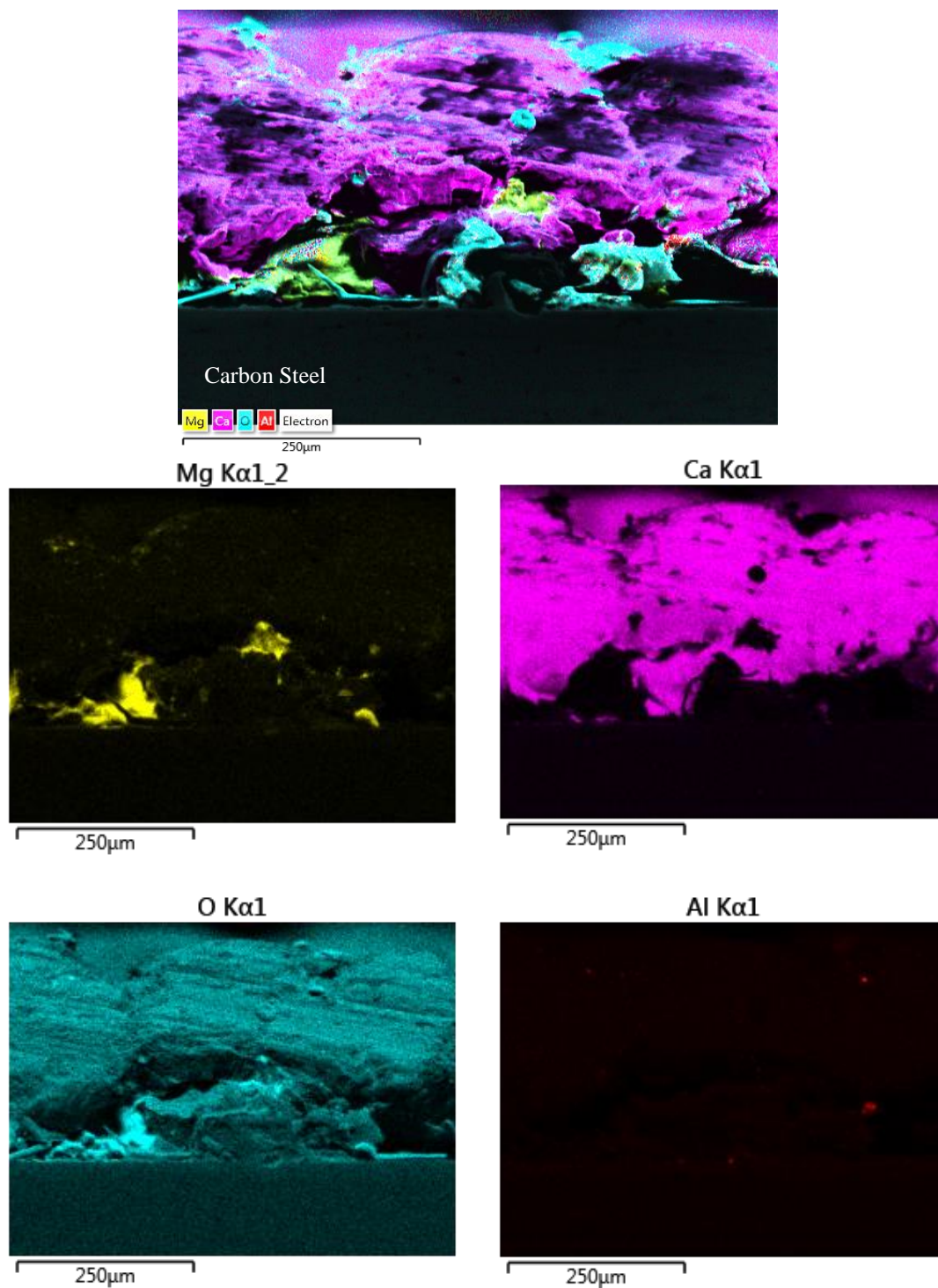
Figure 61 EDS cross-section images of calcareous deposition on carbon steel surface cathodic protected by DSA for 30 days in natural seawater at 40℃.

Table 23 Results from EDS Sum Spectrum on the calcareous deposit on CS at 40℃

Element [wt%]	Map sum Spectrum
O	63.95
Mg	2.4
Ca	33.65
Fe	0
Total	100

7   Discussion

In this chapter, the electrochemical results and the surface characterization for prior and post exposure will be discussed. The chapter is mainly focused on the electrochemical behaviour with respect to time and temperature.

7.1 Effect of Time and Temperature

7.1.1 Open-Circuit Potential

For TSA and DSA immersed in seawater at 10℃, the initial potential was quite high, at -700 mV$_{Ag/AgCl}$ and -900 mV$_{Ag/AgCl}$, but decreased to respectively -950 and -1110 mV$_{Ag/AgCl}$ during the first days of exposure. The development is in accordance to what Gartland et al. and Fischer et al. observed for TSA applied by flame spray, see Figure 8 [1, 19]. As described in Section 2.2.1, the initial increased cathodic potential when immersion is due to localized corrosion around impurities in the coating material contributing to a temporary increased rate of anodic dissolution reactions, but reaches a steady state value as impurities corrodes, detaches and passivation encounters [23]. Also, as corrosion occurs, pores in the coating tend to get filled up by corrosion products, increasing the barrier properties of the coating, reducing the self-corrosion rate, thus the resulting increased OCP.

The initial potential drop occurred faster for DSA than for TSA, at approximately 5 and 10 days respectively. The reduced activation time was most likely caused by alloying elements like Indium and Zinc. As described in Section 2.3.2, a synergic interaction between indium (In) and zinc (Zn) occurs reducing the activation time of the alloy.

The OCP increased with time to a steady state value at -935 and -1000 mV$_{Ag/AgCl}$ for TSA and DSA respectively. For TSA, this is in the range of what P.O. Gartland and T.G. Eggen measured for TSA (Al99.6). The potential of DSA is approximately the same as has been measured for flame sprayed AlMg5 [4]. The more negative potential is caused by Zn and In additives. With respect to the corresponding anode specimen, the OCP for DSA was between 80 and 90 mV more positive, i.e. more noble than the bulk material. This is the opposite as what C. Holager observed for solid -and thermally sprayed AlMg5[33] and what Magome at el. observed for TSA [63]. This indicates that the ability for Al-Zn-In alloy to cathodically protect CS can have been reduced during the thermal spraying process. The less active behavior in addition to longer activation time for the coating is probably caused by a reduction of Zinc and Indium in the DSA, as a result of the spraying process[5]. In addition, increased oxidation properties for thermally sprayed coatings (TSCs) compared to solid aluminum, as mention

---

[5] A coating scrap-off was performed on DSA specimens, both prior -and post exposed, and the powder was sent to SINTEF MOLAB for a full chemical analyze. Unfortunately, the results was not achieved in time for this report.

in Section 2.2.1, has increased the passive behavior in some degree. This can be seen when comparing the anodic polarization curves in Figure 40. Higher current density i.e. higher dissolution rate of the material, can be observed for the anode specimen from OCP up to −900 mV$_{Ag/AgCl}$.

With increased temperature, the potential was more negative for both DSA and TSA during the first days. The initial negative potential is a result of increased kinetic reactions with increasing temperature. Due to some instability in the temperature, the effect of temperature can clearly be seen as an increased temperature resulted in a decreasing potential and vice versa. This effect corresponds to what Thomason observed for TSA with an 8% holidays when lowering the temperature from 25℃ to 3℃ the potential became more positive, from −855 mV$_{Ag/AgCl}$ to −755 mV$_{Ag/AgCl}$ [64]. Nevertheless, the potential increased in the anodic direction with time, and after 1 month of exposure, the OCP of TSA stabilized at the same value measured at lower temperature. This shows that at high temperature, the potential may be low for a short period, before it gradually increases to a value close to what is expected at low temperature. This is in accordance to what Fischer et al observed for TSA, that the OCP may increase to a higher value with increased temperature, see Table 3.

For DSA at 40℃, the OCP has not fully stabilized after one month of exposure, but it's likely that it will move in the same direction as for TSA, i.e. the potential will increase and stabilize close to −1000 mV$_{Ag/AgCl}$ which was the measured steady state potential for DSA freely exposed at 10℃, after 40 days.

7.1.2 Couplings Potential

The coupling potential development with respect to time followed the same trend as for the free corrosion potential, i.e. OCP. The negative coupling potential during the first days is caused by the initiation of corrosion around impurities in the TSCs, followed by a gradually more positive potential as the intermetallic particles detaches and repassivation of the surface encounters. For the solid sacrificial anode, passivation does not occur due to activating elements, Zn and In, which continuously breaks down the protective film as described in Section 2.3.2. Therefore, the coupling potential is stable throughout the exposure period. This is not the case for DSA couplings, whom experienced the same development as for the freely exposed DSA -and TSA specimens, meaning an initial high potential followed by a rapid decreasing potential during the first days, before gradually increase to a more positive value with time. As mentioned, this may be caused by reduced activating elements in the coating, and the fact that the oxidation properties for TSCs increases with respect to its bulk material, due to the thermal spray process [32].

The anode coupling potential seemed to be un-affected by the reduced anode:cathode area ratio, suggesting high anodic activity. This was also observed for the DSA couplings, where the coupling potential for DSA-CS were −975 mV$_{Ag/AgCl}$ and −1000 mV$_{Ag/AgCl}$, simulating a 1% and 10% coating holiday respectively. The potential with 10% defect is the same potential measured for freely corroding

DSA specimen after 40 days. Polarization curves obtained after 30 days of exposure, Figure 40, support this statement. The anodic polarization curves are quite similar for DSA and anode, with a more active behavior compared to TSA where a passive behavior can be observed from OCP to the pitting potential at −600 mV$_{Ag/AgCl}$.

TSA galvanic coupled to CS, simulating 1% and 10% coating holidays, experienced a more positive coupling potential than what DSA with similar coating defect experienced, Figure 29. As mentioned, the OCP for respectively TSA and DSA were −935 and −1000 mV$_{Ag/AgCl}$. Galvanic coupling simulating a 10% defect, lifted the potential in the positive direction for the TSA coupling to approximately −822 mV$_{Ag/AgCl}$ after 2 months, whereas for the DSA coupling the potential was the same as for freely exposed specimens, at −1000 mV$_{Ag/AgCl}$. This implies that the anodic properties are more favorable for DSA when it comes to providing effective cathodic protection to CS. The lower protection capabilities for TSA is most likely caused by its passivating abilities, as Al99.5 (TSA coating) is inside the passive region of the Pourbaix diagram, Figure 4. Increasing the simulated coating holidays for the TSA couplings will further increase the coupling potential, and with defect >20%, the coupling potential will probably be higher than the recommended value for CS at −800 mV$_{Ag/AgCl}$ [7]. Higher degree of defects can most likely be more effective protected with DSA coating, due to the results in this thesis. However, increased defect will increase the dissolution rate of the coating, thus decrease the lifetime of the coating.

The effect of increased temperature on the coupling potential was similar as for the OCP development, with an initial high potential followed by a rapid decreasing potential during the first 5 days, before it gradually increased in the positive direction as the coupling reached its steady state potential. However, for the Anode-CS (10:1) couplings, the potential were 40-50 mV more positive throughout the exposure period of 30 days at 40℃, in comparison to exposure at 10℃. According to literature, Al-Zn-In anodes experiences a reduction in the current capacity and ennoblement of the operating potential with increased temperature. According to K. Fagbayi and D. Scantlebury, this ennoblement may be caused by inward diffusion of insoluble indium atoms with increasing temperature, i.e. the indium content at the anode surface is reduced [65]. This may also be the reason for the high potential fluctuation at 40℃ as active alloying elements are reduced at the surface, a passivation-activation fluctuation may occur as reduced In contributes to reduced break down process of the aluminum oxide, thus allowing oxidation to some extent. According to literature, the spontaneous fluctuation in potential as well as the current density is associated with the initiation of localized pitting corrosion, followed by general corrosion as the fluctuation increases [66]. Comparing the pictures of the anode surface exposed at 10℃ and 40℃, Figure D. 2 and Figure D. 3, small pits can visually be observed on the anode surface exposed at higher temperature. This is just a plausible explanation for the extreme fluctuation behavior. Polarization curves for the anode at 40℃ should have been performed in order to

determine if increased tendency of passivation is observed. Unfortunately, this was not done in this project. This was in fact observed for DSA, Figure 41, and may therefore be a plausible explanation. However, further research should be conducted in this field in order to provide a more conclusive explanation.

7.1.3 Protection Current Density

For DSA-CS couplings, the initial high current density on the CS at day 5 is caused by the negative coupling potential during the first days of exposure, as can be seen from the OCP development for DSA in Figure 27 and Figure 28. The big potential differences between the coupled materials will contribute to high current flow. The galvanic current density from DSA (anode) to the CS (Cathode) decreased and reached equilibrium due to polarization of the CS holiday, reducing the potential differences caused by calcareous deposition which acts as a barrier to oxygen reduction, thus protects the surface against corrosion. Also, the OCP for DSA increased with time, reducing its self-corrosion rate, thus the potential difference in the coupling decreased, hence the current density decreased.

DSA couplings reached its equilibrium current density over a shorter period compared to the anode couplings, Figure 32. This is probably caused by the higher initial current density during the first days, contributing to a more effective polarization of the CS area. As described in the theory part of the report, Section 2.4, calcareous deposition is affected by the applied potential. According to J. F. Yan et al, the lower potential at the CS surface will increase the cathodic reactions at its surface, which increases the formation of OH^- at the surface, thus increases the rate of calcareous deposition [67]. The initial high current density is favorable in order to achieve rapid polarization and formation of calcareous deposition, reducing the current density with time in order to maintain a long life CP system.

For DSA-CS (10:1) exposed at 10℃, the cathodic current density decreased to 172 mA/m² after 1 month, see Table 24. This implies that the current output from DSA is 17.2 mA/m² due to the different area ratio. Adding the self-corrosion rate of DSA from polarization curves obtained after 30 days, the total corrosion rate of the coating will be approximately 54 µm/year, see Appendix C – Corrosion Rate Calculation. This implies that for a 1 mm tick DSA coating with a 10% holiday, it can be expected a service lifetime at around 18 years. As the protective calcareous layer continuous to increase on the CS surface, the current density will decrease, thus the lifetime of the coating will be greater.

TSA supplied the lowest current density to the corresponding CS specimens, with an initial value of 242 mA/m² and 160 mA/m² for respectively 1% and 10 % holidays. This is substantial lower than the initial current density supply from DSA and Anode coupled to CS, whom all reached an initial value above 1000 mA/m². The values at both 10℃ and 40℃ are summarized below in Table 24. The reason is due to reduced anodic capability for TSA compared to DSA and anode alloy, in addition to the more positive OCP for TSA contributing to a smaller potential difference, thus low current flow. Applying

the obtained polarization curves, Figure 40, it's evident that the high pitting potential for TSA contra DSA and anode contributes to reduced anodic properties when it comes to providing effective CP.

Table 24 Average current density on CS and coupling potential after the first days of exposure (initial) and after 1 month.

Couplings	Holiday [%]	Average Current Density and Coupling Potential Values							
		Temperature 10±2℃				Temperature 40±5℃			
		Initial		1 Month		Initial		1 Month	
		[mA/m²]	[mV$_{Ag/AgCl}$]	[mA/m²]	[mV$_{Ag/AgCl}$]	[mA/m²]	[mV$_{Ag/AgCl}$]	[mA/m²]	[mV$_{Ag/AgCl}$]
DSA-CS	10	1072	-1075	172	-1027	4800	-1060	38	-1010
	1	1239	-1102	130	-1013	-	-	-	-
TSA-CS	10	160	-930	39	-875	-		-	
	1	241	-976	64	-930	-		-	
Anode-CS	10	1035	-1090	249	-1085	3350	-1035	45	-1035

According to DNV [7], the initial, mean and final recommended protective current density for exposed CS in seawater relevant for this study, are:

$$T=7\text{-}11°C: \quad i_{initial}=200\,mA/m^2 \quad i_{mean}=100\,mA/m^2 \quad i_{final}=130\,mA/m^2$$

$$T=40°C: \quad i_{initial}=165\,mA/m^2 \quad i_{mean}=85\,mA/m^2 \quad i_{final}=115\,mA/m^2$$

Comparing the recommended values from DNV with the obtained values listed in Table 24, only TSA coupling with 10% holiday supply a lower current density to the CS surface than what is recommended. The protective current density continued the rather low value after 1 month, which should not be sufficient in order to protect the CS surface from corrosion. According W. H. Thomason, a 50% holiday can be protected by TSA coating for a few years. He also found that the corrosion potential for a TSA with 8% holiday were −895 mV/$_{Ag/AgCl}$ [64]. The measured potential is in accordance to the measured coupling potential for a 10% holiday in this study, after 1 month of exposure. Applying the recommended protective current density values from DNV, the CS surface should not be protected, implying that the ability for TSA to protect a local defect in the coating is limited. Visual surface examination also approve this to some degree, where some (but little) brown corrosion products were discovered on the CS surface, Figure 50. The low current density achieved form the TSA coating will reduce calcareous deposit and will not be favorable with respect to long term exposure, as the current density decrease more slowly, resulting in an overall higher consumption rate of the TSA coating compared to DSA and conventional sacrificial Anode. This can undoubtedly be observed from cross-section examination in Figure 52. Severe coating degradation was observed for TSA coupled to CS with a thickness reduction of 50-70%, which further supports this statement.

Further, surface examination of the calcareous deposition on the carbon steel surface protected by the TSA coating showed a clear difference when comparing the deposition formed on the CS surfaces CP from DSA and the sacrificial anode. The thickness of the deposition was substantial smaller, contributing to reduced barrier for corrosion protection. Increased Ca/Mg-ratio was observed for the TSA coupling, Table 21 compared to DSA coupling at 10℃, Table 22. This is in accordance to what is mention in the theory, Section 2.4.1. According to T. Okstad et al, the Ca/Mg ratio degreases with decreasing potential, which contributes to an increased driving force for precipitation of $Mg(OH)_2$. The low coupling potential for DSA-CS (10:1), ergo high current density, increased precipitation of Mg. However, since cross-section examination of the calcareous deposition for the TSA coupling was not possible due to the small thickness, and the fact that calcium precipitated at the outer surface according to Figure 57, the Ca/Mg-ratio may not be representative.

A plausible explanation for the low current density from TSA to CS may be caused by insufficient coating thickness. Experiences with the use of TSA from Shell Malaysia, the most critical factor of achieving adequate TSA performance is the applicator of the coating[6]. Cross-section examination for prior exposed TSA in Figure 46, may indicate higher degree of porosity in the coating in comparison to the DSA coating, contributing to increased permeability of the coating. In addition, freely exposed TSA specimen at 10℃ showed some major areas rich of iron after 30 days of exposure, Figure 49. Over such a short period, corrosion of the substrate should not occur as literature studies suggests that a 200 µm thick TSA coating could protect a 5.7% coating holiday for 30 years, with a current density demand of 40 mA/m^2, Table 1. A thickness reduction above 50% over a period of 30 days, Figure 52, is most likely not introduced from the CS holiday alone. This is a clear evidence of imperfect coating deposition, which contributes to increased cathode area for exposed CS, thus the small current density. In other words, the coating holiday may in fact be larger than 10%.

For Anode coupled to DSA with an area ratio of 1:1 and 1:100, the initial current density were 75 mA/m^2 and 35 mA/m^2. After 20 and 28 days of immersion, a shift in the polarity was observed. This indicated that the DSA coating acted as an anode and supplied protection current to the anode surface. Similar behavior has been observed for TSA coatings at high temperatures [58, 60]. However, the polarity shift lasted for a short period, and increased to an average value at 8 and 7 mA/m^2 after 30 days of exposure. The values are lower than the recommended DNV design for aluminum at 10 mA/m^2, however a steady state value was not reached during the 30 days of exposure, which was the main time frame for this study.

Therefore, new measurements of the current density were manually performed after 86 days of exposure for Anode-DSA (1:1) and after 76 days for Anode-TSA (1:1). The current density demand for DSA and TSA seemed to have stabilized between 8-10 mA/m^2 and 6-7 mA/m^2, respectively. Both

values are in the range of the recommended current density values from DNV, and are far lower than what S. Egtvedt measured for TSA polarized to -1050 mV$_{Ag/AgCl}$ after 4 months, at 25 mA/m^2 [26]. The current density requirement is higher for DSA compared to TSA. With respect to the OCP, DSA which has a more negative potential than TSA should generally have a lower current density demand. However, there are no facts that says that DSA should have similar cathodic properties as for those of sacrificial anode. Looking at the polarization curved obtained for DSA and TSA after 30 days of exposure, Figure 40, the cathodic curves are almost identical from -1100 mV$_{Ag/AgCl}$ to -1550 mV$_{Ag/AgCl}$, thus with a coupling potential of -1090 mV$_{Ag/AgCl}$ the cathodic current density demand should be in the same range for DSA and TSA. Also, DSA is an active metal contra TSA whom experienced a passive behavior. Passivation of the TSA surface will fill up the pores in the coating, increasing its barrier properties, thus decrease the cathodic current density demand. Further, calcareous deposition have been found to precipitate around intermetallic particles on TSA [58, 60], which will reduce cathodic reactions at its surface, hence reduce the current density demand. Calcareous deposition on DSA under cathodic polarization have not been investigated, hence it cannot be concluded that it precipitates.

The effect of increased temperature was observed by an initial higher current density demand from the CS surface, but decreased at a much faster rate due to increased rate of calcareous deposition, contributing to a denser protective layer on the CS surface over a shorter period of time than at low temperature. EDS analysis showed increased Ca/Mg-ratio with increased temperature, Figure 57 and Figure 61, supporting this statement.

7.1.4 **Potentiodynamic Polarization Curves**

The potentiodynamic polarization curves for anode and the corresponding extruded wire experienced similar behavior during 30 days of exposure, Figure 38, thus the electrochemical properties were not affected by the extrusion process. Active dissolution were observed for both specimens with no passive tendency. This is, as mentioned earlier caused by the alloying element In, which due to its high nobility contributes to a cathodic shift in the pitting potential, reducing the passive region of the metal.

For DSA and TSA there are clear differences in the anodic properties suggesting that DSA will perform better as a CP system, i.e. protecting defects where CS is exposed. The most important difference is the potential range from OCP where passivation encounters. For TSA, whom has a more positive OCP than DSA, has a clear tendency to passive behavior from OCP to +319 mV after 30 days of exposure, as illustrated in Figure 62 . This is substantial higher than for DSA with +94 mV. In addition, it can be discussed if this initial small increasing slope for DSA actually can be called a tendency of passivation. However, the anodic current density has decreased to some extend compared to the bulk material, suggesting that either alloying element like Zn and In have been reduced during the thermal spray

process and/or the small passive behavior is a result of increased oxidation for TSCs. Nevertheless, there are a close agreement between DSA and Anode suggesting that the protective abilities for DSA are similar to those of conventional sacrificial anodes.
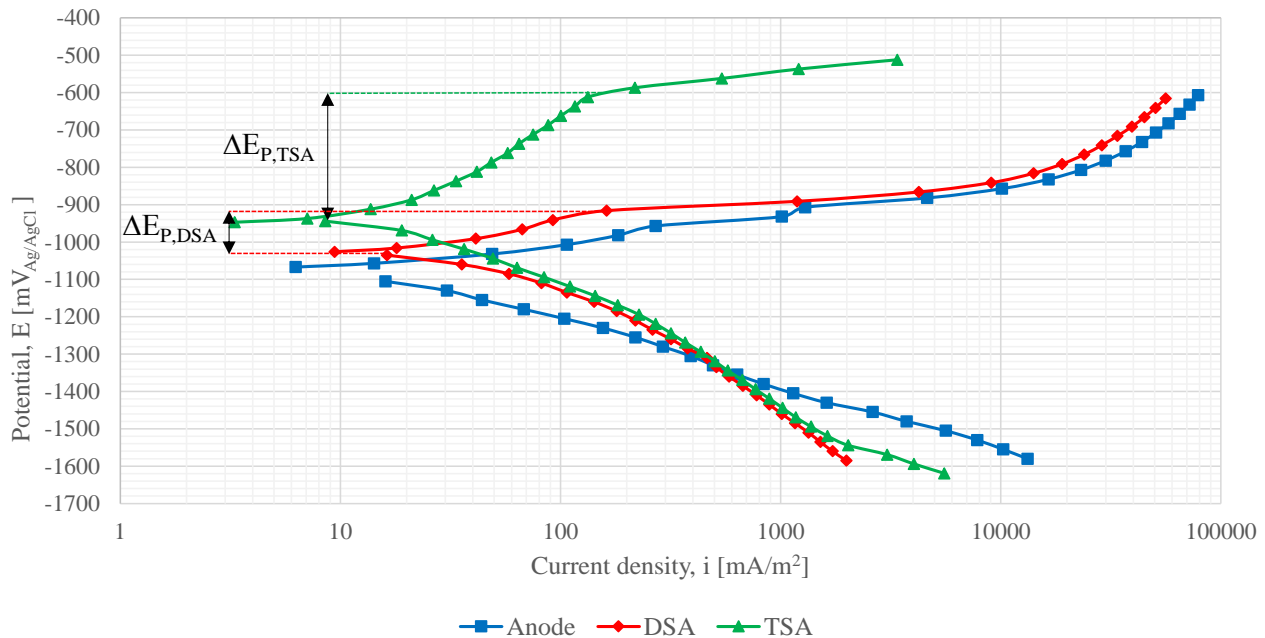
Figure 62 Polarization curves for Anode, DSA and TSA obtained after 30 days of exposure to natural seawater at $10 \pm 2\,^\circ\text{C}$ under nearly stagnate conditions. Increased passive region can be observed for TSA compared to DSA and Anode specimens.

The anodic protective abilities for TSA is limited due to passivation. As mentioned, TSA coupled to CS with are ratio 10:1, did not supply the amount of current density needed to protect the CS surface in accordance to DNV standards. In Figure 40, it was shown that with a maximum allowed potential in order to protect CS against corrosion according to DNV (-800 mV$_{Ag/AgCl}$), TSA could only supply 50 mA/m^2. The measured coupling potential for TSA with a 10% defect was -875 mV$_{Ag/AgCl}$ and -822 mV$_{Ag/AgCl}$ after respectively 1 and 2 months. It's evident that the coupling potential for TSA is strongly affected by increased cathode area. Increasing the potential above the pitting potential would lead to high consumption rate of the coating. According to P.O. Gartland et al, TSA should not be anodic polarized above -670 mV$_{Ag/AgCl}$ as the life time of the coating is considerable reduced to a few weeks [4].

For DSA, this is not the case, as the potential increased little with increased cathode area. Thus, DSA can protect a substantial larger defect in the coating compared to TSA. However, there must be a balance in order to avoid rapid coating degradation. Anodic polarization above -900 mV$_{Ag/AgCl}$ will substantially increase the current density output. At this potential, DSA can supply approximately 200 mA/m^2, respective 19,000 mA/m^2 at -800 mV$_{Ag/AgCl}$ according to the polarization curves obtained at day 30, Figure 40. The initial high current density is as mentioned favorable for increased calcareous

deposit, and will rapidly be reduced to an acceptable low value as a dense and coherent protective calcareous layer is formed on the CS surface, as shown in Table 24. Higher anodic polarization can therefore be performed. Nevertheless, such high defects will most likely not occur due to the high mechanical properties of TSCs.

According to theory mentioned in Section 2.2.3 regarding the effect of increased temperature, the pitting potential should decrease in the cathodic direction with increased temperature in addition to a shift of the passive region towards lower pH, destabilizing the oxide film, contributing to increased corrosion. This deviates from the result obtained for DSA and TSA exposed at 40℃.

From the polarization curves obtained at 40℃, the anodic and cathodic curves for DSA experienced a shifted to the left, indicating reduced anodic -and cathodic current density with respect to the polarization curves obtained at 10℃. For TSA, only reduced anodic current density was observed. In addition, a more negative OCP can be observed, as discussed in Section 7.1.1. For DSA, the most noticeable effect of increased temperature, is the increased potential range of passivation. The pitting potential increased from −916 to −888 mV$_{Ag/AgCl,}$ for DSA and from −600 to −550 mV$_{Ag/AgCl}$ for TSA, Table 13. A tendency for passive behavior can be observed from OCP to +175 mV and +395 mV for respective DSA and TSA. For DSA, the potential range is almost 2 times higher than at 10℃. The increased pitting potential and reduced corrosion rate with increased temperature is not fully understood. A contributing factor may be due to the temperature drop at day 28. The lower temperature may contributed to increased passivation of TSA. This increased oxide layer may still be intact at day 30 when the polarizations curves were obtained, thus increased passive behavior. However, DSA should not passivate. The increased passive range for DSA is most likely contributed by the short exposure time. After 30 days of exposure, steady state OCP for DSA was not reached. It can therefore be expected that the passive potential range for DSA will be reduced with time as the OCP becomes more positive. Further research should performed in order to understand this deviation from the literature [22].

7.1.5 **Corrosion Rate**

The corrosion rate for all test specimens experienced an initial high corrosion rate during the first days of exposure (day 1-8), before it gradually decreased. This is in accordance to theory mentioned in Section 2.2.1, that it can be expected an initial high corrosion rate for TSA caused by dissolution of the oxide layer, increasing exposure of intermetallic particles causing localized pitting corrosion around these particles. This can be observed by an initial low OCP. But over time, these particles should detach followed by repassivation of the pits and thereby reduce the corrosion rate with increased OCP. Also, for the TSCs the corrosion rate should decrease as corrosion products fill up the pores in

the coating, inhibiting further corrosion. However, this affect may be limited for DSA as it's an active metal, thus passivation should not occur.

DSA and TSA experienced very low corrosion rate during the first day of exposure, at 0.013 and 0.019 mm/year, respectively. For TSCs, we have earlier stated that increased oxidation properties can be expected versus the bulk material. This will contribute to increased exposure time before oxide-destabilization. Impurities/intermetallic particles in the coating may therefore not be exposed after one day of exposure, thus the resulting low corrosion rate.

The highest corrosion rate for DSA and TSA exposed at 10℃, was observed at day 8, at respectively 0.07 mm/year and 0.039 mm/year, using the graphical values obtained from Tafel extrapolating. Comparing the OCP development, Figure 27, with the obtained corrosion rate values, the OCP was lowest between day 5 and 10 for DSA and TSA. Low corrosion potential is associated with high corrosion rate [58] due to localized corrosion around impurities in the coating material contributing to a temporary increased rate of anodic dissolution reactions, but reaches a steady state value as impurities corrodes, detaches and passivation encounters, thus the measured corrosion rate is in accordance with the OCP development. Also, close agreement with the LPR measured values, Figure C. 1, suggests that the measured corrosion rates are correct. After 30 days the corrosion rate decreased to a value of 0.031 and 0.017 mm/year for DSA and TSA respectively, suggesting a service life at 30 years for a 1 mm thick DSA coating. P. O. Gartland measured the corrosion rate for TSA (Arc sprayed) after 2 months exposure under similar conditions to be 0.007 mm/year, and 0.0033 mm/year after 11 months, indicating a lifetime of more than 50 years. It can therefore be assumed that the corrosion rate will continue to decrease further with time. Nevertheless, longer exposure time for DSA is necessary in order to determine if the corrosion rate decreases to similar or acceptable values. Shouldn't the corrosion rate decrease to such values, a sealer should be considered in order to increase the barrier properties of the coating. Applying a silicon sealer have shown to reduce the self-corrosion rate by a factor of 2-3 and the cathodic current density demand by an order of magnitude [68]. However, this will reduce the anodic capabilities and will not be suited if DSA shall be used as the primary CP system, i.e. without sacrificial anodes.

During the entire period of exposure (except for day 1), the self-corrosion rate for DSA is higher than that for TSA. This is expected as passivation of TSA will occur, whereas continuously cracking and rupture of the oxide layer occurs at the DSA surface due to the synergic interaction between In and Zn as described in the theory part. However, the corrosion rate for DSA is 2.3 times higher compared to the corresponding anode specimen, i.e. the bulk material, whom experienced a stable OCP at -1085 ± 5 $mV_{Ag/AgCl}$ throughout the exposure period. The higher corrosion rate for TSCs is most likely contributed by their porosity, which could have led to penetration of the electrolyte through open pores

96

accelerating the corrosion rate due to galvanic corrosion with the substrate. For DSA, this is less likely due to the thickness of the coating. Another factor may in fact be that the used porosity for the corrosion rate calculation (10%) is way too conservative. Reducing this value will reduce the corrosion rate of the coating, thus reduce the deviation between the DSA and the bulk material. Analyzing the degree of porosity was unfortunately not performed in this study due to time limitations, but is strongly recommended for further work as it direct affect the estimated service life of the coating.

Effect of Temperature

Comparing the result from low temperature exposure (10℃) with high temperature exposure (40℃), the corrosion rate is reduced with increasing temperature. According to general theory, this is the opposite effect. Increased temperature should contribute to an increase of the underlying chemical reactions, and at temperature above 40℃, the pitting potential should decrease substantial for TSA. In addition, a shift of the passive region towards lower pH should occur as illustrated in Figure 9, destabilizing the oxide layer thus increasing the corrosion rate.

A possible explanation for the lower corrosion rate for DSA at 40℃ may be due the ennoblement process which was proposed as a possible explanation for the more positive OCP of the anode-CS (10:1) couplings at 40℃. According to theory mentioned in Section 2.3.2, the current efficiency decreases with increased amount of indium, thus inward diffusion of the insoluble indium atoms with increasing temperature will result in increased efficiency for DSA, meaning that the self-corrosion rate decreases. However, reduced content of In at the surface should also give a more positive OCP, which is not possible to determine at this point due to a stable OCP is not reached for DSA at 40℃. Also, lower corrosion rate were experienced for TSA as well, where the content of Indium is zero.

Alternatively, the lower corrosion rate at 40℃ is most likely caused by the limited exposure time. Similar experiments were conducted by H. Wilson who observed that the corrosion rate was higher for TSA at 10℃ after 30 days of exposure, compared to exposure at temperature ranging from 30-70℃. This was due to a more rapid decreasing corrosion rate during the first month at high temperatures. However, with time the corrosion rate for low temperature decreased to a lower value than those at high temperature. It is therefore likely that with time, the corrosion rate for DSA and TSA will be higher at 40℃ than at 10℃.

7.2 **Adhesion Strength**

According to P. O. Gartland, Adhesion strength is one of the most important properties of the coating. Even if the electrochemical properties of the coating are favorable, poor adhesion will contribute to increased dangers for blistering and delamination of the coating, thus not recommended to be used [68].

The measured adhesion strengths for DSA were lower than for TSA. This is most likely due to the thickness of the coatings. It's known, that with increased coating thickness the adhesion strength will be reduced. The reduction is said to be related to increased residual stresses with increased thickness, which will increase the driving force for interface crack propagation [69]. Another contributing factor of the reduced adhesion for DSA contra TSA, may be due to the dual layer. The majorities of failure were adhesive failure in the interface between TSA and DSA. In Figure 54, cross-section examination of DSA revealed increased oxygen content at the TSA/DSA interface. A dual layer may not be favorable when high adhesion is desired, thus a single layer of DSA may be more beneficial. Nevertheless, the average measured adhesion strengths for prior exposed specimen were 8.82 MPa and 13.53 MPa for DSA and TSA respectively. This is higher than what Fischer et al. measured for the tethers and risers at the Hutton TLP (6.9MPa) coated with TSA, which showed good performance.

No reduction of adhesion strength was observed after 30 days of exposure. In fact, the adhesion strengths increased with exposure time. The adhesion increased by 3-5 MPa for both coatings. P. O. Gartland experienced similar increased adhesion after exposure [68]. Increased adhesion is common for organic paints after immersion due to the continued curing process. This is not possible for TSCs coatings. The cause may be related to decreased tensions within the coating due to corrosion products filling the pores, thus increased extraction strength. This is just pure speculations and should be further investigated in order to find a more plausible explanation. Nevertheless, with such high values, increased thickness of DSA should be possible to some extend in order to increase the life time of the coating and CP system. It should be said that a longer exposure time is necessary in order to fully evaluate the mechanical performance of the coating. As no sealer is applied on the DSA surface, blistering may occur as the barrier effect is lower than for a sealed coating.

8   Conclusions

Electrochemical Properties

- DSA has similar anodic properties as for those of conventional sacrificial anodes, and can supply sufficient CP to a substantial larger defect compared to TSA coatings, contributing to a more effective polarization of exposed CS. An initial high current output can be delivered from DSA to CS, but will rapidly be reduced due to effective polarization and formation of calcareous deposit, maintaining a long life CP system.

- Increased temperature contributes to increased passivity for DSA and TSA –stronger tendency for TSA than DSA, reducing the anodic protection properties.

- The initial corrosion rate for thermally sprayed coatings (TSCs) is low due to intact oxide layer, but increases during the first 8 days due to destabilization process, exposing impurities/intermetallic particles in the coating. After 30 days in natural seawater at 10℃, the corrosion rate was 31 µm/year and 17 µm/year, for respectively DSA and TSA.

- At 40℃, the corrosion rate decreases faster and is lower compared to at 10℃, measured at 10 µm/year and 9 µm/year after 30 days, for respectively DSA and TSA.

DSA under Cathodic Protection

- DSA drains current from the anode.

- At cathodic polarization between −1100 and −1550 $mV_{Ag/AgCl}$, DSA and TSA have similar current density demand. When connected to a separate sacrificial anode, the current density for DSA and TSA are in the same range, between 6-10 mA/m^2. The current density demand is in accordance to DNV standard.

- The current density demand is 2-3 mA/m^2 higher for DSA than for TSA due to the passivating abilities for TSA.

- A temporary shift in the current direction will occur during the first month due to the periodically more negative open circuit potential (OCP) for DSA.

Electrochemical Potential

- TSCs experiences an initial high OCP, but decreases rapidly during the first days due to localized corrosion around impurities in the coating, contributing to a temporary increased rate of anodic dissolution reactions. The potential will gradually increase in the positive direction as impurities detaches from the matrix followed by passivation.

- The OCP for DSA and TSA in natural seawater at 10℃ is −1000 $mV_{Ag/AgCl}$ and −935 $mV_{Ag/AgCl}$, respectively.

- At higher temperature (40℃), the initial OCP drop is higher for DSA and TSA, but will move in the anodic direction with time, reaching a steady state value close to the measured value at 10℃.

- The OCP for DSA is 80-90 mV nobler than the bulk anode material. The increased potential is caused by either reduced content of alloying element like zinc and indium and/or due to increased oxidation properties.

- The OCP for conventional sacrificial anode and corresponding extruded wire, CORAL A grade, are identical at approximately -1085 mV$_{Ag/AgCl}$ when immersed in natural seawater at 10℃.

- The potential for DSA and anode is practically not affected by increased cathode area when coupled to CS with 10 to 1 area ratio. The coupling potential is nearly the same as for freely exposed DSA and anode, at respective -1000 mV$_{Ag/AgCl}$ and -1085 mV mV$_{Ag/AgCl}$. TSA has limited protective abilities. The coupling potential for TSA with a 10% holiday was -822 mV$_{Ag/AgCl}$, after 2 months in natural seawater at 10℃.

- At 40℃, the coupling potential of anode-CS (10:1) experienced a more noble potential than at 10℃. This is possible contributed by inward diffusion of indium atoms.

Adhesion Strength

- The adhesion strength for DSA and TSA is in the range between 9-20 MPa, before and after exposure, but higher after 30 days of exposure.

- A dual layer may not be favorable when high adhesion is desired as the majorities of failures will occur at the TSA/DSA interface, thus a single layer of DSA may be more beneficial.

Calcareous Deposit

- Increased temperature will increase the rate of calcareous deposition, thus decrease the current density demand from the anode over a shorter period than at low temperature.

- The calcareous deposition is affected by the temperature, where increased temperature contributes to an increased Ca/Mg-ratio.

Final Remarks:

- ❖ DSA has similar anodic properties as for those of conventional sacrificial anodes.

- ❖ DSA does not eliminate the cathode area, but drains current from connected sacrificial anodes with the same current demand as for those of TSA.

- ❖ DSA has not the same electrochemical potential as sacrificial anodes, but is 80-90 mV more positive.

- ❖ DSA is an alternative to TSA and sacrificial anodes due to its protective capabilities.

9   Suggestions for further studies

GE assumed that DSA would be best suited for un-insulated gas systems operating at elevating temperature up to 140℃. In this study, ennoblement of conventional sacrificial anode was observed at 40℃. It is therefore strongly recommended that similar experiments will be conducted for DSA at higher temperatures.

Suggesting for further work include:

- Obtain the correct porosity of the DSA coating as it direct affect the estimated lifetime of the coating, i.e. the corrosion rate.
- Obtain polarization curves for conventional sacrificial anode (CORAL A Graded) and DSA at higher temperatures in order to determine if the alloy experiences increased passive behavior and increased OCP.
- Similar study with only a single layer of DSA, i.e. no TSA as a first coating.
- Study the effect of increased coating thickness with respect to adhesion strength for DSA. Also, as blistering have shown to increase with increased thickness for TSA, this should be investigated for DSA as well.
- Anodic properties for DSA with applied sealer.
- High temperature have shown to cause blistering on TSA, which will significantly reduce the service lifetime of the coating. The susceptibilities for blistering on DSA should be investigated.
- Investigate if calcareous deposition precipitate on DSA surface when connected to a conventional sacrificial anode.
- For subsea structures, increased water depth will contribute to increased number of anodes for protection due to an increased OCP of the anodes. The effect of increased hydrostatic pressure on the performance of DSA should be investigated.

References

[1] K. P. Fischer, W. H. Thomason, T. Rosbrook, and J. Murali, "Performance history of thermal-sprayed aluminum coatings in offshore service," *Journal Name: Materials Performance; Journal Volume: 34; Journal Issue: 4; Other Information: PBD: Apr 1995,* pp. Medium: X; Size: pp. 27-34, 1995.

[2] W. H. Thomason, "Offshore Corrosion Protection With Thermal-Sprayed Aluminum," 1985.

[3] S. L. Wolfson, "Corrosion Control of Subsea Piping Systems Using Thermal Sprayed Aluminum Coatings."

[4] P. O. Gartland and T. G. Eggen, "Cathodic and Anodic Properties of Thermally Sprayed Al- and Zn-based Coatings in Seawater," 1990.

[5] S. Papavinasam, M. Attard, B. Arseneult, and R. W. Revie, "State-of-the-Art of Thermal Spray Coatings for Corrosion Protection," *Corrosion Reviews,* vol. 26, pp. 105-145, 2008.

[6] D. K.-K. Tiong and H. Pit, "Experiences On "Thermal Spray Aluminum (Tsa)" Coating On Offshore Structures."

[7] DnV, "Cathodic Protection of Structures," vol. DnV-RP-B401, ed, 2010.

[8] M. Iannuzzi, L. Årtun, K. Nordholm, A. Fjeldly, and A. Q. M, "Chatodic Protection by Distributed Sacrificial Anodes (DSA) - Unpublished Work," Oslo, 2016.

[9] M. R. Dorfman, "19 - Thermal Spray Coatings," in *Handbook of Environmental Degradation of Materials (Second Edition)*, M. Kutz, Ed., ed Oxford: William Andrew Publishing, 2012, pp. 569-596.

[10] J. R. Davis, J. R. Davis, C. Thermal Spray Society Training, and S. Thermal Spray, *Handbook of Thermal Spray Technology*. Materials Park: A S M International, 2004.

[11] T. G. Eggen, "Thermal sprayed coating of al and zn - surface preparation and application," 1991.

[12] V. R. S. Sá Brito, I. N. Bastos, and H. R. M. Costa, "Corrosion resistance and characterization of metallic coatings deposited by thermal spray on carbon steel," *Materials & Design,* vol. 41, pp. 282-288, 10// 2012.

[13] S. Metco. (2013, An Introduction to Thermal Spray. Available: https://www.upc.edu/sct/es/documents_equipament/d_324_id-804-2.pdf

[14] R. C. Tucker Jr, "ASM Handbook, Volume 05A - Thermal Spray Technology," ed: ASM International.

[15] M. Muhamad Hafiz Abd, S. Nor Hayati, A. Sunhaji Kiyai, and S. Noriyati Mohd, "Thermal Arc Spray Overview," *IOP Conference Series: Materials Science and Engineering,* vol. 46, p. 012028, 2013.

[16] M. R. Dorfman, "Chapter 20 - Thermal spray coatings," in *Handbook of Environmental Degradation of Materials*, M. Kutz, Ed., ed Norwich, NY: William Andrew Publishing, 2005, pp. 405-422.

[17] E. Bardal, *Korrosjon og korrosjonsvern*. Trondheim: Tapir Akademisk Forlag, 1994.

[18] N. s. konkurranseposisjon, "Surface preperation and protective coatings," vol. M-501, ed: NORSOK Standard, 2012.

[19] P. O. Gartland, "Protective properties of Al-based coatings in seawater," SINTEF Corrosion Center (Metallurgy), Trondheim1991.

[20] R. S. C. Paredes, S. C. Amico, and A. S. C. M. d'Oliveira, "The effect of roughness and pre-heating of the substrate on the morphology of aluminium coatings deposited by thermal spraying," *Surface and Coatings Technology,* vol. 200, pp. 3049-3055, 2/8/ 2006.

[21] Y. G. Kweon, R. W. Chang, Y. M. Yang, and S. M. Lee, "Blistering Behavior Of Thermally Sprayed Metallic Coatings In Seawater."

[22] K. Nisancioglu, "Corrosion basics and engineering," in *Lecture Notes for the course TMM4170, Korrosjon*, ed. Trondheim, NTNU, 1994.

[23] K. Nisancioglu, "Corrosion and protection of aluminum alloys in seawater," 2007.

[24] F. M. Reinhart and J. F. Jenkins, *Corrosion of alloys in hydrospace : 189 days at 5,900 feet / by Fred M. Reinhart and James F. Jenkins*. Port Hueneme, Calif. :: Naval Civil Engineering Laboratory, 1972.

[25] S. Gudić, J. Radošević, I. Smoljko, and M. Kliškić, "Cathodic breakdown of anodic oxide film on Al and Al–Sn alloys in NaCl solution," *Electrochimica Acta,* vol. 50, pp. 5624-5632, 9/30/ 2005.

[26] S. Egtvedt, K. Nisancioglu, and R. Johnsen, "Thermally Sprayed Aluminum (TSA) with Cathodic Protection as Corrosion Protection for Steel in Natural Seawater: Characterization of Properties on TSA and Calcareous Deposit," ed: Institutt for materialteknologi, 2011.

[27] M. A. B. Rossana Grilli a, James E. Castle, Barrie Dunn and John F. Watts, "Localized corrosion of a 2219 aluminium alloy exposed to a 3.5% NaCl solution," 2010.

[28] R. Grilli, M. A. Baker, J. E. Castle, B. Dunn, and J. F. Watts, "Localized corrosion of a 2219 aluminium alloy exposed to a 3.5% NaCl solution," 2010.

[29] S. Gustafsson, "Corrosion properties of aluminium alloys and surface treated alloys in tap water ", Teknisk- naturvetenskaplig fakultet, Uppsala University, Sverige, 2011.

[30] I. K. a. J. H. N. Christian Knutsen, "Aluminum applied for subsea structures: possibilities and challenges," presented at the The Eleventh International Offshore and Polar Engineering Conference, Stanvanger, Norway, 2001.

[31] C. Vargel, "Corrosion of Aluminium," ed: Elsevier, 2004.

[32] T. G. Eggen and J. M. Drugli, "Sea water corrosion of thermal sprayed aluminium," SINTEF Corrosion Center1993.

[33] C. Holager, R. Johnsen, and K. Nisancioglu, "Corrosion of Thermally Sprayed Aluminum in Flowing Seawater."

[34] M. Lannuzzi, "Kinetics I : Fundamentals of Aqueous Corrosion," ed. The University of Akron, 2015.

[35] H. Bohnes and G. Franke, "6 - Galvanic (Sacrificial) Anodes," in *Handbook of Cathodic Corrosion Protection (Third Edition)*, ed Burlington: Gulf Professional Publishing, 1997, pp. 179-206.

[36] DnV, "Offshore Standard in Submarine pipeline systems," vol. DnV-OS-F101, ed, 2012.

[37] ISO, "Petroleum, petrochemical and natural gas industries - Cathodic protection of pipeline transportation systems - Part 2: Offshore pipelines," vol. ISO 15589-2, ed, 2012.

[38] S. Hejian and H. Shizhong, "Zn's role in dissolution of al sacrificial anodes," *Chinese Journal of Oceanology and Limnology,* vol. 8, pp. 354-362.

[39] C. B. Breslin and L. P. Friery, "The synergistic interaction between indium and zinc in the activation of aluminium in aqueous electrolytes," *Corrosion Science,* vol. 36, pp. 231-240, 1994/02/01 1994.

[40] F. Bolzoni, G. Contreras, L. Lazzari, and S. Goidanich, "Test Results on Sacrificial Anodes used for Seawater."

[41] W. Li, Y. Yan, G. Chen, and M. Li, "The Effect of Temperature and Dissolved Oxygen Concentration on the Electrochemical Behavior of Al-Zn-Inbased Anodes," *Procedia Engineering,* vol. 12, pp. 27-34, // 2011.

[42] H. Sun, L. Liu, Y. Li, L. Ma, and Y. Yan, "The performance of Al–Zn–In–Mg–Ti sacrificial anode in simulated deep water environment," *Corrosion Science,* vol. 77, pp. 77-87, 12// 2013.

[43] M. A and Y. S.A., "Effect of Zinc Addition on the performance of Aluminum as Sacrificial Anode in Seawater," *Journal of Minerals & Materials Characterization & Engineering,* vol. 10, NO 2, pp. 185-198, 2011.

[44] C. Barchiche, C. Deslouis, D. Festy, O. Gil, P. Refait, S. Touzain*, et al.*, "Characterization of calcareous deposits in artificial seawater by impedance techniques: 3—Deposit of CaCO 3 in the presence of Mg(II)," *Electrochimica Acta,* vol. 48, pp. 1645-1654, 2003.

[45]   Y. Yang, J. D. Scantlebury, and E. Koroleva, "A Study of Calcareous Deposits on Cathodically Protected Mild Steel in Artificial Seawater," *Metals,* vol. 5, pp. 439-456, 2015.

[46]   W. Sun, G. Liu, L. Wang, and Y. Li, "A mathematical model for modeling the formation of calcareous deposits on cathodically protected steel in seawater," *Electrochimica Acta,* vol. 78, pp. 597-608, 9/1/ 2012.

[47]   D. A. Shifler, "Understanding material interactions in marine environments to promote extended structural life," *Corrosion Science,* vol. 47, pp. 2335-2352, 10// 2005.

[48]   T. Okstad, Ø. Rannestad, R. Johnsen, and K. Nisancioglu, "Significance of Hydrogen Evolution during Cathodic Protection of Carbon Steel in Seawater," *Corrosion,* vol. 63, pp. 857-865, 2007.

[49]   Y. F. Yang, R. R. Cottis, D. Scantlebury, and R. Cottis, "CALCIUM AND MAGNESIUM CONTAINING ANTI-CORROSION FILMS ON MILD STEEL," ed: The University of Manchester, Manchester, UK, 2010.

[50]   C. Deslouis, D. Festy, O. Gil, V. Maillot, S. Touzain, and B. Tribollet, "Characterization of calcareous deposits in artificial sea water by impedances techniques: 2-deposit of Mg(OH)2 without CaCO3," *Electrochimica Acta,* vol. 45, pp. 1837-1845, 2/1/ 2000.

[51]   C. Barchiche, C. Deslouis, O. Gil, P. Refait, and B. Tribollet, "Characterisation of calcareous deposits by electrochemical methods: role of sulphates, calcium concentration and temperature," *Electrochimica Acta,* vol. 49, pp. 2833-2839, 7/30/ 2004.

[52]   C. Li, M. Du, J. Qiu, J. Zhang, and C. Gao, "Influence of Temperature on the Protectiveness and Morphological Characteristics of Calcareous Deposits Polarized by Galvanostatic Mode," *Acta Metallurgica Sinica (English Letters),* vol. 27, pp. 131-139, 2014.

[53]   H. Möller, "The influence of Mg2+on the formation of calcareous deposits on a freely corroding low carbon steel in seawater," *Corrosion Science,* vol. 49, pp. 1992-2001, 4// 2007.

[54]   S. American Welding Society. Committee on Thermal, *Corrosion tests of flame-sprayed coated steel; 19-year report*: Miami, Fla. : American Welding Society, [1974], 1974.

[55]   K. P. Fischer, W. H. Thomason, and J. E. Finnegan, "ELECTROCHEMICAL PERFORMANCE OF FLAME-SPRAYED ALUMINUM COATINGS ON STEEL IN SEAWATER," 1987.

[56]   W. H. Thomason, S. Olsen, T. Haugen, and K. P. Fischer, "Deterioration of Thermal Sprayed Aluminum Coatings on Hot Risers Due to Thermal Cycling," 2004.

[57]   W. T. Young and J. Repp, "Application and Performance of Thermally Sprayed Aluminum and Zinc on Steel."

[58]   H. Wilson, R. Johnsen, and A. Barnoush, "Thermal Sprayed Aluminium for Subsea Heat Exchanger Surfaces: Effect of Temperature on Protection Current Requirement and Calcareous Development," ed: Institutt for produktutvikling og materialer, 2014.

[59]   O. Ø. Knudsen, J. Van Bokhorst, and G. Duncan, "Corrosion of Thermal Spray Aluminum Coatings in Subsea Mud," *Materials Performance,* vol. 54, pp. 57-57, 2015.

[60]   R. Johnsen and C. Torres, "ER-Subsea Coating for Cooling TSA Test (Final Report)," The Department of Engineering Design and Materials2015.

[61]   T. C. as. (2016). *Total Coating, Drammen*. Available: http://totalcoating.no/

[62]   "ASTM D4541 - 09e1 Standard Test Method for Pull-Off Strength of Coatings Using Portable Adhesion Testers," ed, 2009.

[63]   M. Magome, Y. Mimte, and K. Vermo, "Sprayed metals and alloys in a galvanic serie based on potential measurments in sea water.," *9th International Thermal Spray Conference, The Hague, Netherlands,* 1980.

[64]   W. H. Thomason, "Cathodic Protection of Submerged Steel with Thermal sprayed Aluminum Coatings," *NACE Corrosion,* vol. 85, 1985.

[65]   K. Fagbayi and D. Scantlebury, "Adverse effect of temperature on the operating-potential behavior of Al-Zn-In Anodes," *The Journal of Corrosion Science and Engineering,* vol. 4, 2003.

[66]   J. Ma, J. Wen, and Q. Li, "Electrochemical noise Analysis of the Corrosion Behaviors of Al-Zn- In based Alloy in NaCl Solution," *Physics Procedia,* vol. 50, pp. 421-426, // 2013.

[67]   J. F. Yan and R. B. Griffin, "Parametric studies of the formation of calcareous deposits on cathodically protected steel in seawater," *Journal of the Electrochemical Society,* vol. 140, 1993.

[68]   Per Olav Gartland and T. G. Eggen, "Thermal sprayed aluminum coatings in sea water with and without cathodic protection," SINTEF, Trondheim1993.

[69]   D. J. Greving, J. R. Shadley, and E. F. Rybicki, "Effects of coating thickness and residual stresses on the bond strength of ASTM C633-79 thermal spray coating test specimens," *Journal of Thermal Spray Technology,* vol. 3, pp. 371-378, 1994.

Appendix A – Technical Data of Coral A Anode

SKARPENORD
CORROSION A.S

TECHNICAL DATA

CORAL® 'A'
HIGH GRADE

Al-In-Zn alloy

Chemical composition according to NORSOK specification no. M-503, rev. 2 and certified according to DNV Type Approval program, IOD-90-TAI, November 1982.

The chemical composition and performance data of CORAL® 'A' High Grade alloy are as follows:

Elements	Analysis (% by weight)
Zn	3,5 – 5,0
In	0,015 – 0,025
Cu	max. 0,003
Fe	max. 0,09
Si	max. 0,10
Others (each)	max. 0,020
Al	Remainder

Specific gravity 2,78 kg/dm³ (theoretically)

Performance data in ambient sea water

Capacity	2585 Ah/kg
Consumption rate	3,39 kg/A.yr
Closed circuit potential	-1,09 volt v.s. Ag/AgCl/sea water

Performance data in sea bottom sediments (mud)

	0-20°C	40°C	60°C	80°C
Capacity (Ah/kg)	2400	1750	1150	600
Consumption rate (kg/A.yr)	3,65	5,00	7,62	14,6
Closed circuit potential (volt v.s. Ag/AgCl/sea water	-1,05	-1,03	-1,01	-1,00

VERSION 1/03 – SKARPENORD CORROSION a.s, NORWAY

Figure A. 1 Technical data for CORAL A High Grade Al-Zn-In alloy

Appendix B – First stage of the extrusion process

Prosjektnummer / navn : 10201xxxx, Ekstrud av 5 mmØ stang/Støping av bolt
Container / matrise / bolster: Ekstrudering 100 mmØ / Ekstrudering av 5 mm stang, A3 / Vinge
Kommentarer: Ekstrud av stang – ArnfinnW / Roy Johnsen

Dato: 2016-01-28

2864

Målte parametre

Log	Forsøk Nr	Materiale	V_STEMPEL (MM/S)		T_BOLT (°C)			T_CONT	T_STEM	T_BÆREFLATE		Kraft (kN)		Kommentarer
			innstilt	ok	ovn	føran	Bak			T1_MAX	T2_MAX	Max	Min	
1	1	7x8	0,8	0,7	496	510	502	430	~50	-	-	2815	2606	ok!
	2		"	0,7	490	511	506	430	~100			2748	2497	"
	3		"	0,7	"	511	501	430	~100			2763	2465	

Figure B. 1 Data from the first stage of the extrusion process from
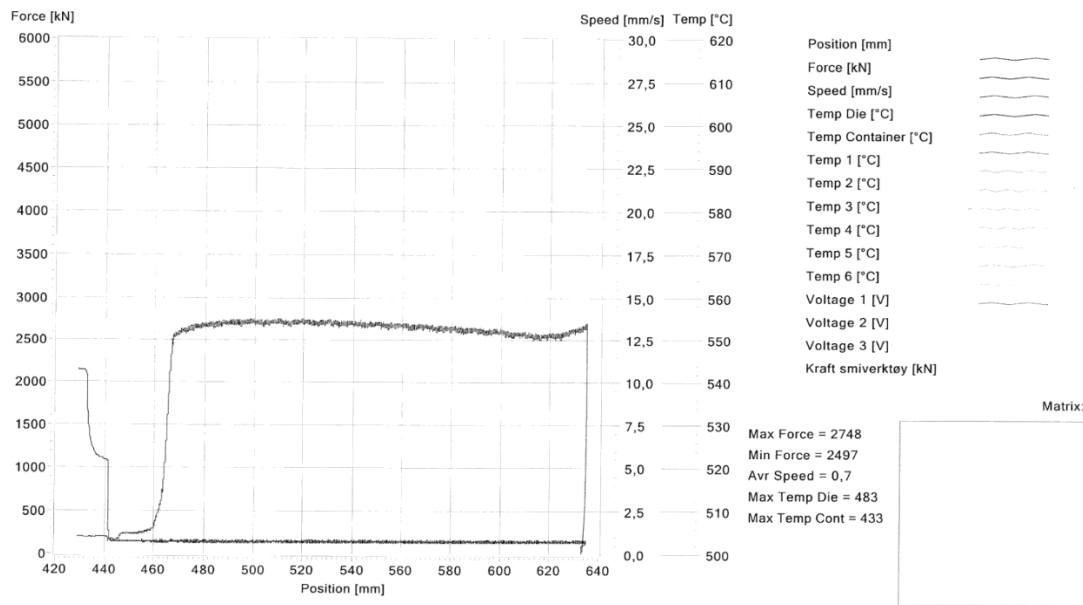
Figure B. 2 First stage of the wire extrusion process.

Appendix C – Corrosion Rate Calculation

Polarization curves were obtained after 1, 8, 15 and 30 days of exposure to natural seawater at 10±2℃. In addition, polarization curves for DSA and TSA exposed at 40℃ were obtained after 30 days of exposure. In Figure C.2-C.17, anodic- and cathodic overvoltage curves are drawn, and the Tafel constants, the slope of the curves, are obtained. Further, the corrosion potential, E_{corr}, and the corrosion current density, i_{corr}, are found by the point of intersection of the tangents, which are presented in the table below each plot. Notice that the polarizations curves are plotted with the logarithmic values for the current density. This is necessary in order to find the Tafel constants.

The corrosion rate was calculated as described in Section 2.2.5. Physical data used for the corrosion rate calculations are shown in Table C. 1.

Table C. 1 Physical data used for the corrosion rate calculation

Property	Value	Unit
Faradays constant, F	96485	C/mol
Density of AlZnIn, ρ_{AlZnIn}	2.95	g/cm^3
Density of DSA, ρ_{DSA}	2.66*	g/cm^3
Density of TSA, ρ_{TSA}	2.43*	g/cm^3
Molar Weight AlZnIn, M_{AlZnIn}	26.98	g/mol
Molar Weight DSA, M_{DSA}	26.98	g/mol
Molar Weight TSA, M_{TSA}	26.98	g/mol

*   Porosity of 10% is added to DSA and TSA

The result from corrosion rate calculation are shown in Figure C. 1 where the left values are obtained from Tafel extrapolation and the right values are obtained from LPR measurements. LPR values and results of calculations can be found in Table C. 2, on the next page.
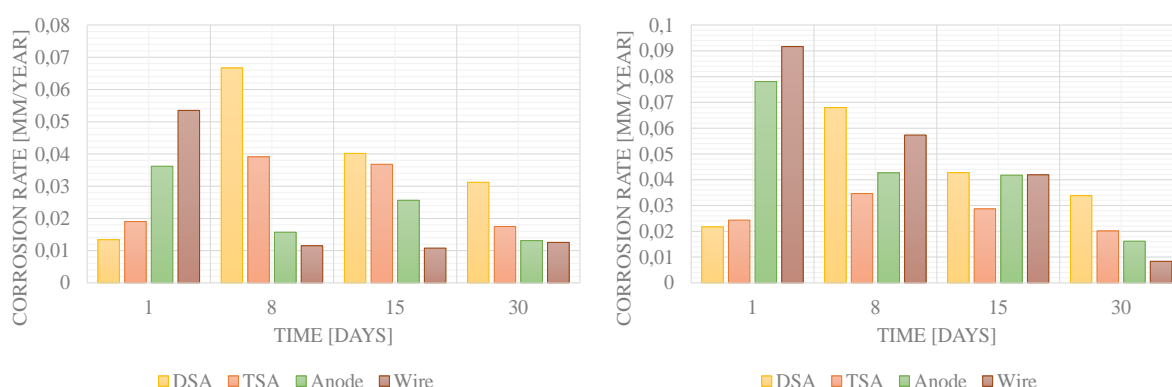

Figure C. 1 Corrosion rate calculation as a function of time, obtained by Tafel extrapolation and LPR measurement respectively.

Linear polarization Resistance Values

Table C. 2 Linear Polarization Resistance (LPR) values with calculated corrosion rate.

Specimen	Days of exposure	B_a [mV/dec]	B_c [mV/dec]	OCP [mV$_{Ag/AgCl}$]	R[ohm]	ΔE (neg) [mV]	ΔE (pos) [mV]	$|\Delta I|$ (neg) [mA]	ΔI (pos) [mA]	Rp [ohm]	I_{corr} [mA]	i_{corr} [mA/cm^2]	CR [mm/year]
TSA	1	-	-	-746	10	-0.1	0.3	0.01	0.03	1000			
	8	254.43	-226.14	-940	100	-2.9	2.6	0.029	0.026	727.27	0.0715	0.002863	0.03452
	15	249.85	-201.21	-948	100	-1.8	3.1	0.018	0.031	816.32	0.0593	0.002374	0.02872
	30	253.34	-213.87	-919	100	-1.7	1.6	0.017	0.016	1212.12	0.0416	0.001664	0.02012
DSA	1	41.86	-101.01	-912	10	-0.4	1.1	0.04	0.11	266.67	0.0491	0.001963	0.02172
	8	168.78	-251.29	-1078	10	-0.6	0.8	0.06	0.08	285.71	0.1534	0.000614	0.06803
	15	115.16	-168.01	-1071	10	-0.6	0.7	0.06	0.07	307.79	0.0965	0.003862	0.04275
	30	128.87	-216.19	-1036	100	-4.0	4.7	0.04	0.047	459.77	0.0763	0.003054	0.03380
Anode	1	108.11	-406.77	-1088	10	-0.5	1.4	0.05	0.14	210.52	0.1764	0.007056	0.07810
	8	86.48	-154.34	-1079	10	-0.4	1.2	0.04	0.12	250	0.0963	0.003856	0.04268
	15	89.07	-203.67	-1083	10	-0.4	1.0	0.04	0.1	285.71	0.0943	0.003772	0.04175
	30	86.38	-163.20	-1080	100	-2.4	3.55	0.024	0.035	672.26	0.0365	0.001461	0.01617
Wire	1	52.64	-243.98	-1093	10	-0.5	1.7	0.05	0.17	181.81	0.1035	0.008283	0.09168
	8	74.63	-148.43	-1090	10	-0.3	0.9	0.03	0.09	333.33	0.0647	0.005181	0.05736
	15	74.52	-137.96	-1088	10	-0.2	0.7	0.02	0.07	444.44	0.0473	0.003786	0.04191
	30	89.196	-268.51	-1090	100	-3.6	0.93	0.0036	0.0093	3093,6	0.0094	0.000753	0.00833
TSA (40ºC)	30	235.49	-159,92	-945	100	-2.2	0.4	0.022	0.004	1538.4	0.0269	0.001076	0.01302
DSA (40ºC)	30	318.44	-217.98	-1063	100	-1.4	0	0.014	0	2857.1	0.0197	0.001231	0.01446

Corrosion rate calculation for DSA with 10% holiday

Simple corrosion rate/dissolution rate calculation for DSA coating with a 10% holiday, i.e. exposed bare CS. The current density was obtained from Table 24 after 30 days of exposure. Physical data can be found in Table C. 1.

Consumption due to CS

$$E_{Coupling} = -1027\,mV_{Ag/AgCl}$$

$$i_{CS} = 172\,mA/m^2$$

$$A_{CS} = 10\,cm^2 \qquad A_{DSA} = 100\,cm^2$$

$$I_{DSA} = I_{CS}$$
$$i_{DSA} \cdot A_{DSA} = i_{CS} \cdot A_{CS}$$
$$i_{DSA} = 17.2\,mA/m^2$$

$$CR = K \cdot \frac{i_{DSA} \cdot M}{n \cdot \rho} = 3268 \cdot \frac{\left(0.00172 \cdot 10^{-3}\,A/cm^2\right) \cdot \left(26.98\,g/mol\right)}{3 \cdot 2.655\,g/cm^3}$$
$$CR = \underline{0.019\,mm/year = 19\,\mu m/year}$$

$$CR_{Total} = (19 + 35)\,\mu m/year = \underline{\underline{54\,\mu m/year}}$$

Consumption due to self − corrosion

$$i_{corr}(-1027) = 31.6\,mA/m^2$$

$$CR = K \cdot \frac{i_{DSA,s} \cdot M}{n \cdot \rho} = 3268 \cdot \frac{\left(31.6 \cdot 10^{-6}\,A/cm^2\right) \cdot \left(26.98\,g/mol\right)}{3 \cdot \left(2.655\,g/cm^3\right)}$$

$$CR = \underline{0.035\,mm/year = 35\,\mu m/year}$$

C.1 Polarization Curves for specimens exposed at 10±2℃

Anode day 1

y = 108,11x - 820,91
R² = 0,9943

y = -406,77x - 2080,8
R² = 0,9991

Cathodic —— Anodic ⋯⋯ OCP ⋯⋯ Linear (Cathodic Tafel) ⋯⋯ Linear (Anodic Tafel)

Point of Interception		
Equation	ax	constant
Anodic tafel	108,11	-820,91
Catodic tafel	-406,77	-2080,8
X-value (log i)		-2,44695851
Y-value (Ecorr)		-1085,45069
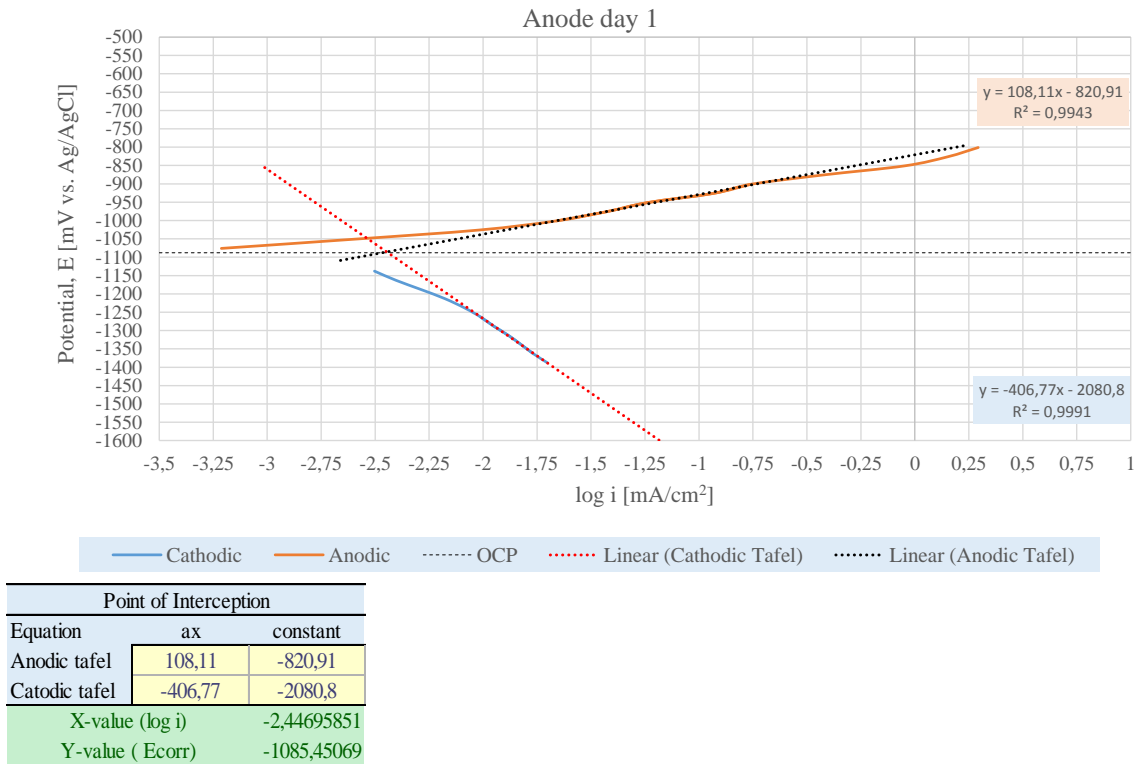
Figure C. 2 Polarization Curves of anode with calculated tafel constant, obtained day 1 in natural seawater at 10℃.


Anode day 8

y = 86,478x - 844,31
R² = 0,982

y = -154,34x - 1519,2
R² = 0,998

Cathodic —— Anodic ⋯⋯ OCP ⋯⋯ Linear (Cathodic Tafel) ⋯⋯ Linear (Anodic Tafel)

Point of Interception		
Equation	ax	constant
Anodic tafel	86,478	-844,31
Catodic tafel	-154,34	-1519,2
X-value (log i)		-2,80248985
Y-value (Ecorr)		-1086,66372
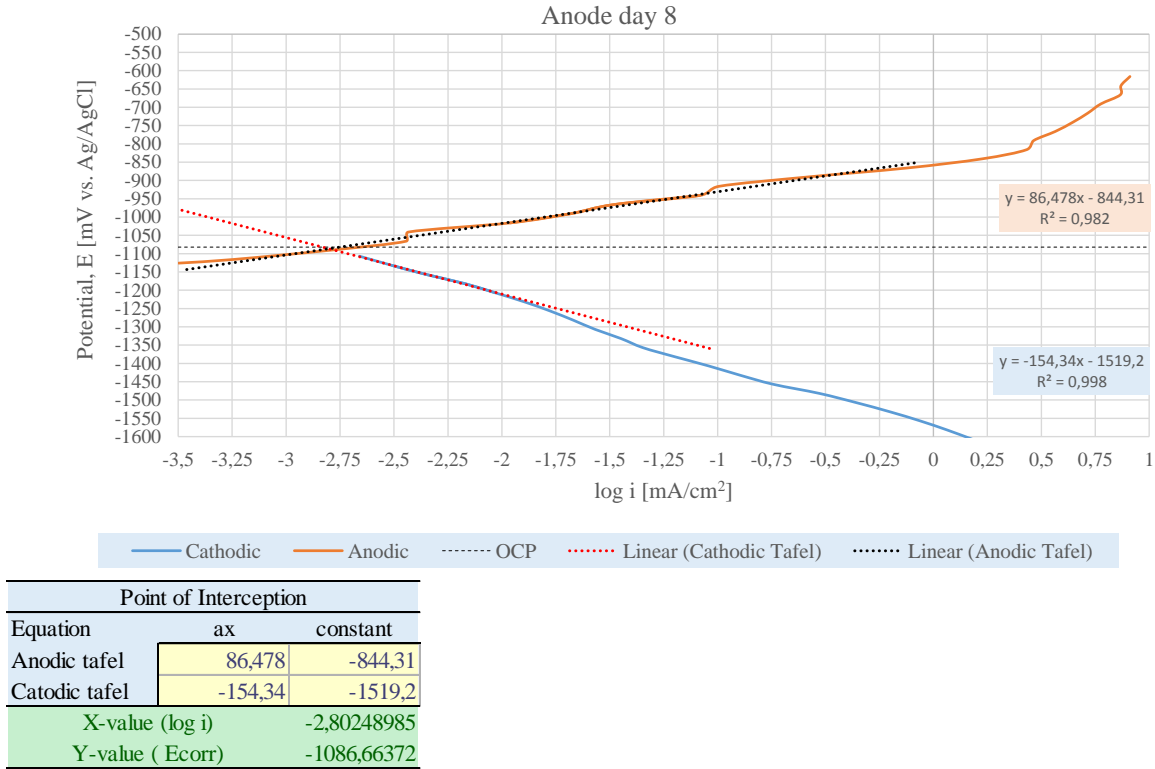
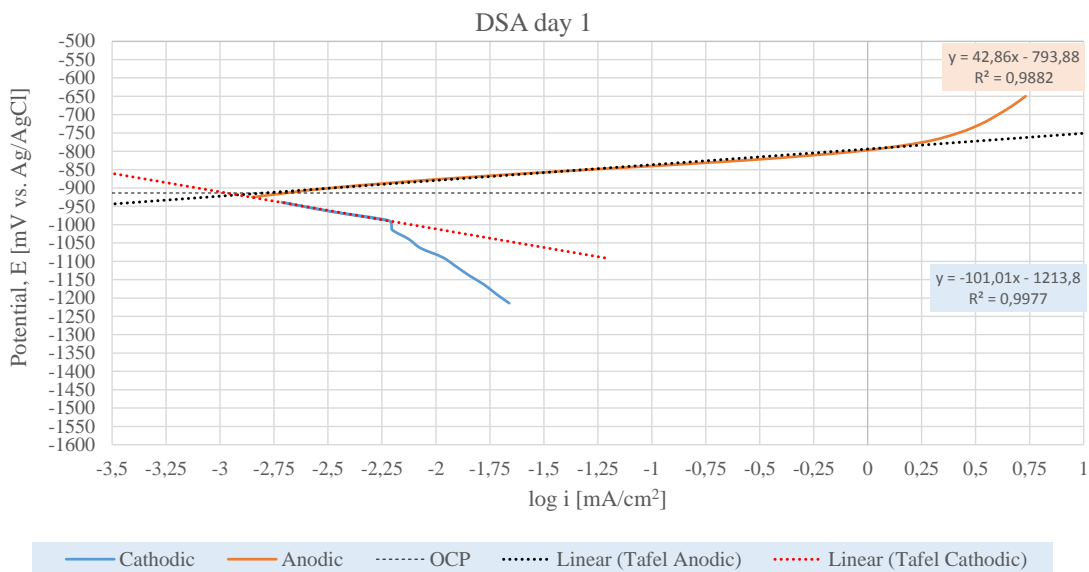**Figure C. 3** Polarization Curves of anode with calculated tafel constant, obtained day 8 in natural seawater at 10℃.
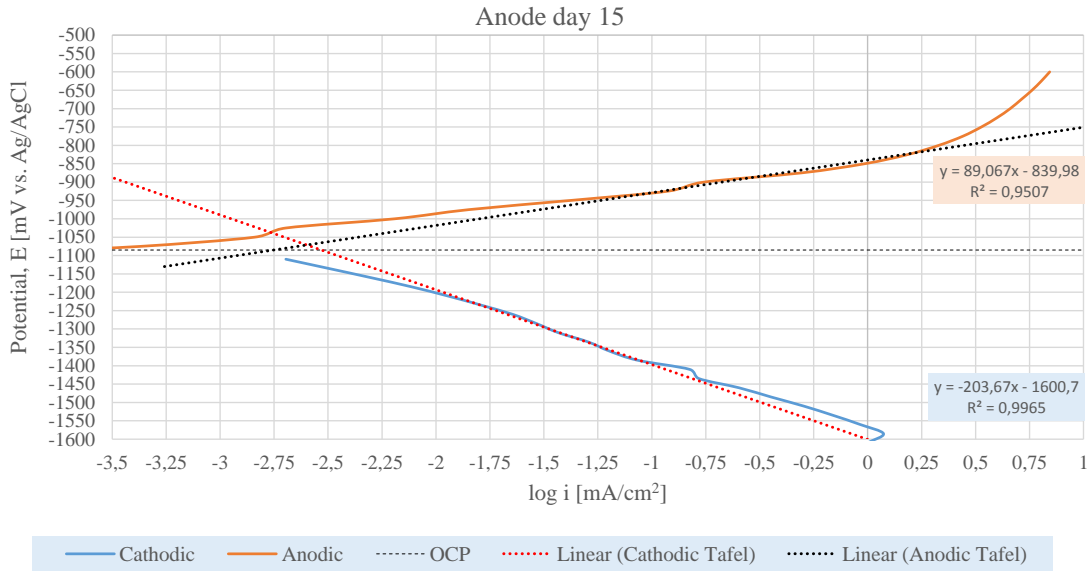
Figure C. 4 Polarization Curves of anode with calculated tafel constant, obtained day 15 in natural seawater at 10°C.
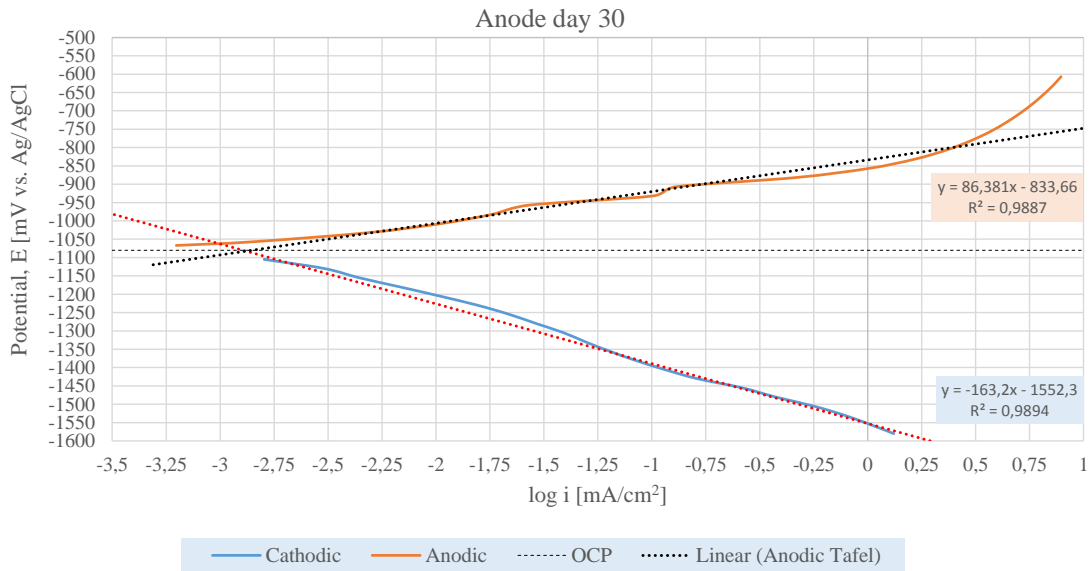
Figure C. 5 Polarization Curves of anode with calculated tafel constant, obtained day 30 in natural seawater at 10°C.
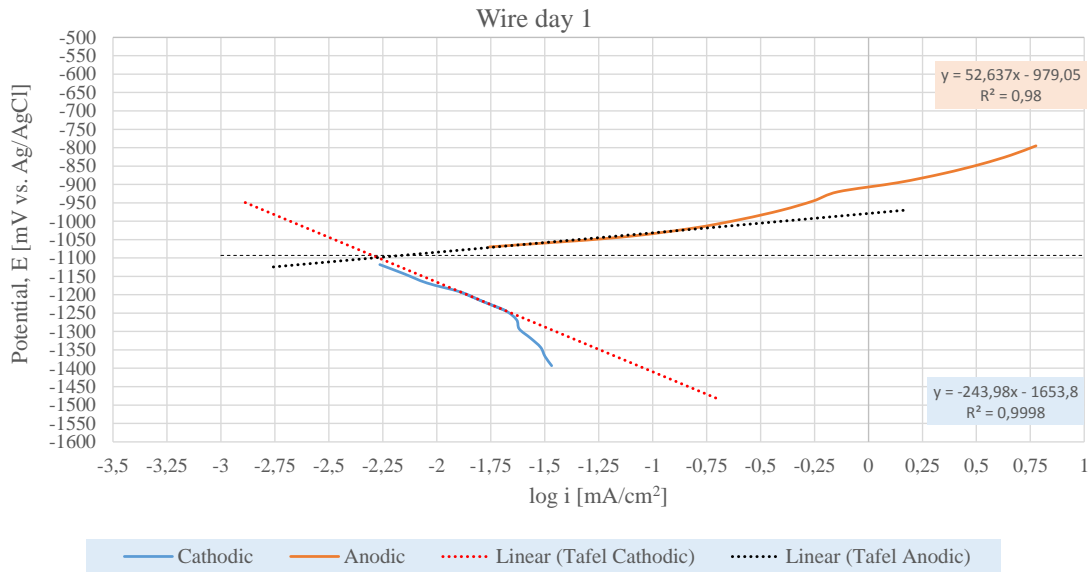
Figure C. 6 Polarization Curves of anode wire with calculated tafel constant, obtained day 1 in natural seawater at 10℃.
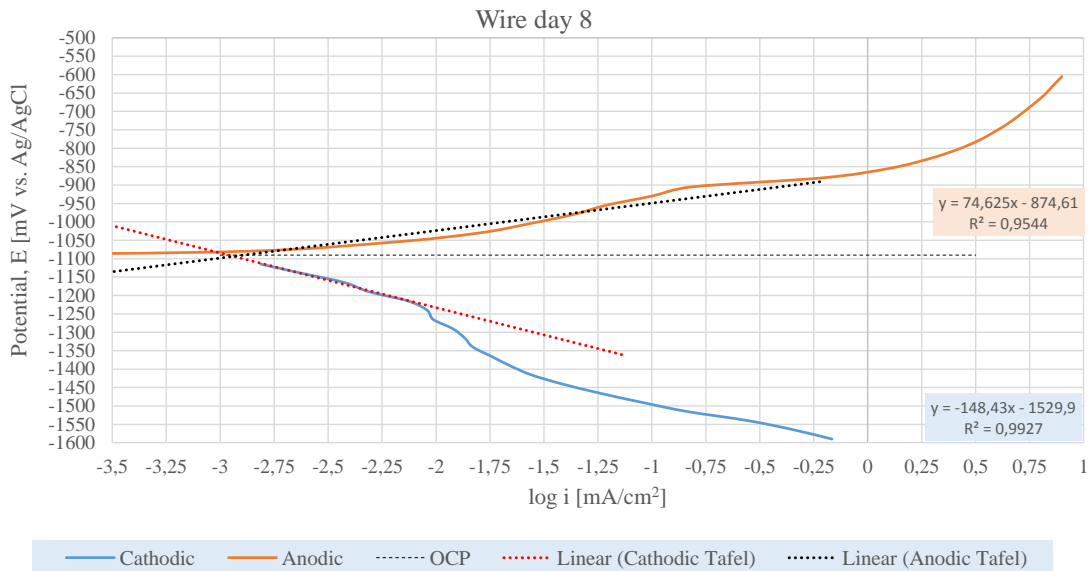
Figure C. 7 Polarization Curves of anode wire with calculated tafel constant, obtained day 8 in natural seawater at 10℃.
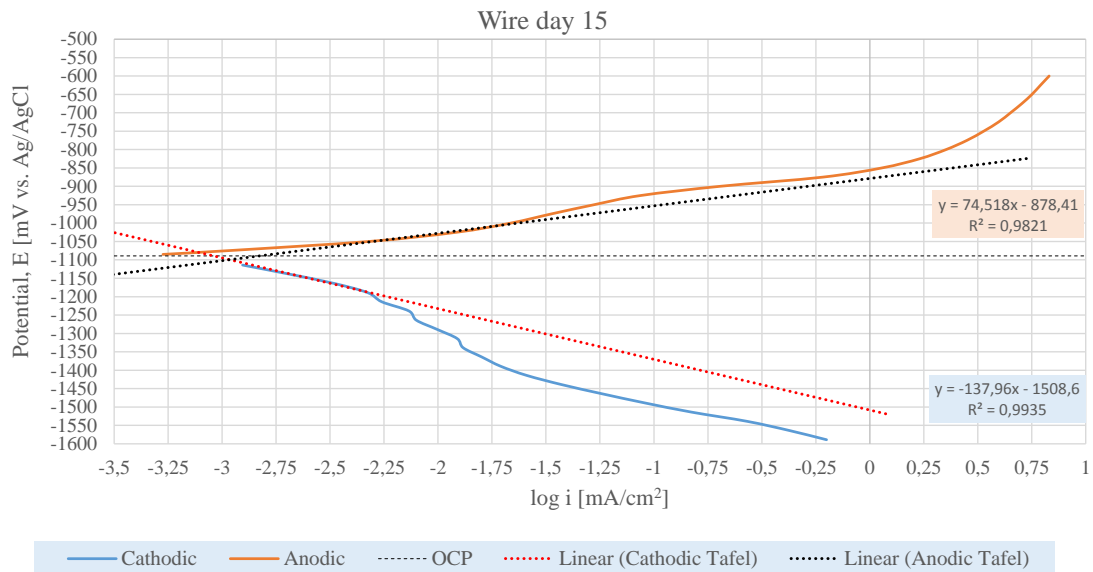
Figure C. 8 Polarization Curves of anode wire with calculated tafel constant, obtained day 15 in natural seawater at 10°C.
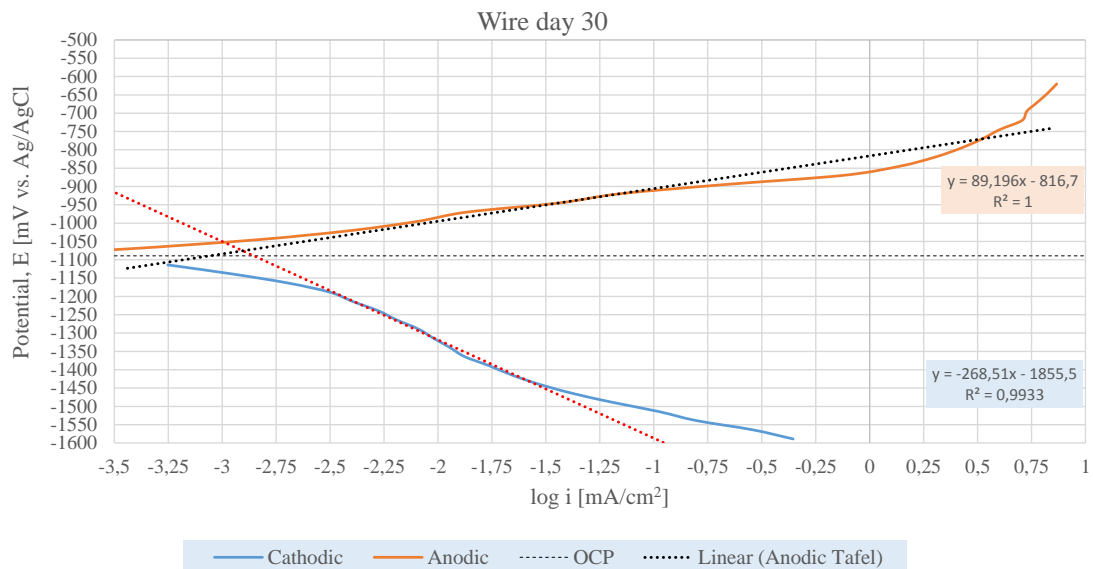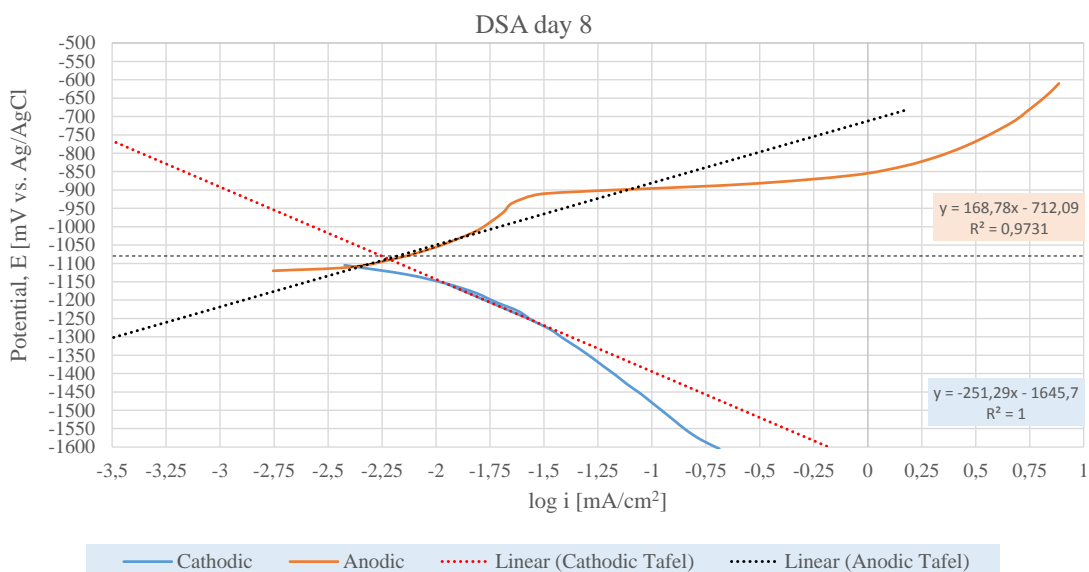

Figure C. 9 Polarization Curves of anode wire with calculated tafel constant, obtained day 30 in natural seawater at 10°C.

DSA day 1

Point of Interception		
Equation	ax	constant
Anodic tafel	42,86	-793,88
Catodic tafel	-101,01	-1213,8
X-value (log i)		-2,9187461
Y-value (Ecorr)		-918,97746

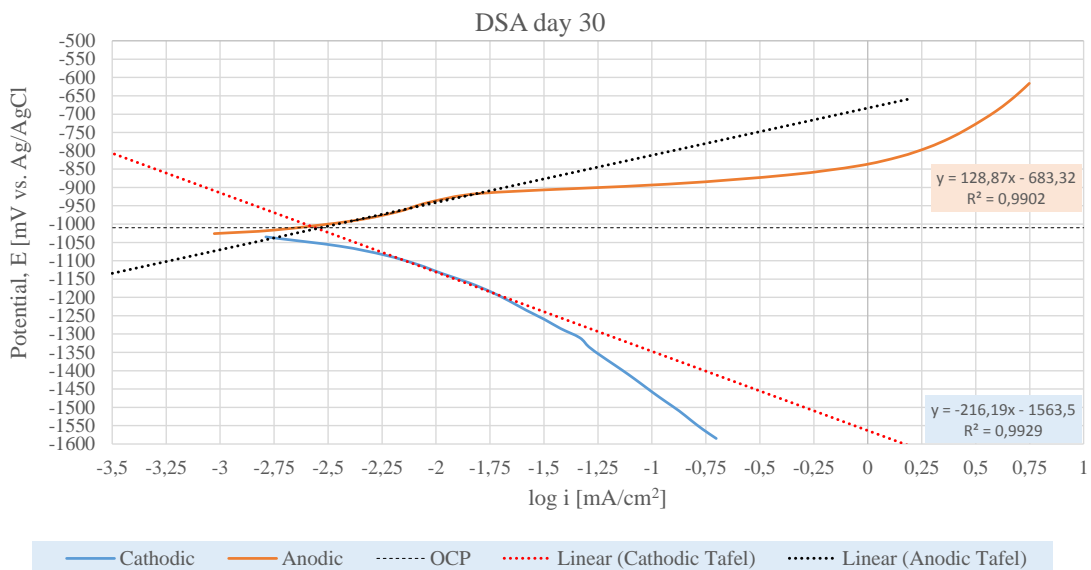**Figure C. 10** Polarization Curves of DSA with calculated tafel constant, obtained day 1 in natural seawater at 10℃.

DSA day 8

Point of Interception		
Equation	ax	constant
Anodic tafel	168,78	-712,09
Catodic tafel	-251,29	-1645,7
X-value (log i)		-2,22251
Y-value (Ecorr)		-1087,21

Figure C. 11 Polarization Curves of DSA with calculated tafel constant, obtained day 8 in natural seawater at 10℃.

DSA day 15
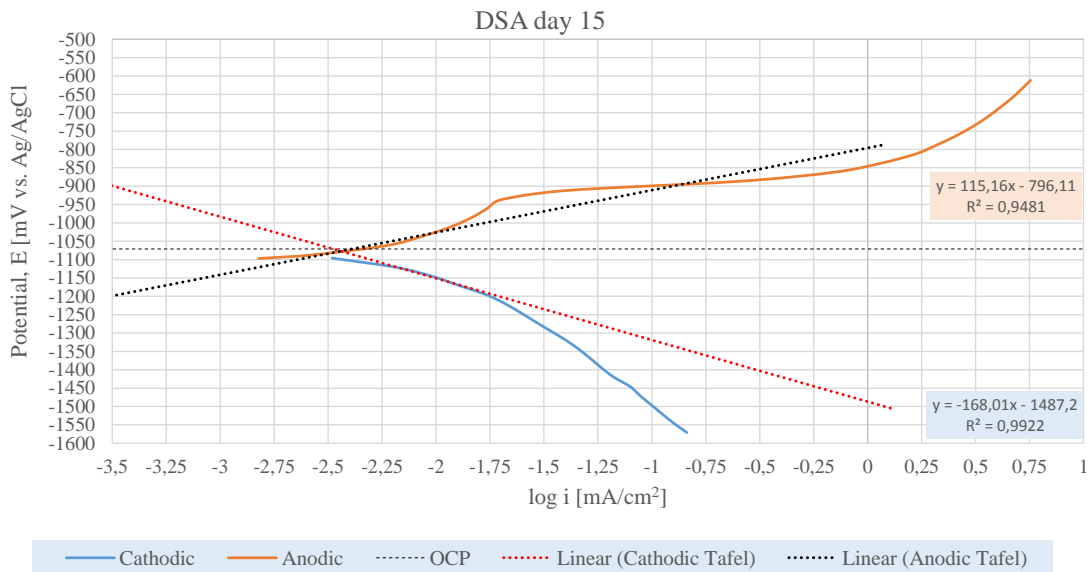
Point of Interception		
Equation	ax	constant
Anodic tafel	115,16	-796,11
Catodic tafel	-168,01	-1487,2
X-value (log i)		-2,44055
Y-value (Ecorr)		-1077,16

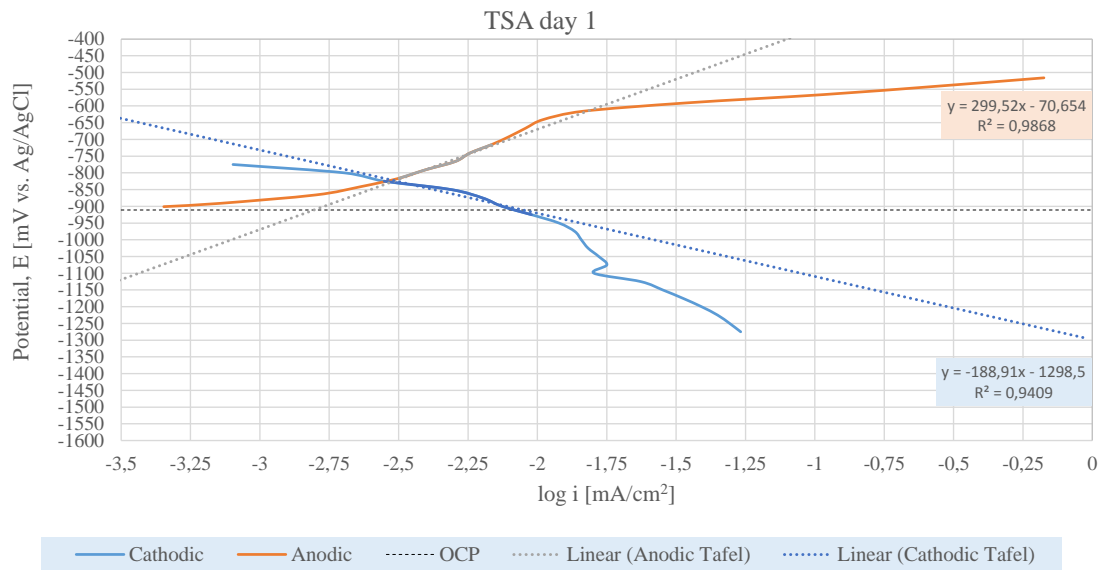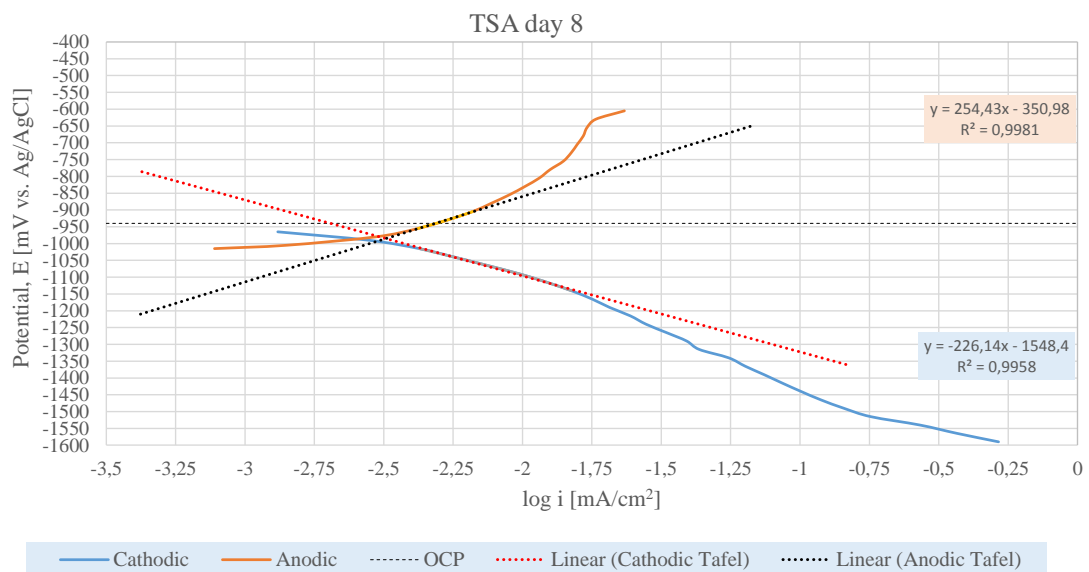**Figure C. 12** Polarization Curves of DSA with calculated tafel constant, obtained day 15 in natural seawater at 10°C.

DSA day 30

Point of Interception		
Equation	ax	constant
Anodic tafel	128,87	-683,32
Catodic tafel	-216,19	-1563,5
X-value (log i)		-2,5508
Y-value (Ecorr)		-1012,04

Figure C. 13 Polarization Curves of DSA with calculated tafel constant, obtained day 30 in natural seawater at 10°C.

TSA day 1

Point of Interception		
Equation	ax	constant
Anodic tafel	299,52	70,654
Catodic tafel	-188,91	-1298,5
X-value (log i)		-2,803173433
Y-value (Ecorr)		-768,9525067

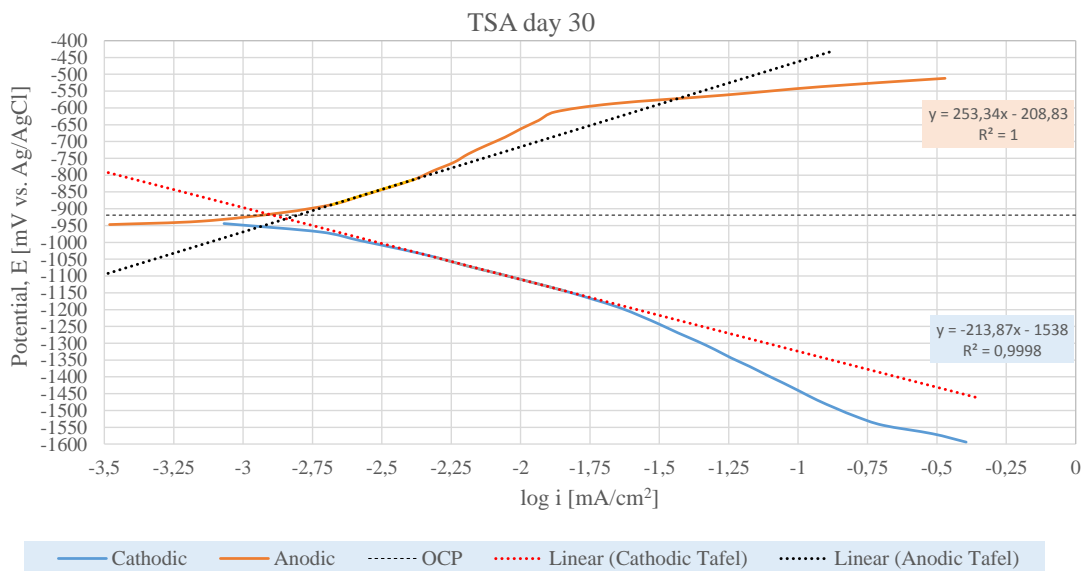**Figure C. 14** Polarization Curves of TSA with calculated tafel constant, obtained day 1 in natural seawater at 10℃.

TSA day 8

Point of Interception		
Equation	ax	constant
Anodic tafel	254,43	-350,98
Catodic tafel	-226,14	-1548,4
X-value (log i)		-2,4916661
Y-value (Ecorr)		-984,93462

Figure C. 15 Polarization Curves of TSA with calculated tafel constant, obtained day 8 in natural seawater at 10℃.

Figure C. 16 Polarization Curves of TSA with calculated tafel constant, obtained day 15 in natural seawater at 10℃.
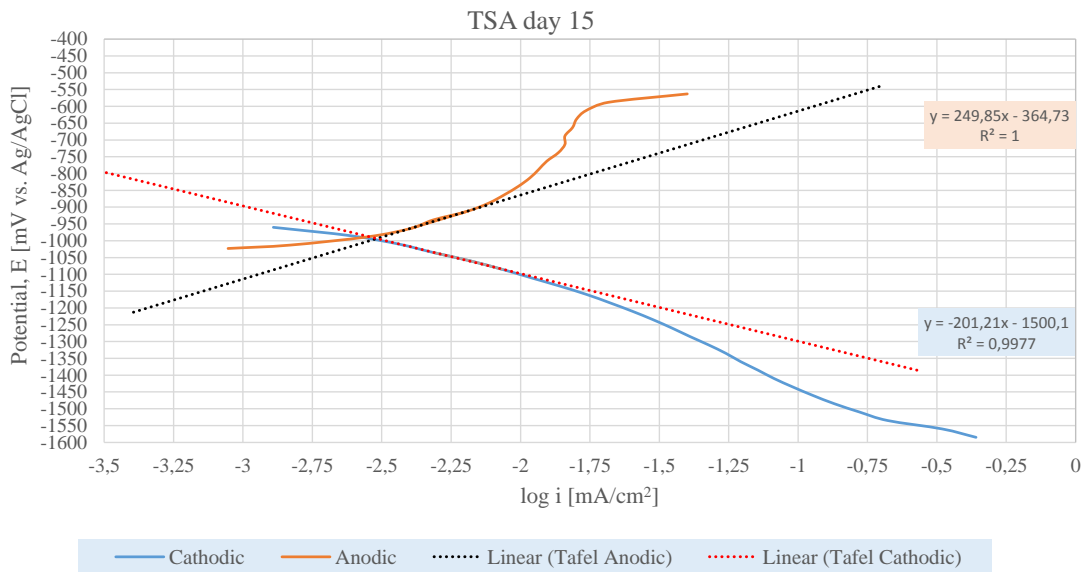
Point of Interception		
Equation	ax	constant
Anodic tafel	249,85	-364,73
Catodic tafel	-201,21	-1500,1
X-value (log i)		-2,51712
Y-value (Ecorr)		-993,631

Figure C. 17 Polarization Curves of TSA with calculated tafel constant, obtained day 30 in natural seawater at 10℃.
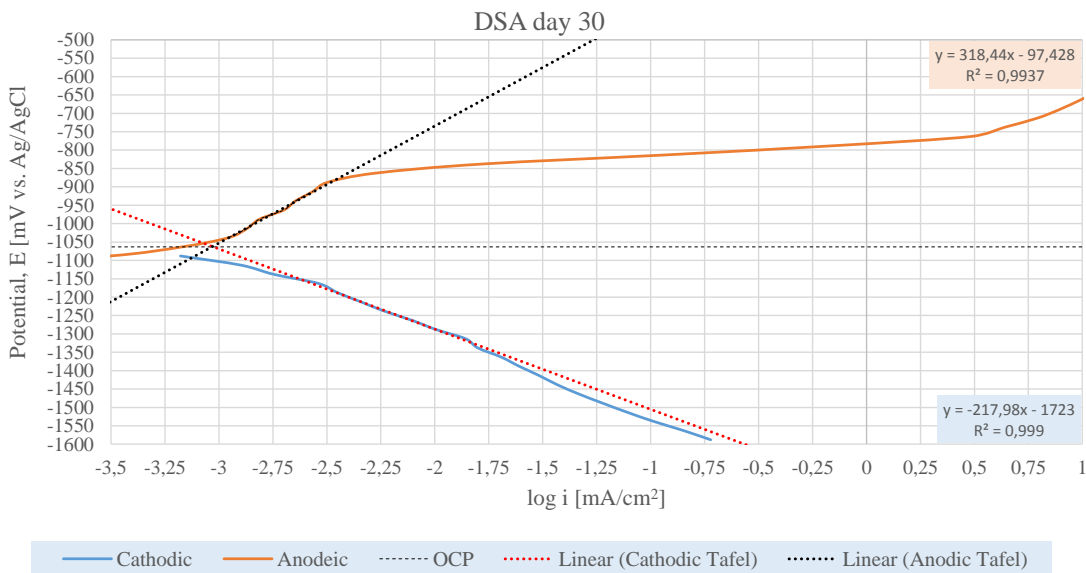
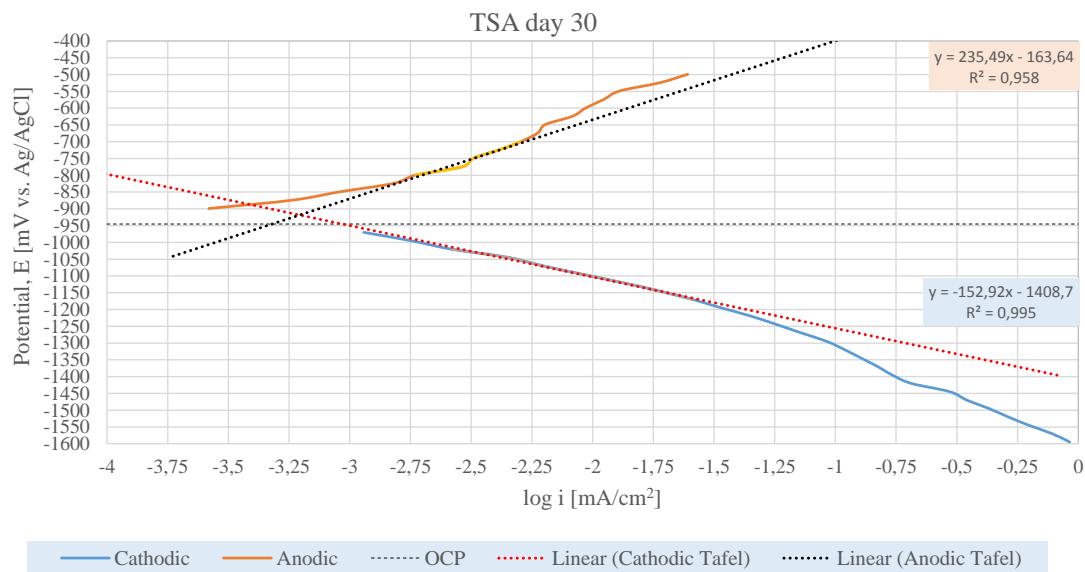| Point of Interception		
Equation	ax	constant
Anodic tafel	253,34	-208,83
Catodic tafel	-213,87	-1538
X-value (log i)		-2,8449091
Y-value (Ecorr)		-929,55928

C.1 Polarization Curves for specimens exposed at 40℃

The temperature varied a lot throughout the exposure period. However, when the polarization curves for DSA and TSA were obtained after 30 days of exposure, the temperature was 40.05℃. The anodic and cathodic polarization curves with the corresponding Tafel slopes can be seen on the next page.

Point of Interception		
Equation	ax	constant
Anodic tafel	318,44	-97,428
Catodic tafel	-217,98	-1723
X-value (log i)		-3,030409008
Y-value (Ecorr)		-1062,431444

Figure C. 18 Polarization Curves of DSA with calculated tafel constant, obtained day 30 in natural seawater at 40℃.

TSA day 30

y = 235,49x - 163,64
R² = 0,958

y = -152,92x - 1408,7
R² = 0,995

Point of Interception		
Equation	ax	constant
Anodic tafel	235,49	-163,64
Catodic tafel	-159,92	-1408,7
X-value (log i)		-3,148782277
Y-value (Ecorr)		-905,1467383

Figure C. 19 Polarization Curves of DSA with calculated tafel constant, obtained day 30 in natural seawater at 40℃.

Appendix D – Exposed specimens
Photos of galvanic couplings after 30 days exposure at 10±2°C.
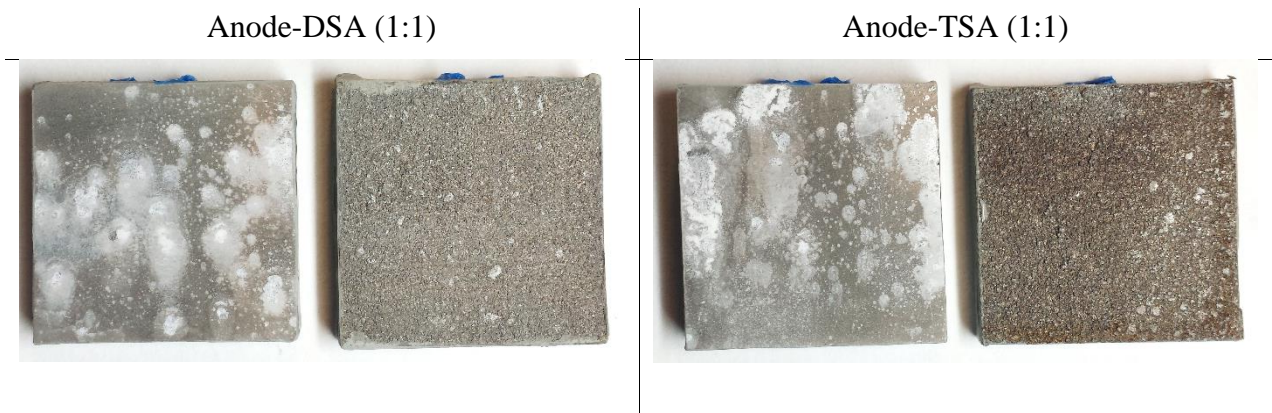
Anode-DSA (1:1)

Anode-TSA (1:1)

Figure D. 1 Galvanic couplings between Coral A anode and DSA and TSA with area ratio 1:1, after 30 days of exposure to natural seawater at 10°C.
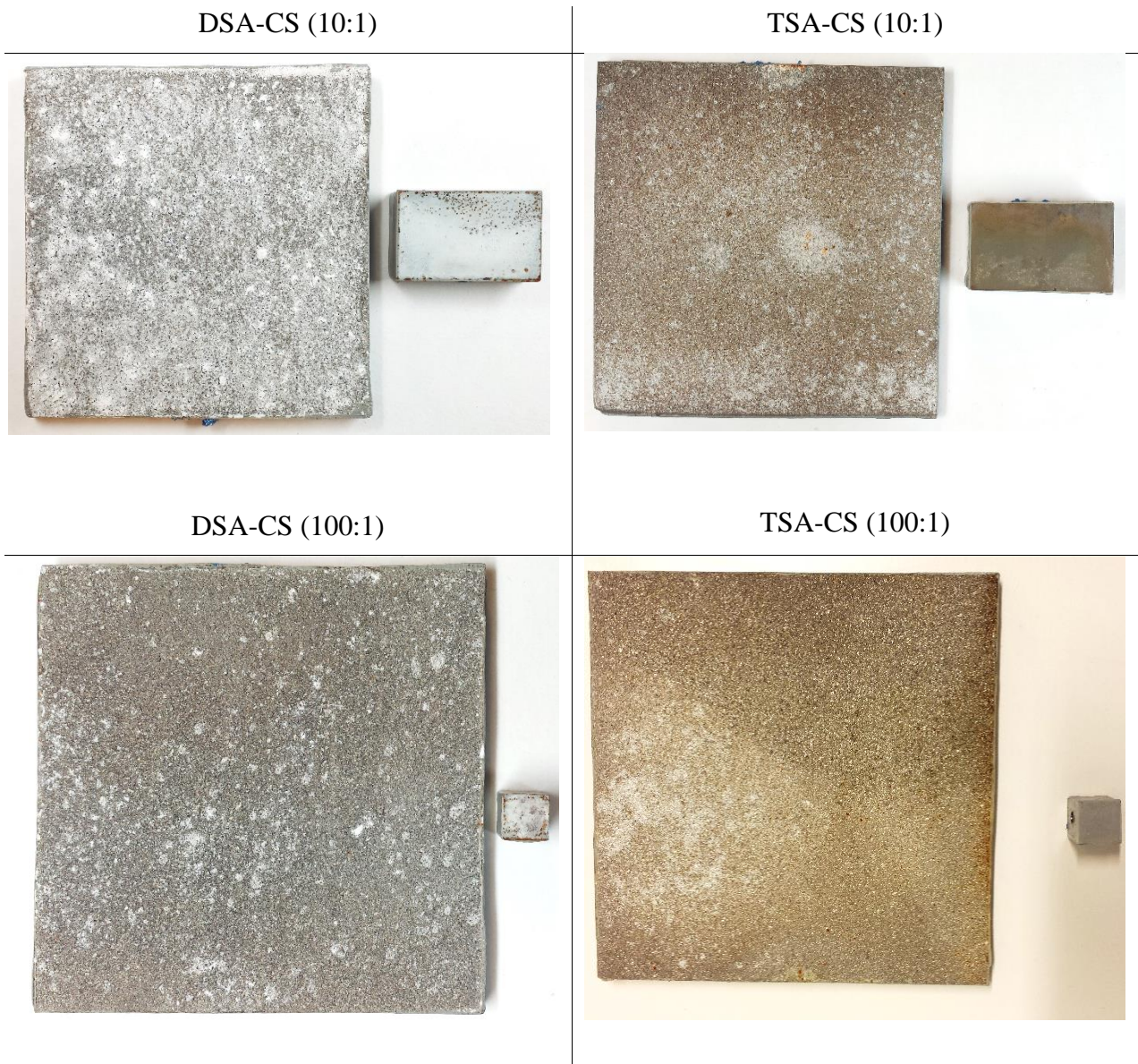
DSA-CS (10:1)

TSA-CS (10:1)

DSA-CS (100:1)

TSA-CS (100:1)

Figure D. 2 Galvanic coupling between DSA and CS with area ratio 10:1 and 100:1, after 30 days of exposure to natural seawater at 10℃

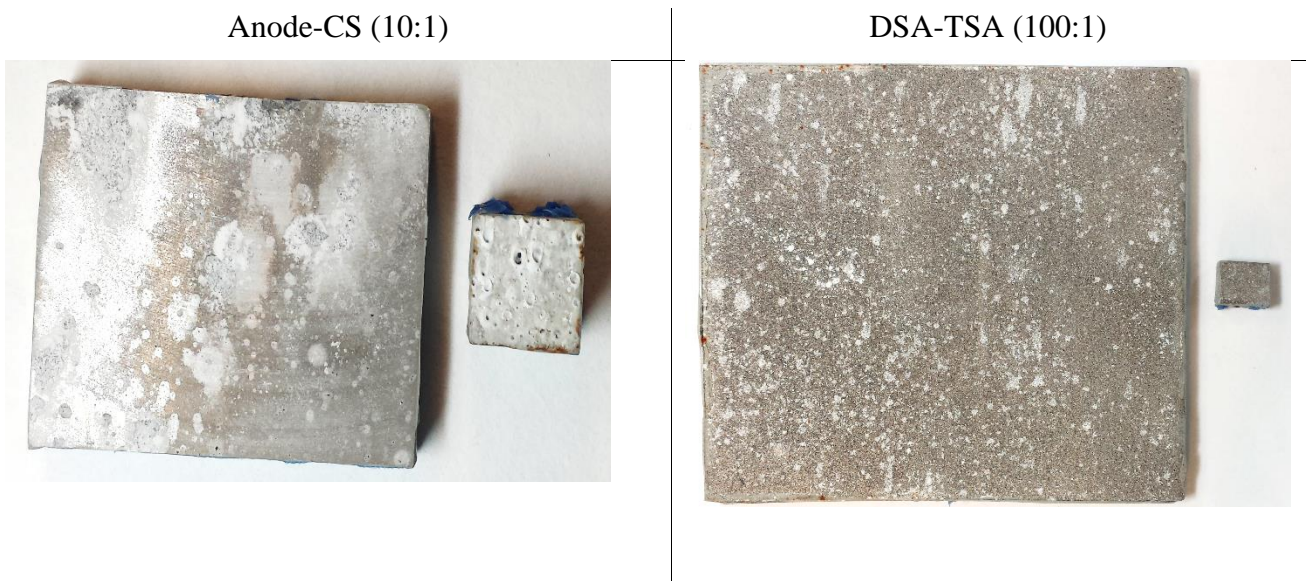| Anode-CS (10:1)	DSA-TSA (100:1)

Figure D. 3 Galvanic coupling between Anode and CS with area ratio 10:1 and coupling between DSA and TSA with area ratio 100:1, after 30 days of exposure to natural seawater at 10℃.

Photos of galvanic couplings after 30 days exposure at 40±10℃.

Before exposure

DSA-CS (10:1)   DSA-TSA (10:1)

Anode-CS (10:1)

Figure D. 4 Galvanic Couplings before and after 30 days of exposure to natural seawater at 40±5℃

Appendix E – Adhesion Pull-Off Test

Results from adhesion pull of test for the "special" plate with incremental coating thickness is presented in Table E. 1. SEM analysis of the cross sections showed that the coating thickness were approximately 1 mm at dolly 1-2, 1.75 mm at dolly 3-5 and 1.55 mm at dolly 5-8. Higher adhesion can be observed for the thinnest layer. However, as the coating thickness was largest in the middle zone (3-5), there are no clear evidence that the adhesion strength of the coating is severely affected by increasing the thickness from 1.55 mm to 1.75. More testing should be done in this area in order to find the right balance between coating thickness and mechanical performance.

Table E. 1 Adhesion pull of test for special coated plate with incremental thickness.

Dollies	MPa	Failure mode
1.	10.13	100% B/C
2.	10.31	100% B/C
3.	10.67	100% B/C
4.	8.89	100% B/C
5.	9.07	100% B/C
6.	8.89	100% B/C
7.	8.89	100% B/C
8.	8.53	100% B/C

Appendix F – Risk Assessment

NTNU
HMS

Kartlegging av risikofylt aktivitet

	Utarbeidet av	Nummer	Dato
	HMS-avd.	HMSRV2601	22.03.2011
	Godkjent av		Erstatter
	Rektor		01.12.2006

Dato: 01.02.16

Enhet:

Linjeleder:

Deltakere ved kartleggingen (m/ funksjon): Geir Quale
(Ansv. veileder, student, evt. medveiledere, evt. andre m. kompetanse)

Kort beskrivelse av hovedaktivitet/hovedprosess: MSc Project by Geir Quale *"Cathodic Protection with Distributed Anodes"*

Er oppgaven rent teoretisk? (NEI):

Signaturer: Ansvarlig veileder: Student:

ID nr.	Aktivitet/prosess	Ansvarlig	Eksisterende dokumentasjon	Eksisterende sikringstiltak	Lov, forskrift o.l.	Kommentar
1	Teoretisk skriving					Ingen risiko
2	Verksted, kapping (klargjøring av prøver 50x50)	Geir Quale (Roy Johnsen)		Vernebriller, hansker, kjeledress	Påbudt verneutstyr NTNU	
3	Verksted, maskinering	Geir Quale (Roy Johnsen)		Vernebriller, hansker, kjeledress	Påbudt verneutstyr NTNU	
4	Korrosjonsforsøket gjennomføres i sealab og i Korrosjonslab ved NTNU. Ulike prøvestykker (TSA, anode, wire etc.) skal eksponeres for sjøvann ved 10 grader og mulig 80 grader. Måling av potensial, LPR, polarisasjonskurver, blandingspotensial og strøm vs. tid	Geir Quale (Roy Johnsen)		Vernebriller	Påbudt verneutstyr NTNU	Eksperimentet inneholder ingen farlige elementer, og det er svært liten risiko for en ulykke å intreffe. Experimentet blir gjennomført på laboratorie hvor det finnes farlige elementer.

131

NTNU HMS	Kartlegging av risikofylt aktivitet			Utarbeidet av	Nummer	Dato
				HMS-avd.	HMSRV2601	22.03.2011
				Godkjent av	Erstatter	
				Rektor		01.12.2006

| 5 | Metallografi, prøvene kappes i to, slik at tversnittarealet kan undersøkes | Geir Quale (Roy Johnsen) | | Vernebriller | Påbudt verneutstyr NTNU | Varsom oppførsel er viktig. Kappingen foregår i maskin som brukes til slike formål. |

NTNU | | | Utarbeidet av | Nummer | Dato
| HMS | Risikovurdering | HMS-avd. | HMSRV2601 | 22.03.2011
| | Dato: | Godkjent av | Erstatter | 01.12.2006
| | | Rektor | |

Enhet:

Linjeleder:

Deltakere ved kartleggingen (m/ funksjon):
(Ansv. Veileder, student, evt. medveiledere, evt. andre m. kompetanse)

Risikovurderingen gjelder hovedaktivitet: MSc Project by Geir Quale *"Cathodic Protection with Distributed Anodes"*

Signaturer: *Ansvarlig veileder:* _____ *Student:* _Geir Quale_

ID nr	Aktivitet fra kartleggings-skjemaet	Mulig uønsket hendelse/ belastning	Vurdering av sannsyn-lighet (1-5)	Menneske (A-E)	Ytre miljø (A-E)	Øk/ materiell (A-E)	Om-dømme (A-E)	Risiko-Verdi (menn-eske)	Kommentarer/status Forslag til tiltak
1	Teoretisk skriving	Ingen uønsket hendelse							
2	Verksted, kapping	Kappe/Skade av kroppslegemer	3	C	A	B	A	C2	Være årvåken, kjenne maskinen, bruke påkrevd verneutstyr.
3	Verksted, maskinering	Kappe/Skade av kroppslegemer, Øyeskade	3	C	A	B	A	B1	Være årvåken, tilstrekkelig luftavsug, sveisekunnskap, bruke påkrevd verneutstyr
4	Verksted, exp. forsøk	Ingen uønskede hendelser	-	-	-	-	-	-	Bruk vernebriller
5	Metallografi, kapping	Kappe/Skade av kroppslegemer	2	B	A	B	A	B2	Være årvåken, kjenne maskinen, bruke påkrevd verneutstyr, riktig instillinger, passe på at beskyttelsesluka på maskinen er fulstedning lukket under arbeidet.

Risikovurdering

Sannsynlighet vurderes etter følgende kriterier:

Svært liten 1	Liten 2	Middels 3	Stor 4	Svært stor 5
1 gang pr 50 år eller sjeldnere	1 gang pr 10 år eller sjeldnere	1 gang pr år eller sjeldnere	1 gang pr måned eller sjeldnere	Skjer ukentlig

Konsekvens vurderes etter følgende kriterier:

Gradering	Menneske	Ytre miljø Vann, jord og luft	Øk/materiell	Omdømme
E Svært Alvorlig	Død	Svært langvarig og ikke reversibel skade	Drifts- eller aktivitetsstans >1 år.	Troverdighet og respekt betydelig og varig svekket
D Alvorlig	Alvorlig personskade. Mulig uførhet.	Langvarig skade. Lang restitusjonstid	Driftsstans > ½ år Aktivitetsstans i opp til 1 år	Troverdighet og respekt betydelig svekket
C Moderat	Alvorlig personskade.	Mindre skade og lang restitusjonstid	Drifts- eller aktivitetsstans < 1 mnd	Troverdighet og respekt svekket
B Liten	Skade som krever medisinsk behandling	Mindre skade og kort restitusjonstid	Drifts- eller aktivitetsstans < 1uke	Negativ påvirkning på troverdighet og respekt
A Svært liten	Skade som krever førstehjelp	Ubetydelig skade og kort restitusjonstid	Drifts- eller aktivitetsstans < 1dag	Liten påvirkning på troverdighet og respekt

Risikoverdi = Sannsynlighet x Konsekvens
Beregn risikoverdi for Menneske. Enheten vurderer selv om de i tillegg vil beregne risikoverdi for Ytre miljø, Økonomi/materiell og Omdømme. I så fall beregnes disse hver for seg.

Til kolonnen "Kommentarer/status, forslag til forebyggende og korrigerende tiltak":
Tiltak kan påvirke både sannsynlighet og konsekvens. Prioriter tiltak som kan forhindre at hendelsen inntreffer, dvs. sannsynlighetsreduserende tiltak foran skjerpet beredskap, dvs. konsekvensreduserende tiltak.

134

NTNU			
	utarbeidet av HMS-avd.	Nummer HMSRV2604	Dato 08.03.2010
HMS/KS	godkjent av Rektor	Erstatter	09.02.2010

Risikomatrise

MATRISE FOR RISIKOVURDERINGER ved NTNU

KONSEKVENS					
Svært alvorlig	E1	E2	E3	E4	E5
Alvorlig	D1	D2	D3	D4	D5
Moderat	C1	C2	C3	C4	C5
Liten	B1	B2	B3	B4	B5
Svært liten	A1	A2	A3	A4	A5
	Svært liten	Liten	Middels	Stor	Svært stor
	SANNSYNLIGHET				

Prinsipp over akseptkriterium. Forklaring av fargene som er brukt i risikomatrisen.

Farge	Beskrivelse
Rød	Uakseptabel risiko. Tiltak skal gjennomføres for å redusere risikoen.
Gul	Vurderingsområde. Tiltak skal vurderes.
Grønn	Akseptabel risiko. Tiltak kan vurderes ut fra andre hensyn.